Aus der

Kinderklinik und Kinderpoliklinik im Dr. von Haunerschen Kinderspital

Klinikum der Ludwig-Maximilians-Universität München

IL1RL2 in immunity and intestinal homeostasis-
Insights from patients with VEO-IBD

Dissertation
zum Erwerb des Doctor of Philosophy (Ph.D.)
an der Medizinischen Fakultät
der Ludwig-Maximilians-Universität München

vorgelegt von
Leyla Atac

aus
Hatay / Türkei

Jahr
2024

_____

Mit Genehmigung der Medizinischen Fakultät der
Ludwig-Maximilians-Universität München

Erstes Gutachten: Prof. Dr. Dr. Christoph Klein

Zweites Gutachten: Priv. Doz. Dr. Dr. Daniel Kotlarz

Drittes Gutachten: Priv. Doz. Dr. Christian Schulz

Viertes Gutachten: Prof. Dr. Barbara Schraml-Schotta

Dekan: Prof. Dr. med. Thomas Gudermann

Tag der mündlichen Prüfung: 02.12 2024

TABLE OF CONTENT

ABSTRACT

Very early onset inflammatory bowel disease (VEO-IBD) is distinguished by intense, early-onset inflammation in the gastrointestinal tract and is often connected to genetic mutations. VEO-IBD patients usually exhibit intense disease indications that are unresponsive to treatments. Several signatures, including *IL10R*, *RIPK1*, *MD2*, and *CASP8* deficiencies, have been identified in our laboratory as prominent monogenic causes of IBD. Nevertheless, the majority of VEO-IBD patients remain without a genetic diagnosis, highlighting the essential need to comprehend the pathophysiology for effective clinical management. Our laboratory has utilized whole exome sequencing to examine one of the largest international cohorts of VEO-IBD, with the objective of identifying previously unexplored genetic markers. This genetical screen revealed compound heterozygous missense mutations (c.[952A>G];[965A>C]) and splice region mutation (c.1298-4C>T) in *IL1RL2* (Interleukin 1 receptor-like 2) as a novel risk factor for VEO-IBD.

This assessment purposed to enlighten the molecular mechanisms of *IL1RL2* deficiency in macrophages and epithelial cells. The study utilized various advanced techniques, including CRISPR/Cas9-mediated genetic engineering, induced pluripotent stem cell (iPSC) differentiation towards macrophages and colonic organoids, and various immunological assays to investigate the impact of *IL1RL2* mutations. Western blot analysis demonstrated reduced activation of the NFκB and MAPK signaling pathways in patient-derived macrophages. Functional assays showed that the c.[952A>G];[965A>C] deficiency in *IL1RL2* results in decreased expression of CD14, CD163, and CD273, indicating impaired macrophage polarization. Additionally, HCT116 cells expressing the c.952A>G or c.965A>C variants exhibited reduced NFκB and MAPK activation, impaired wound healing, altered *CCL20* expression, and increased cell death. iPSC-derived colonic organoids expressing c.[952A>G];[965A>C] or c.1298-4C>T exhibited impaired wound healing, altered *IL1RL2* and *CCL20* expression. This comprehensive study provides new insights into the molecular mechanisms underlying VEO-IBD and underscores the critical role of *IL1RL2* in gut immunity. The findings suggest potential therapeutic targets for treating IBD through modulation of IL1RL2 signaling.

LIST OF TABLES

LIST OF FIGURES

LIST OF ABBREVIATIONS

AMP	Antimicrobial protein
ATG16L1	Autophagy Related 16 Like 1
bFGF	Basic fibroblast growth factor
BMDCs	Bone marrow-derived dendritic cells
BMP	Bone morphogenetic protein
BSA	Bovine serum albumin
Cas9	CRISPR-associated 9
CASP8	Caspase 8
CCL	Chemokine (C-C motif) ligand
CD	Crohn's disease
CO	Colonic organoid
CRISPR	Clustered Regularly Interspaced Short Palindromic Repeats
CXCL	Chemokine (C-X-C motif) ligand
CXCR	Chemokine (C-X-C motif) receptor
DAPI	4′,6-diamidino-2-phenylindole
DCs	Dendritic cells
DE	Definitive endoderm
dH$_2$O	Deionized water
DMEM	Dulbecco's Modified Eagle's Medium
DNA	Deoxyribonucleic Acid
DSS	Dextran sodium sulfate
EDTA	Ethylenediamine tetraacetic acid
EGF	Epidermal growth factor
ERK	Extracellular signal-regulated kinase
FACS	Fluorescence-Activated Cell Sorting
FGF	Fibroblast growth factor
FLT3L	Fms like tyrosine kinase 3 ligand
FoxP3	Forkhead box P3
GFP	Green fluorescent protein
GI	Gastrointestinal tract
GM-CSF	Granulocyte–macrophage-stimulating factor
GWAS	Genome-Wide Association Study
gRNA	Guide RNA
HCl	Hydrochloric acid
HDR	Homologous-directed repair
HE	Hindgut endoderm
HGF	Hepatocyte growth factor
HSPC	Hematopoietic stem and progenitor cell
IBD	Inflammatory bowel diseases
IBD-U	IBD-undifferentiated
IEC	Intestinal epithelial cells
IESCs	Intestinal epithelial stem cells
IFN	Interferon
Ig	Immunoglobulin
IGF	Insulin-like growth factor

IKK	IκB kinase
IL-10	Interleukin-10
IL-12	Interleukin-12
IL-12B	Interleukin-12 B
IL-1R	Interleukin-1 receptor
IL-1RAcP	IL-1-related accessory protein
IL-1Rrp2	IL-1R–related protein 2
IL1RL2	Interleukin 1 receptor like 2
IL-23	Interleukin-23
IL-23R	Interleukin-23 receptor
IL1RL2	Interleukin-36 receptor
ILCs	Innate lymphoid cells
IMDM	Iscove's Modified Dulbecco Medium
IRAK	IL-1 receptor-associated kinase
IRGM	Immunity related GTPase M
IκB	Inhibitor of NFκB
iPSC	Induced pluripotent stem cells
JAK2	Janus kinase 2
JNK	C-Jun-N-terminale Kinase
KCl	Potassium chloride
KGF	Keratinocyte growth factor
KI	Knock-in
KO	Knock-out
LAP	Latency Associated Peptide complex
LB	Lysogeny broth, Luria broth, or Luria-Bertani medium
LPS	Lipopolysaccharide
MAPK	Mitogen-activated protein kinases
M-CSF	Macrophage colony-stimulating factor
MDCs	Monocyte-derived dendritic cells
MDP	Muramyl dipeptide
min	Minute
MMPs	Matrix metalloproteinases
MRI	Magnetic Resonance Imaging
MUC	Mucin
NaCl	Sodium chloride
NFκB	Nuclear Factor-kappa B
NO_2	Nitrogen dioxide
NOD2	Nucleotide-binding oligomerization domain containing 2
PBMC	Peripheral Blood Mononuclear Cell
PBS	Phosphate-buffered saline
PBS-T	PBS containing 0.1% Tween
PCR	Polymerase Chain Reaction
PEI	Polyethylenimine
PGs	Prostaglandins
PI3K	Phosphatidyl inositol 3-kinase
PIC	Protease inhibitor cocktail
PMSF	Phenylmethylsulfonyl fluoride
PVDF	Polyvinylidene fluoride
REGIIIγ	C-type lectin regenerating islet-derived protein IIIγ

RELMβ	Resistin-like molecule-β
RFP	Red fluorescent protein
RNA	Ribonucleic Acid
RT	RT
SCF	Stem cell factor
SDM	Site-directed mutagenesis
SDS	Sodium dodecyl sulfate
SDS-PAGE	Sodium dodecyl sulfate-polyacrylamide gel
sec	Seconds
SNP	Single-nucleotide polymorphism
SO_2	Sulfur dioxide
STAT3	Signal transducer and activator of transcription 3
TAE	TRIS-Acetate-EDTA
TBE	Tris-boric acid-EDTA
TE	Tris-EDTA
TFF3	Trefoil factor 3
TGFβ1	Transforming growth factor beta 1
Th	T helper
TIR	Toll/IL-1 receptor
TLR	Toll-like Receptor
TNF	Tumor Necrosis Factor
TPO	Thrombopoietin
Tregs	Regulatory T cells
UC	Ulcerative colitis
USA	United States of America
UV	Ultraviolet
VEGF	Vascular endothelial growth factor
VEO-IBD	Very early onset IBD

1.   INTRODUCTION

1.1.   Inflammatory Bowel Disease

Inflammatory bowel diseases (IBD) are complex immune disorders characterized by persistent or recurring inflammation of the gastrointestinal (GI) tract. Types of IBD include Crohn's disease (CD), ulcerative colitis (UC), and unclassified IBD (IBD-U) [1, 2]. IBD-U are terms used to categorize patients with apparent symptoms of IBD but for whom neither CD nor UC can be distinguished [3]. IBD-U is considerably more typical in children than adults, in whom 5-10% of patients of IBD are initially categorized as IBD-U [3, 4].

CD and UC exhibit significant differences in various aspects, including the site of the disease through the GI tract, characteristics of inflammatory responses, clinical symptoms, associated complications, and findings observed during endoscopic examination. Besides these differences, UC and CD share similar manifestations, such as diarrhea, hematochezia, and abdominal pain, but vary in inflammation location, depth, intricacies, and prevalence [5]. CD can influence any area of the GI tract [5, 6]. Nonetheless, CD most frequently impacts the terminal ileum and the proximal colon. The CD is characterized by a patchy distribution, with areas of normal tissue interspersed between inflamed regions. In contrast, UC is restricted to the colon as well as the rectum. Inflammation typically initiates in the rectum and extends varying degrees to the proximal colon [5, 6]. In CD, inflammation can infiltrate the transmural site of the bowel wall. This deep inflammation can result in the development of fistulas, strictures, and abscesses. Neutrophilic inflammation is the most common phenotype in UC [7]. In contrast, in UC, inflammation is generally limited to the submucosa and mucosa and does not typically affect the deeper layers of the bowel wall [5, 6]. Typical symptoms of CD subsume abdominal pain, diarrhea (sometimes with blood), weight loss, and fatigue. Other symptoms may include mouth sores, anal pain, or drainage due to fistulas and malnutrition. On the other hand, typical manifestation of UC includes abdominal pain, bloody diarrhea, and tenesmus. UC patients may also experience weight loss and fatigue, particularly during flare-ups [5, 6].

CD is more likely to cause other complications like arthritis, skin rashes, eye inflammation, and liver disorders [8, 9]. Due to the deeper inflammation, complications like strictures and fistulas are more frequent [8-11]. While extra-intestinal manifestations can occur in UC (such as joint pain and liver issues), they are less common compared to CD [8, 9]. The primary complications are related to the colon itself, including an increased risk of colon cancer and toxic megacolon [8, 9].

1.1.1. Incidence of IBD

IBD can manifest at any age, with an early peak of incidence between 15 and 29 years of age for both UC and CD [12]. There is evidence of a second smaller peak later in life, particularly for UC in older adults, although some studies show more of a plateau effect rather than a distinct second peak [13, 14]. Approximately 25% of individuals diagnosed with IBD experience onset during childhood, with the majority of pediatric-onset cases occurring during adolescence. Within this group, there exists a subset of patients who exhibit symptoms of IBD before the age of six, a condition defined as VEO-IBD [5, 15]. IBD is associated with significant morbidity and mortality, resulting in significant patient load and costs to healthcare strategies [16, 17]. IBD poses a substantial public health challenge due to the rising prevalence and mortality rates worldwide. In 2019, IBD had a notable impact globally, affecting an estimated 4.9 million individuals. China and the United States reported 911,405 and 762,890 cases, equating to incidence rates of 66.9 and 245.3 cases per 100,000 individuals, respectively [18, 19].

1.1.2. Pathomechanisms of IBD

The precise cause of IBD remains elusive; nonetheless, it has been widely acknowledged that IBD arises from a multifaceted interplay of genetic predisposition, environmental factors, microbial influences, and immune responses. Among these factors, genetic research on gut inflammation has shown notable progress within IBD pathogenesis. (Figure 1) [20-22].
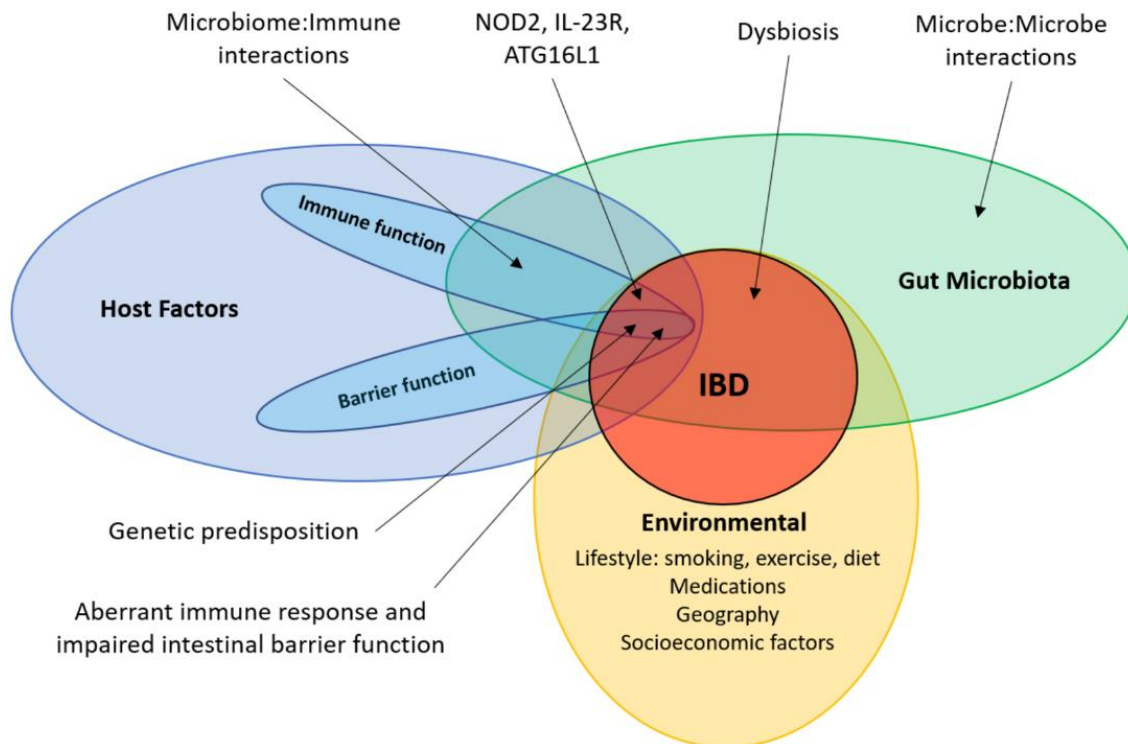
Figure 1: Diverse factors influence the pathomechanism of IBD.
The development of IBD is prompted through the convoluted interaction of the gut microbiota, host, and external factors. These interactions are mutual, constantly influencing and modulating one another to maintain a delicate physiological balance. [22].

1.1.3. Genetic Factors in IBD

The investigation of genetic susceptibility in IBD is predominantly centered on outlining the complicated landscape of monogenic, which adheres to Mendelian inheritance patterns and biallelic forms with complex inheritance patterns [23]. Monogenic IBDs originate from highly penetrant genetic variants within a single gene, differing from the predominantly polygenic nature of most IBD cases [23]. Roughly 50 genetic variants have thus far been linked to monogenic IBDs [24]. Monogenic IBDs typically manifest as VEO-IBD, onset <6 years, or in infantile/neonatal stages [23-25]. Genes associated with monogenic IBD include *IL10*, *IL10RA*, *IL10RB*, and others impacting immune regulation or epithelial barrier function [24, 25]. Biallelic (two mutated alleles) loss-of-function variants in genes like IL10, IL10RA, and IL10RB in the IL-10 signaling pathway are completely penetrant for VEO-IBD [25]. Some monogenic IBDs may exhibit incomplete penetrance, where additional genetic factors, such as the polygenic burden of IBD variants, might influence the phenotype [25]. Various approaches like whole exome sequencing (WES), and whole genome sequencing (WGS), are utilized to diagnose monogenic IBD [23, 24]. RNA sequencing can complement these techniques by identifying splice variants and evaluating cell-specific gene expression patterns [24]. Overall,

while the majority of IBD cases are polygenic, there exists an expanding spectrum of monogenic disorders, often featuring biallelic variants, which can manifest as early-onset or VEO-IBD [23, 24]. Several genes have been connected in IBD, and each has a distinct function in immune regulation, epithelial barrier function, or mucosal homeostasis [26]. Among the extensively researched genes linked to IBD is NOD2 (nucleotide-binding oligomerization domain-containing protein 2) which is involved in recognizing bacterial components and initiating innate immune responses [27, 28]. Mutations in NOD2 have been linked to impaired bacterial sensing, leading to dysregulated immune activation and increased susceptibility to CD [27, 28]. The mutations in X-linked inhibitors of apoptosis protein (XIAP) impair apoptotic signaling pathways, leading to aberrant immune cell activation and dysregulated inflammatory responses within the GI [29, 30].

Genome-Wide Association Study (GWAS) has significantly enhanced our comprehension of the genetic underpinnings of IBD [31]. These investigations, conducted with extensive cohorts comprising over 75,000 individuals affected by IBD and control subjects, have collectively unveiled more than 200 genetic susceptibility loci linked to IBD. Particularly noteworthy is the latest and most extensive GWAS, which identified 163 susceptibility loci, comprehensively portraying the genetic landscape associated with IBD susceptibility. Within this pool, 110 loci were observed to confer risk for both CD and UC, while 30 loci were specific to CD and 23 to UC. Furthermore, a subsequent multiple ethnic or racial groups study, encompassing more than 20,000 individuals, divulged an additional 38 new IBD loci, thus augmenting our understanding and elevating IBD risk loci to approximately 240 (Figure 2) [30-32].

The collective outcomes from these large-scale GWAS highlight the intricate polygenic nature of IBD, wherein an array of genetic variants distributed across numerous loci collectively contribute to disease susceptibility and pathogenesis. This substantial body of evidence, derived from a diverse array of investigations, substantially supports the contention concerning the complex genetic architecture of IBD, as elucidated through GWAS [30].
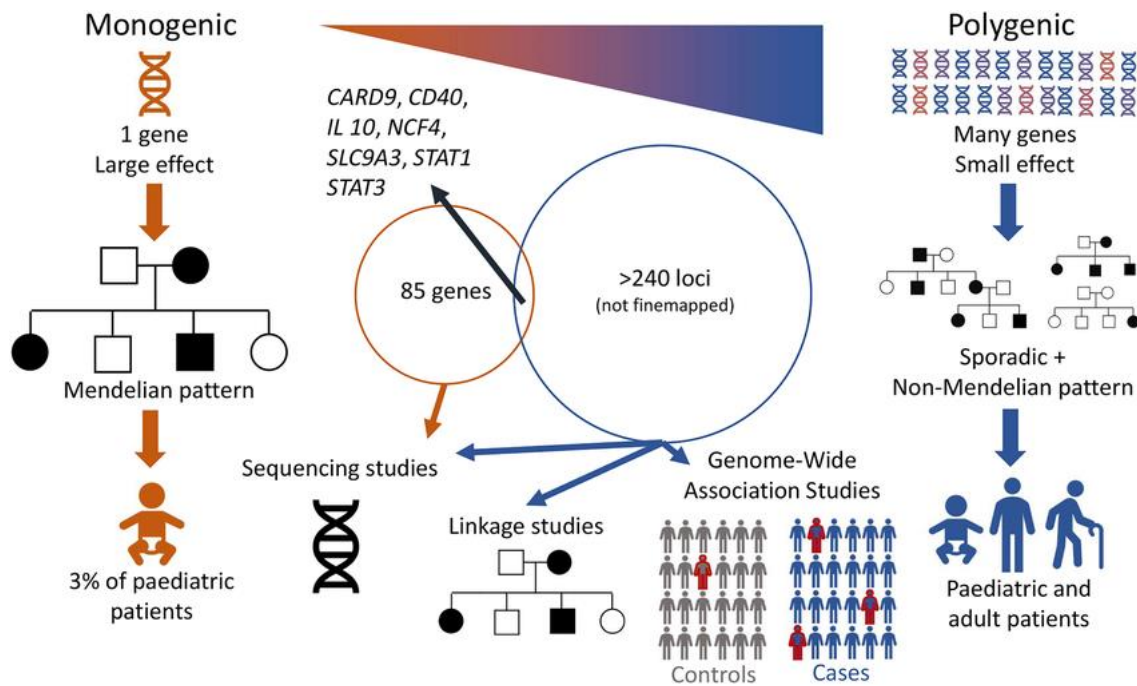
Figure 2: Genetic susceptibility in IBD.
The picture contrasts the genetic mechanisms of monogenic and polygenic IBD. Monogenic diseases arise from mutations in single genes, exerting significant effects and adhering to Mendelian inheritance patterns, primarily affecting pediatric patients. The research employs sequencing and linkage studies with implicated genes such as CARD9, CD40, IL10 and so on. In contrast, polygenic diseases involve mutations in multiple genes, each with modest effects, and exhibit complex, non-Mendelian inheritance patterns, affecting both pediatric and adult populations. GWAS are pivotal in identifying associated genetic variations. The diagram reveals 85 genes shared between monogenic and polygenic studies and over 240 loci requiring fine-mapping from GWAS data [32].

1.1.4. Environmental and Microbial Factors in IBD

Substantial geographical variations exist in the prevalence of IBD. The prevalence of IBD is most heightened in Western nations and industrialized regions such as North America, Europe, and Australia [33]. In contrast, prevalence rates are lower but increasing rapidly in newly industrialized countries in Asia, South America, and Africa. Notably, the highest prevalence rates are observed in Canada, the United Kingdom, and parts of Scandinavia [33, 34]. While IBD incidence rates stabilize in Western nations, they continue to rise in newly industrialized regions [34, 35]. There is no clear north-south gradient in IBD incidence among women in the United States [35]. However, some studies have identified a north-south gradient in Europe, with higher incidence rates in northern latitudes for both CD and UC [35, 36]. The rising incidence of IBD in developing nations is attributed to factors such as industrialization, urbanization, and the adoption of a more "Westernized" diet and lifestyle. Improved sanitation and hygiene may also play a role by altering the gut microbiome and immune development,

thereby increasing the risk of IBD [34]. Genetic susceptibility alone does not account for the geographical differences, suggesting that environmental factors are significant [34, 36]. Additionally, better access to healthcare and diagnostic tools in high-income regions may contribute to the higher reported prevalence [34]. Overall, there are distinct geographical differences in IBD epidemiology. Western nations bear the highest burden, while newly industrialized regions in Asia and Africa are experiencing a rapidly rising incidence, likely driven by environmental and lifestyle factors associated with economic development [33-35, 37].

The factual reason for IBD is not thoroughly comprehended, and several environmental elements have been involved in its pathomechanism [38]. The factors compromise diet, smoking, antibiotics, stress, and geography (Figure 1).

Studies point out that diet may recreate a function in the progression of IBD. For example, certain dietary components, like sugar, unhealthy fats, and processed foods, can indeed exacerbate symptoms or increase the risk of developing IBD. These types of foods may trigger inflammation in the gut and worsen symptoms such as abdominal pain, diarrhea, and fatigue [39].

Smoking has been linked to an elevated risk of CD, while it might protect people against UC [40]. Antibiotics can change the gut microbiome, which might influence the development and advancement of IBD [41, 42]. Although stress does not cause IBD, it can worsen the symptoms of IBD [43].

High air pollution may contribute to the incidence of UC and CD development. It has been studied that the levels of NO_2 and SO_2 are linked to the risk of IBD [44]. Current studies suggest that while environmental factors may contribute to the likelihood of developing IBD, they are not the only determinants of the condition.

The microbiome has a paramount function in the pathomechanism and progression of IBD, with dysbiosis, contributing to intestinal inflammation and immune dysregulation seen in IBD [42]. The enteric microbiome contains the four phyla Firmicutes, Bacteroidetes, Proteobacteria, and Actinobacteria [45]. At the same time, Bacteroides and Firmicutes generally predominate in the healthy gut microbiota and provide energy and nutrients to the host [45]. A robust enteric microbiota promotes resilience against pathogens while also offering essential nutritional, metabolic, and immunological support in humans [45]. A disruption in the balance and role of the microbiota leads to dysbiosis, which changes how the host's immune system interacts with the microbiota. Several studies have demonstrated marked differences in the microbiota of individuals with IBD compared to those without the condition, and an abnormal immune

reaction to the microbiome triggers inflammation in the intestines in IBD [46-49]. Many researchers contend that a combination of environmental, microbial, and immune-related factors influences the development of IBD in individuals with a genetic predisposition [1, 50]. Similarly, the transplantation of bacteria or microbiota from afflicted mice to healthy counterparts has been observed to impact inflammation, while the inoculation of mice with gut microbiota derived from individuals with IBD exacerbates colitis by modulating immune reactions [49]. The gut microbiota has essential functions in shaping the progression of the host's immune mechanism, which is reciprocally influenced by the host's immune response. Investigations conducted on mice devoid of gut microbiota reveal compromised immune maturation, evidenced by underdeveloped lymphoid tissues, diminished intestinal lymphocyte populations, and decreased levels of antimicrobial peptides and immunoglobulin (Ig) A [51, 52].

Genetic mutations associated with IBD have impacts on the microbiome and immune system. For instance, NOD2 binds with peptidoglycan in gram-positive and -negative bacteria. NOD2 has a defensive role against intracellular bacteria in epithelial cells. Based on this, it has been studied that NOD2-deficient mice had an imbalanced microbiome, which induced colitis [53, 54]. *NOD2* mutations in patients associated with imbalanced microbiota are distinguished by lowered *Faecalibacterium* species and many *Escherichia* species [55, 56].

1.1.5. Immunological factors in IBD

IBD manifests as epithelial injury, amplifying inflammation induced by intestinal flora and infiltrating numerous cell types into the lamina propria, such as T cells, B cells, macrophages, dendritic cells (DCs), and neutrophils [2, 57]. Innate and adaptive immunity compromise the intestinal immune system [58]. The intestinal mucosa, antibacterial proteins, innate immune cells, as well as cytokines and molecules, and defensins constitute intestinal innate immunity [2, 57-60]. Specific to particular pathogens, adaptive immunity is initiated when innate immune responses are unable to prevent the invasion of pathogens. Upon encountering a pathogen, activating adaptive immune responses involving T and B cells typically requires several days. [57]. The innate immune system acts as the first line of defense against infections, initiating rapid responses and inflammation through the secretion of various molecules, ultimately facilitating the activation of the adaptive immune system [61]. The adaptive immune response has a major role in IBD pathogenesis. CD4$^+$ T helper (Th) cells, especially the Th17 subset, are key drivers of inflammation. Th17 cells produce copious amounts of IL-17, which recruits and

activates neutrophils, leading to tissue injury [62, 63]. The ratio between Th17 and regulatory T cells (Tregs) is critical, as Tregs normally suppress excessive Th17 responses [62, 63]. Innate lymphoid cells (ILCs) have also arisen as novel pathogenic cells that contribute to gut inflammation in IBD [62, 63]. ILCs produce elevated concentrations of IL-17 and Interferon (IFN)-γ), driving tissue damage [64].

Cytokines and chemokines secreted by immune cells (e.g., TNF-α, IL-6, IL-1β, and IL-8) are also vital in sustaining the inflammatory condition in the gut [65]. Anti-TNF therapies have been shown to modulate the peripheral immune system in IBD, declining neutrophil frequencies and increasing lymphocyte populations [62]. In addition to the well-characterized roles of T cells and cytokines, other immune components are also involved in IBD pathogenesis. B cells exhibit a dual role in IBD, having both pro-inflammatory and anti-inflammatory functions [66, 67]. Elevated B cell counts and the generation of pro-inflammatory antibodies exacerbate inflammation in IBD patients, notably in UC, while dysregulated B cells hinder regulatory T cell function, further exacerbating inflammation [66, 67]. Additionally, the development of tertiary lymphoid structures rich in B cells heightens chronic inflammation, particularly in CD. Conversely, B cells aid in maintaining gut balance by producing IgA antibodies against beneficial bacteria, and regulatory B cells producing IL-10 help suppress inflammation [63, 66]. However, therapy involving B cell depletion with anti-CD20 antibodies might worsen UC by reducing regulatory B cell numbers and IL-10 production, resulting in increased T cell activity and release of pro-inflammatory cytokines [66, 67]. The delicate equilibrium among pro-inflammatory and anti-inflammatory B cell responses is pivotal in shaping IBD's development and clinical outcomes [66, 67]. Macrophages are immune cells that can produce inflammatory cytokines and contribute to tissue injury in the intestines of individuals with IBD [68]. An increased number of CD14^{+} macrophages accumulate in the inflamed intestinal mucosa of IBD patients [69, 70]. Macrophages, notably in CD patients, demonstrate heightened inflammation, displaying an elevated M1 phenotype distinguished by the upregulation of markers such as CD40, CXCL9, and MMP12 [71]. Macrophages also show heightened expression of markers associated with the anti-inflammatory M2 phenotype, along with pathways linked to fibrosis and the formation of granulomas, particularly evident in CD [71]. In IBD patients, DCs within inflamed intestines adopt a pro-inflammatory phenotype, generating inflammatory cytokines and fostering Th1/Th17 responses [72, 73]. Conversely, DCs in healthy intestines exhibit reduced responsiveness to inflammation, facilitating regulatory T-cell development and preserving intestinal equilibrium [72]. In UC, DCs demonstrate an impaired ability to produce retinoic acid, crucial for regulatory T cell induction,

even during remission, indicating compromised tolerogenic function [68, 72]. DCs facilitate antigen presentation and T cell activation, a process spurred through an increased expression of chemokines and addressins, which attract DCs to the inflamed gut [72].

1.1.6. Intestinal Epithelial Barrier Dysfunction in IBD

The largest mucosal surface in the body is found in the intestinal epithelium, where intestinal epithelial stem cells (IESCs) in the crypts drive a continual renewal process, initiating proliferation and differentiation [74]. Specialized epithelial cells shape the intestinal barrier, providing a dual defense against commensal and pathogenic microorganisms through physical and biochemical means. Within the gut, the epithelial barrier comprises distinct cell types. Intestinal epithelial cells (IECs) primarily employ secretory defenses, notably through goblet cells' production of highly glycosylated mucins, particularly Mucin 2 (MUC2), essential for structuring the mucous layers on the colon's epithelial surface, serving as the initial barrier against microbial invasion [75]. Goblet cell-produced molecules, including Trefoil factor 3 (TFF3) and resistin-like molecule-β (RELMβ), play a pivotal role in microbial defense by enhancing mucus structure through crosslinking with mucin, thus assisting in epithelial homeostasis, IECs migration, and resilience to cell death [76, 77]. RELMβ controls adaptive T-cell responses and macrophage activation during inflammation and directly inhibits parasite chemotaxis in case of nematode infection concurrently with MUC2 [78, 79].

Antimicrobial protein (AMP) secretion by IECs sustains intestinal barrier functions. For instance, C-type lectin regenerating islet-derived protein IIIγ (REGIIIγ) is produced from enterocytes to the small intestine and colon, protecting the epithelial surface from bacterial invasion [80]. In the small intestine, the main productions of Paneth cells are defensins, including pore-forming cathelicidins and lysozyme. These pore-forming defensins support the epithelial barrier from bacterial invasion by disrupting bacterial membranes and peptidoglycans of the bacterial walls [81]. Interaction of AMPs, such as REGIIIγ and mucins, provides a physical and antibacterial barrier to control bacterial attachment and invasion and restrict the diversity of the bacteria that can transit the epithelial barrier [82].

1.2. IL1RL2-mediated Signaling

1.2.1. IL36 receptor complex

The interleukin-36 receptor (also named as interleukin 1 receptor-like 2, IL1RL2) is a member of the IL-1 receptor (IL-1R) superfamily. IL1RL2 shares a sequence homology with IL-1R [83, 84]. The IL1RL2 forms a heterodimeric assembly by associating the subunit IL-1R–related protein 2 (IL-1Rrp2) with the co-receptor subunit IL-1 related accessory protein (IL-1RAcP). [85]. The IL1RL2 has proinflammatory agonists named as IL-36α, IL-36β, and IL-36γ. IL1RL2 signaling is inhibited by the binding of IL-36Ra (also called IL-1F5) [71-73]. The intracellular domain of IL1RL2 includes a Toll/IL-1 receptor (TIR) responsible for maintaining signal transduction to downstream pathways [86, 87]. The TIR domains located on every subunit of IL1RL2 trigger the initiation of intracellular signaling pathways through phosphorylation and the dimerization of both IL1RL2 subunits [88]. The IL-1Rrp2 and IL-1RAcP initiate downstream signaling through an interaction between TIR domains and MyD88/IL-1 receptor-associated kinase 1 (IRAK/IRAK2). Once the IL1RL2 receptor complex is dimerized, the signal transduction is triggered, and NFκB and MAPK pathways are activated (Figure 3) [85, 89]. The dimerization of IL-1Rrp2 and IL-1RAcP is sustained by the hydrogen bond formation between the IL1RL2 and IL-36 cytokines. The amino acid residues on the IL1RL2 engaged in hydrogen bond formation are Asp150 for IL-36α, Asn148 for IL-36β, Ala162 for IL-36γ, and Ser185 for IL-1RAcP [90]. Disulfide bonds and N-linked glycosylation in the ectodomain of IL1RL2 regulate protein accumulation and the trafficking of IL1RL2 to the membrane. Studies have shown that A471T, a single nucleotide polymorphism (SNP) within the TIR domain of IL1RL2, reduces signal transduction by dampening its interaction with IL-1RAcP [87].

Numerous studies revealed the essential involvement of IL1RL2 in intestinal inflammation. For instance, the knockout of *IL1RL2* in mice showed increased disease activity and decreased survival, pointing to the protective role of IL1RL2 [91]. Moreover, *Il1rl2*$^{-/-}$ deficiency showed impaired recovery and decreased IL-22 production, mediating epithelial proliferation, restitution, and mucosal protection in mice colitis models induced with dextran sodium sulfate (DSS). This is corroborated by the enhanced expression of IL-22 and IL-23 observed in IL-36γ-treated colonic explants [92].
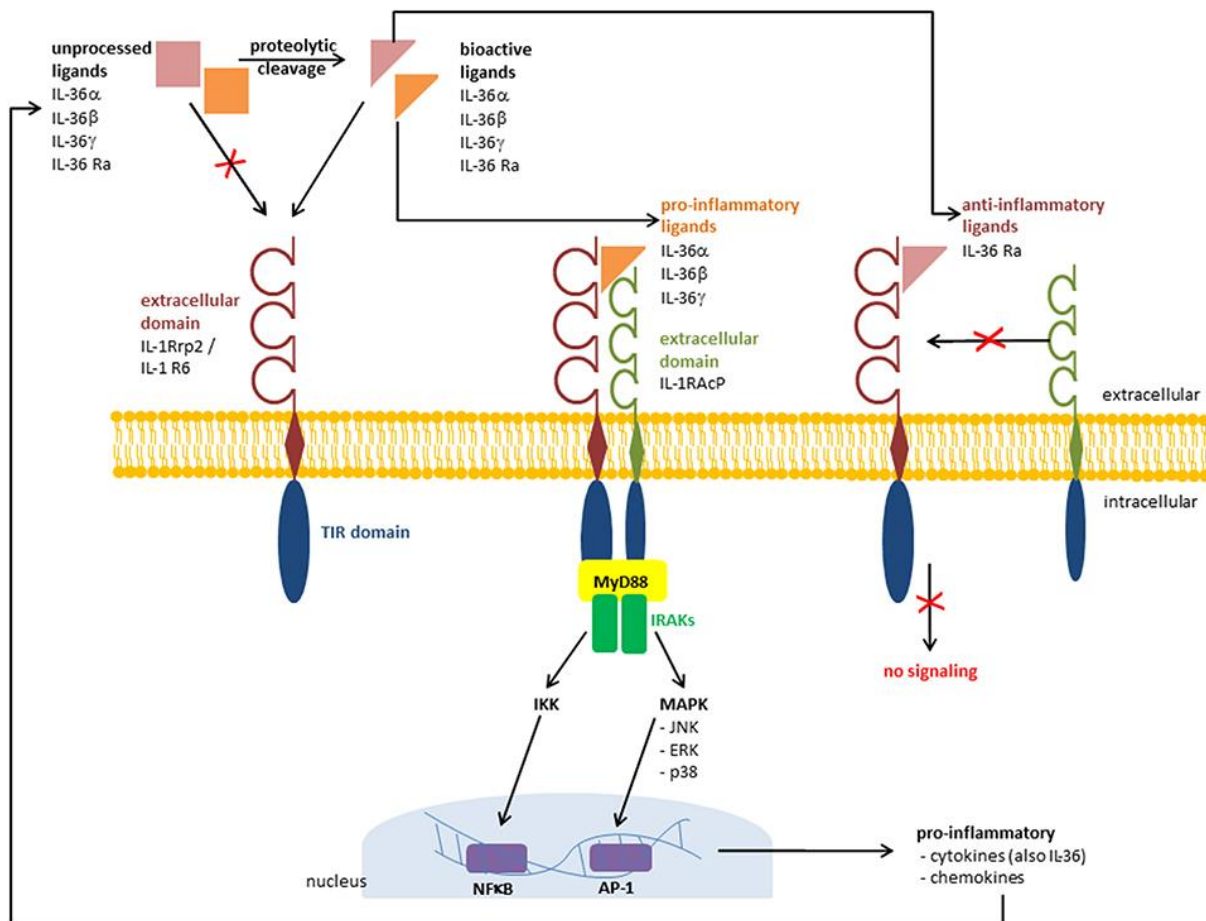
Figure 3: IL-36 receptor signaling.
The illustration depicts the IL-36 receptor-mediated signaling cascade, wherein unprocessed ligands (IL-36α, IL-36β, IL-36γ, IL-36Ra) undergo cleavage to produce bioactive forms. Proinflammatory ligands engage with the receptor complex (IL-1Rrp2/IL-1RAcP), initiating the MyD88 pathway and activating NFκB and AP-1. These transcription factors lead to the production of proinflammatory cytokines and chemokines. Contrarily, the anti-inflammatory ligand IL-36Ra binds to the receptor but inhibits signaling, thereby preventing an inflammatory response. This delicate equilibrium between pro-inflammatory and anti-inflammatory signals governs the inflammatory response [85, 89].

1.2.2. IL-36 Cytokines

IL-36 cytokines coding genes are located in interleukin genes on human chromosome 2q13 [93]. The IL-36 cytokines exhibit sequence similarity, share similar gene positioning, and possess a widely distributed organization within the IL-1 and IL-36 loci across both human as well as murine genomes [94]. IL-36 cytokines are synthesized as precursor forms and undergo complete activation through proteolytic post-translational alterations [95]. Precursor forms of IL-36 cytokines are truncated by cathepsin G, elastase, and proteinase from the N-terminal [96]. This N-terminal truncation removes a few amino acids from the precursor forms, dramatically increasing their binding affinity for the IL1RL2 and potentiating their pro-inflammatory activity

by 1,000 to 36,000-fold [97]. Specifically, IL-36α requires the removal of 9 N-terminal amino acids after the A-X-Asp motif at position K6 for full activation. IL-36β is activated by cleavage after R5. IL-36γ is activated by removing 18 N-terminal residues after S18 [97]. Truncation of precursor forms of IL-36 increases the biological activity of cytokines by intensifying binding affinity for IL1RL2 [88, 98]. Different proteases facilitate the cleavage of IL-36 cytokines in various tissue contexts. For instance, within the skin, cathepsin G and elastase mediate the cleavage of IL-36α, cathepsin G is involved in the cleavage of IL-36β, and elastase facilitates the cleavage of IL-36γ [97, 99]. In the antigen-presenting cells, the IL-36γ is trimmed and activated by Cathepsin S, which is expressed in those cells [100]. IL-36 cytokines and IL1RL2 have ubiquitous expression and mediate various clinical conditions, including psoriasis, arthritis, IBD, allergic rhinitis, and fibrotic disorders (Figure 4) [101-103].

Various cell types, including keratinocytes, monocytes, DCs, epithelial cells, B cells, T cells, and neutrophils, express IL-36 cytokines [104, 105]. Immune cells like monocytes, B cells, T cells, and epithelial cells mainly express IL-36α during embryonic development [85]. IL-36α is proinflammatory and regulates skin barrier function and homeostasis [85, 106]. Human epithelial cells, myelomonocytic cells, DCs, macrophages, and T cells express IL-36β [85]. In epithelial cells, epidermal growth factor (EGF) regulates IL-36β expression [107]. Murine neurons and glial cells express IL-36β, but its expression is not affected by lipopolysaccharide (LPS) or IL-1β treatment [108]. It has been demonstrated that IL-36β promotes Th2 responses in DSS-induced colitis in mice [109]. Keratinocytes, epithelial cells, human monocytic THP1 cells, and peripheral blood lymphocytes express IL-36γ [110-112]. The expression of IL-36 cytokines can be stimulated autonomously, through interactions with bacterial components, or via other molecules such as IL-1β and TNF-α [113]. The regulation of IL-36 cytokine expression within a particular tissue varies. Studies have demonstrated decreased levels of IL-36α and IL-36β but increased levels of IL-36γ in the luminal and glandular epithelia during early pregnancy, suggesting diverse functional roles for IL-36 cytokines [97, 101].
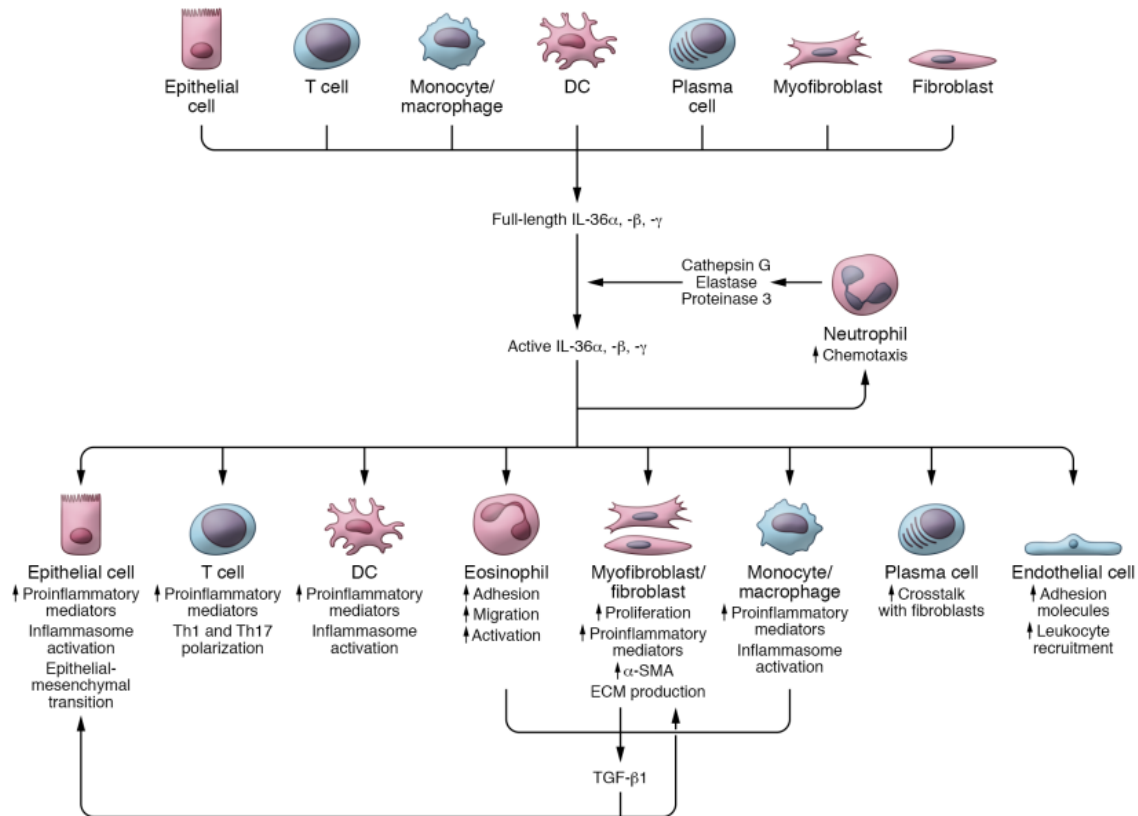
Figure 4: Pleiotropic functions of IL-36 cytokines across various cell types
The image illustrates the activation and impacts of IL-36 cytokines on various cells. Neutrophils convert full-length IL-36 cytokines into active forms using enzymes like Cathepsin G, Elastase, and Proteinase 3. Active IL-36 cytokines then act on different cells, including epithelial cells, T cells, DCs, eosinophils, myofibroblasts, fibroblasts, monocytes/macrophages, plasma cells, and endothelial cells, promoting proinflammatory responses. These responses include increased production of proinflammatory mediators, cell migration, adhesion, activation, and inflammasome activation. The image also shows feedback mechanisms, such as TGF-β1 promoting extracellular matrix production by myofibroblasts and fibroblasts [101].

1.2.3. Function of the IL1RL2

The IL1RL2 pathway is a crucial mediator of inflammatory responses, and dysregulation is linked to diverse inflammatory diseases. Targeting this pathway via receptor blockade or balancing agonists and antagonists holds promise as a therapeutic strategy. The IL-36 functions at barrier locations (e.g., skin, lung, and intestine) to protect the body from environmental interferences like bacterial, viral, and fungal infections [114-116].

The binding of IL-36 cytokines to IL1RL2 initiates pro-inflammatory pathways, augmenting the antimicrobial functions of associated cells [96, 117-122]. This encompasses the differentiation of myeloid cells, elevated cytokines such as TNF, IL-6, and IL-8, enhanced bacterial clearance by macrophages, and elevated production of antimicrobial peptides by keratinocytes [96, 117-122]. The expression of *CXCL1*, *CXCL2*, *CXCL8*, *CCL3*, and *CCL20*

are induced by IL1RL2 mediated signalling. [96, 117-122]. Additionally, IL-36γ inhibits the Tregs differentiation and polarization of T cells towards Th9 cells [123]. It has been studied that *IL1RL2* deficiency in mice results in diminished resolution of intestinal injury in DSS-induced mouse models [124]. *IL1RL2* expression is observed in human monocyte-derived dendritic cells (MDCs). Following exposure to IL-36 cytokines, production of pro-inflammatory cytokines such as IL-2, IL-23, IL-6, IL-12, granulocyte–macrophage-stimulating factor (GM-CSF), and TNF-α are triggered. Therefore, the differentiation of naive CD4^{+} T cells towards Th1, Th17, and Th9 effector cells is mediated, while the progression of FoxP3 Treg is simultaneously repressed [117, 123, 125]. Furthermore, IL1RL2 signaling controls the movement of innate immune cells by promoting the generation of chemoattractants. [91, 92, 117, 123, 125].

1.2.4. IL1RL2 signaling in gut immunity

IL1RL2 signaling can be pathogenic or protective in the intestine, contingent upon the timing of its expression and the disease stage in murine models. In murine models of intestinal inflammation, heightened expression of IL-36α and IL-36γ was reported, and clinical research has confirmed elevated levels of colonic IL-36α in patients with active disease [92, 124, 126-128]. DSS exerts toxicity on the colonic epithelium, disrupting the integrity of the intestinal epithelial barrier and leading to the infiltration of luminal bacteria and their antigens into the mucosa, thereby facilitating the dissemination of proinflammatory contents into the underlying tissue [129, 130]. Studies have shown that during the pathological stage of the disease in *Il1rl2^{-/-}* mice, there is a decrease in disease activity attributed to diminished infiltration of innate inflammatory cells following DSS treatment [124, 127]. Nevertheless, *Il1rl2^{-/-}* mice exhibited compromised wound healing and could not recuperate from DSS-induced injury in the healing phase, as indicated by several studies. These results imply the crucial role of IL1RL2-mediated signaling in resolving acute intestinal injury [92, 124, 128].

Promoting mucosal healing in the gut via IL1RL2 involves two mechanisms: stimulating IL-22 and antimicrobial peptides (AMPs) and boosting the expansion of intestinal epithelial cells and fibroblasts. Inflammatory macrophages and epithelial cells trigger the production of IL-36α and IL-36γ upon gut tissue injury. Subsequently, these cytokines bind to the IL1RL2 complex on DCs, colonic myofibroblasts, and intestinal epithelial cells, resolving intestinal damage. Upon ligand binding, MyD88-mediated signaling activates NFκB, c-rel, and p50, upregulating IL-23 and promoting IL-22 production in the colon, facilitating wound healing and AMP production

in the gut [92, 124]. IL-36 cytokines trigger the activation of colonic fibroblasts expressing IL1RL2 via MyD88, prompting the function of GM-CSF and IL-6 in wound healing following mucosal damage in the intestine [128]. Studies in mouse models have shown that administering IL-36 cytokines enhances mucosal recuperation by stimulating intestinal epithelial cell proliferation and boosting AMP production [128]. The findings indicate that IL-36 assumes a pathogenicity role during the acute phase of intestinal damage, exacerbating the inflammatory response. Nevertheless, in the subsequent recovery phase, IL1RL2-mediated signaling has an indispensable function in coordinating immune and non-immune cellular activities, thereby promoting healing and augmenting the synthesis of antimicrobial factors to facilitate the restoration of the intestinal barrier (Figure 5) [91, 92, 124, 126, 128].
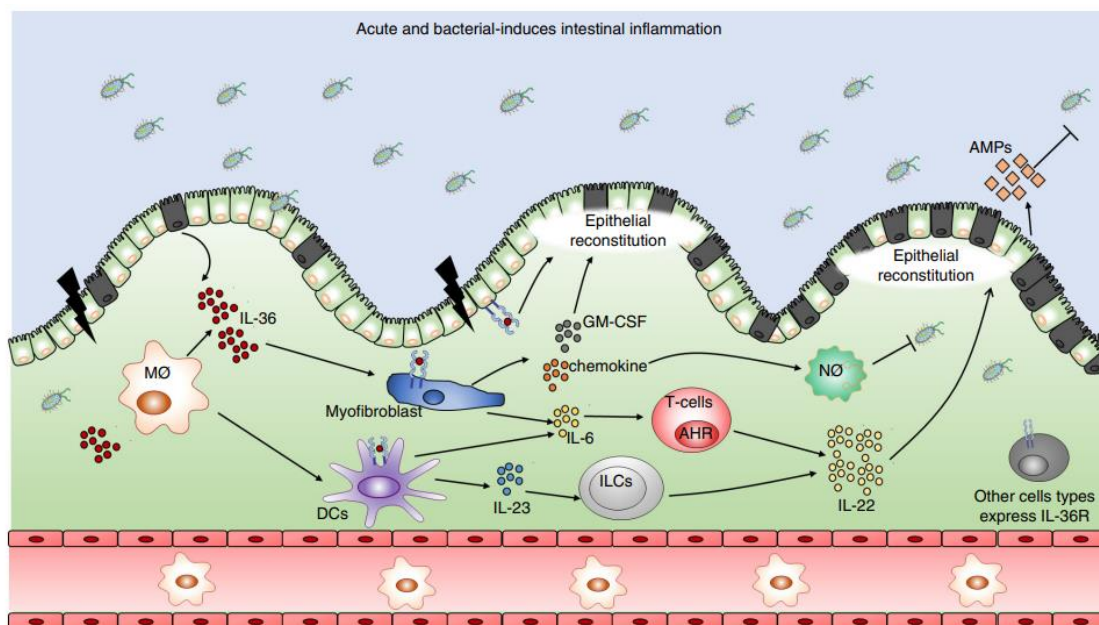
Figure 5: IL1RL2 signaling facilitates host defense mechanisms in intestinal inflammation induced by bacteria.
Damaged epithelial cells trigger the release of various immune signals, such as IL-36, which activate macrophages (MΦ) and dendritic cells (DCs). These cells produce IL-23 and GM-CSF, promoting the activation of T-cells and innate lymphoid cells (ILCs), which in turn release IL-22 and IL-6 to stimulate epithelial reconstitution. Chemokines and nitric oxide (NO) further support this regenerative process, while antimicrobial peptides (AMPs) help control bacterial populations. The cycle aims to restore the integrity of the intestinal barrier and manage inflammation [131].

It has been studied that IL1RL2 signaling has a pathogenic role in chronic intestinal inflammation [127, 132]. The IL-36γ triggers inhibition of FoxP3^{+} Treg expansion in the mice model of colitis [127, 132]. Activation of IL1RL2 signaling triggers the conversion of naive CD4^{+} T cells into IL-9-producing pathogenic CD4^{+} T cells (Th9) through an IL-2-STAT5 and

IL-2-STAT6-dependent pathway. IL1RL2-deficient mice are protected from effector T cell-induced intestinal inflammation, showing elevated colonic Th9 cell counts and reduced Treg cell populations [123]. In experimental models of intestinal inflammation, namely DSS and TNBS, the release of IL-36α from CD64^{+} macrophages initiates inflammatory cytokines and collagen type VI production, resulting in fibrosis [91, 128, 131, 133] (Figure 6).
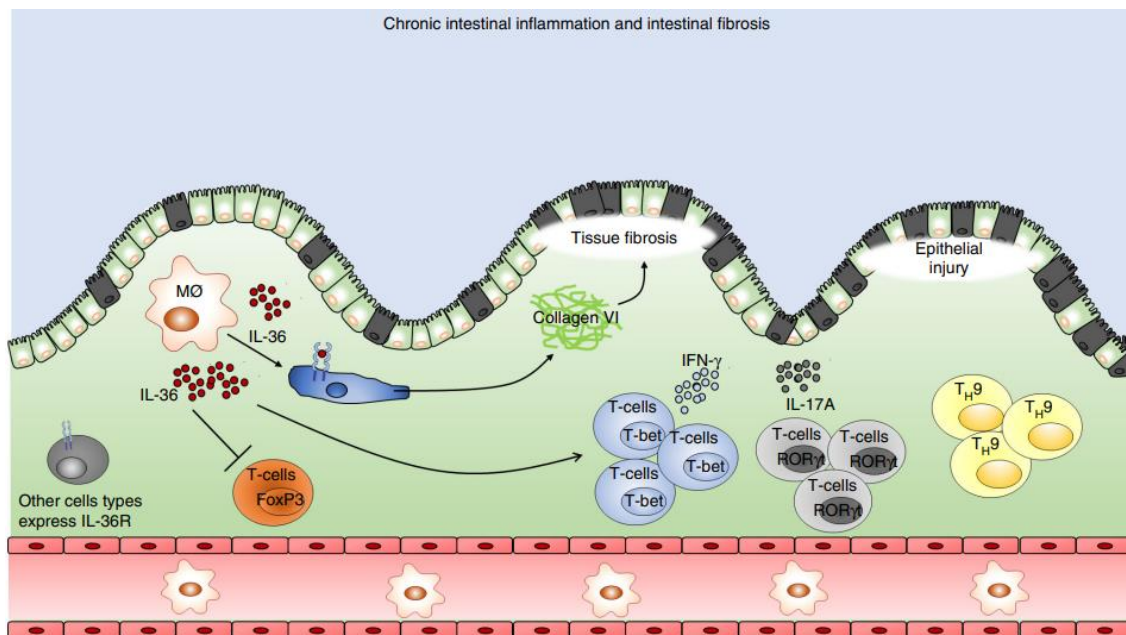
Figure 6: The pathogenic role of IL1RL2-mediated signaling in intestinal inflammation. IL-36 produced by macrophages (MΦ) and other cell types expressing IL1RL2 activates FoxP3^{+} T-cells. These activated T-cells release cytokines that contribute to tissue fibrosis, with an accumulation of Collagen VI. T-bet[+] T-cells secrete IFN-γ, promoting further inflammatory responses. RORγ[+] T-cells produce IL-17A, exacerbating the inflammatory process. Additionally, Th9 cells are involved in epithelial injury, further contributing to the pathology of chronic intestinal inflammation [131].

It has been shown that *Il1rl2* deficiency causes failure to control infection with the enteropathogenic bacterium *Citrobacter rodentium* [126]. *Il1rl2*^{-/-} mice exhibited diminished Th1 but enhanced Th17 responses upon infection with *Citrobacter rodentium* [126, 127]. IL1RL2-mediated signaling regulates IL-22 production, which manages enteropathogenic bacterial infections in the intestine. Upon *Citrobacter rodentium* infection, inflammatory monocytes produce IL36 cytokines that bind to receptor complexes on DCs, initiating a signaling cascade that modulates IL-23 and IL-6 secretion, acting on intestinal epithelial cells to promote IL-22 and antimicrobial peptide production, thereby enhancing early infection protection [126, 127].

1.2.5. Prospects for IBD treatment through IL1RL2 inhibition

Inhibiting the IL1RL2 emerges as a promising therapeutic strategy for managing IBD. Research indicates enhanced levels of IL-36α in the serum of newly diagnosed, treatment-naive pediatric IBD patients, highlighting its significance in disease onset and progression [134]. IL1RL2 expression on CD4$^+$ T cells exacerbates intestinal pathology in murine models of colitis by enhancing Th1 responses, inhibiting regulatory T cell generation, and inducing gut-homing receptors on pro-inflammatory T cells [134].

Experimental findings demonstrate that disrupting or inhibiting IL1RL2 signaling in mice alleviates DSS-induced chronic colitis and intestinal fibrosis. Notably, neutralizing antibodies against IL1RL2 have proven effective in reducing fibrosis in mice with chronic inflammation in the intestine, suggesting the therapeutic potential of IL1RL2 blockade, while also triggering the expression of genes regulating fibrosis, tissue remodeling, and collagen type VI production in both human and murine fibroblasts, thus further emphasizing its role in intestinal fibrogenesis [133].

Phase 2 trials, such as TUSCANY and ARTEMIS-UC, evaluating an anti-IL1RL2 antibody (TEV-48574), have shown promising results, expanding therapeutic options for IBD. Inhibiting IL1RL2 signaling holds promise for demonstrating both antifibrotic and anti-inflammatory properties, targeting two critical pathological processes central to IBD pathophysiology [135]. Furthermore, IL1RL2 targeting represents a novel therapeutic approach surpassing conventional treatments like aminosalicylates, corticosteroids, immunomodulators, and biologics, providing renewed hope for individuals with IBD [135, 136].

2. OBJECTİVE

Children suffering from VEO-IBD frequently present with a severe and potentially fatal illness resistant to standard treatments. Comprehending the molecular pathways involved is vital for improving the medical care of VEO-IBD patients. Through an extensive genome-wide investigation, we have determined inherited variants in the *IL1RL2* as a previously unrecognized genetic risk factor contributing to VEO-IBD. The primary objective of this PhD study was to delve into the mechanisms driving intestinal inflammation in individuals with *IL1RL2* mutations.

2.1. Specific Aims

1. Investigation of the immune dysregulations associated with *IL1RL2* mutations through the assessment of macrophage polarization, inflammasome activation, and cytokine expression in macrophages derived from patient's monocytes or induced pluripotent stem cells (iPSCs), genetically engineered to harbor variants, including c.952A>G, c.965A>C, c.[952A>G];[965A>C], or c.1298-4C>T.

2. Investigating the effect of *IL1RL2* mutations on wound healing in iPSC-derived colonic organoids and HCT116 colon carcinoma cells expressing *IL1RL2* variants.

3. Analysis of phosphorylation of NFκB and MAPK pathways in HCT116 colon carcinoma cells overexpressing *IL1RL2* variants.

4. Investigation of cell death response in HCT116 colon carcinoma cells overexpressing *IL1RL2* variants.

3.   MATERIAL

The materials listed below were used in this thesis study.

3.1.   Chemicals

Chemical name	Company	Catalog Number
Agar-Agar	Carl Roth	5210-2
Agarose	Applicchem	A8963-0500
Boric acid	Carl Roth	6943.3
Bromophenol blue	Carl Roth	A512.1
Deoxy nucleoside triphosphate (dNTP)	Applicchem	A9823,1000
Dimethyl sulfoxide	Sigma Aldrich	D8418
Na_2HPO_4 (Di-sodium hydrogen phosphate)	Carl Roth	P030-2
Ethanol	VWR	83.813.440
Ethidium Bromide	Applicchem	A1152,0010
Glycerol	Carl Roth	3783.1
Glycine	Carl Roth	3908.3
Hydrochloric acid	Carl Roth	K025.1
LB-Medium	Carl Roth	X968.4
Lipopolysaccharide	Sigma Aldrich	L2654
Methanol	Honeywell	32213-2.5L
Nigericin	Sigma Aldrich	N7143-5MG
Phenylmethylsulfonylfluorid (PMSF)	Abcam	ab120297
H_3PO_4 (Phosphoric acid)	Carl Roth	6366.1
KCl (Potassium chloride)	Carl Roth	6781.1
Potassium dihydrogen phosphate (KH2PO4)	Carl Roth	P018.2
PIC (Protease inhibitor cocktail)	Sigma Aldrich	P8340
Rotiphorese 30 % Acrylamide	Carl Roth	3029.1
20 % sodium dodecyl sulfate (SDS)	Carl Roth	1057.1
NaCl (Sodium chloride)	Carl Roth	9265.2
NaoH (Sodium hydroxide)	Carl Roth	P031.2

Na$_3$VO$_4$ (Sodium orthovanadate)	Sigma Aldrich	S6508-10G
TEMED (Tetramethylethylenediamine)	Carl Roth	2367.3
Tris	Carl Roth	5429.2
Triton X-100	Carl Roth	9090.3
Tween 20	Applicchem	1.423.121.611
Versene solution	TFS	15040066
β-mercaptoethanol	Sigma Aldrich	M7522/M6250

3.2. Consumables

Product	Company	Catalog number
100 mm dish	Sarstedt	833.902.300
12-well plate	Sarstedt	833.921.300
12x75 mm tubes with filter	Corning/Falcon	352235
24-well plate	Sarstedt	833.922
48-well plate	Sarstedt	833.923
Competent *Escherichia coli*	NEB	C2988J
6-well plate	Sarstedt	833.920
96-well flat bottom plate	Sarstedt	833.924
Advanced DMEM/F12	TFS	12634-028
Ampicillin	Sigma Aldrich	A9518
Bambanker	Niippon Genetics	BB01
Protein Marker	Jena Bioscience	PS-103
Bovine Serum Albumin (BSA)	Applichem	A6588,0100
Cell lysis buffer (10X)	Cell Signaling Technologies	9803S
DMEM	TFS	11960044
Human CD14$^+$ Selection Kit II	Stemcell	17858
E6 medium	TFS	A1516401
Fetal bovine serum (FBS)	TFS	10270106
Ficoll-Paque	GE Healthcare	17-1440-03
GlutaMax	TFS	35050-038
HEPES	TFS	15630056

IMDM	TFS	21980065
IntestiCult™ ODM Human Basal Medium	Stemcell	100-0212
L-Glutamine	TFS	25030123
MethoCult H4435 Enriched	Stemcell	H4435
Mid-Range DNA Ladder (100bp - 3000bp)	VWR	M-203L
Milk powder	Carl Roth	T145.3
mTeSRplus	Stemcell	100-0276
OptiMEM	TFS	11058021
Organoid Supplement	Stemcell	100-0191
Penicillin/Streptomycin	TFS	15140-122
peqGOLD 1kb DNA Ladder	VWR	25-2030
Phosphate-buffered saline (PBS)	TFS	14190-169
PVDF (Polyvinylidene fluoride) membrane	GE Healthcare	10600023
Puromycin	TFS	A11138-03
RPMI 1640 Medium	TFS	61870010
Sodium pyruvate	TFS	11360088
StemPro-34 SFM Complete Medium	TFS	10639011
Chemiluminescent Substrate	TFS	34577
0.45 μm filter	VWR	514-0063
T175 flask	Sarstedt	833.912.002
T75 flask	Sarstedt	833.911.002
TMB Solution (1X)	TFS	00-4201-56

3.3. Cytokines

Cytokines	Company	Catalog Number
bFGF (Basic fibroblast growth factor)	Peprotech	100-18B
BMP4 (Bone morphogenetic protein 4)		120-05
Flt3/Flk-2 Ligand		300-19
GM-CSF		300-03
IFN-γ		300-02
IL-10		200-10
IL-1β		200-01B
IL-3		200-3
IL-36β		200-36B
IL-36γ		200-36G
IL-4		200-04
M-CSF		300-25
SCF (Stem cell factor)		300-07
TGF-β		100-21
TPO (Thrombopoietin)		300-18
VEGF (Vascular endothelial growth factor)		100-20
Y-27632 (Rho kinase inhibitor)	Biotrend	Y-5301-10 mg
RiboLock RNase Inhibitor	TFS	EO0381
SB431542	Selleckchem	S1067
SCR7	Stemcell	74102
CHIR99021	Milipore	361571

3.4. Antibodies and dyes

Product name	Company	Catalog number	Usage
Phospho-p44/42	Cell Signaling	4370S	WB
p44/42 MAPK		9102S	
p-p38-MAPK		4511S	
p38-MAPK		9212S	
Phospho-NF-kappaB p65		3033S	
NF-κB p65		8242S	
β-Actin	Santa Cruz	sc-47778	
IL1β	R&D	AF-201-NA	
CD45-FITC	Biolegend	304038	FACS
CD34-BV421		343610	
CD14-APC		301808	
CD163-PE		333606	
CD33-PE	eBioscience	12033941	
Annexin V-APC		88800774	
CD86-BV421	BD	562432	
HLA-DR-PE-Cy7		335830	
CD273 BV786		563843	
DAPI	Sigma	D9542-10MG	

3.5. Enzymes

Product	Company	Catalog number
Accutase	Merck Milipore	SCR005
Collagenase Type IV	Stemcell	7909
Alkaline Phosphatase	TFS	EF0651
AgeI		FD1464
BamHI		FD0054
BpiI		FD1014
SpeI		FD1254
illustra ExoProStar	Sigma Aldrich	GEUS78211
OneTaq polymerase Mix	TFS	M0482L
SYBR Green		A25777
Protease	Qiagen	19155
Q5 High Fidelity Polymerase	NEB	M0491S

T4 ligase	TFS	EL0011	
Trypsin-EDTA	Sigma Aldrich	T3924-100ML	

3.6. Plasmids

Plasmid	Usage	Catalog number	Company
pSpCas9(BB)-2A-GFP	Delivery of gRNA-Cas9 particles	48138	Addgene
pSpCas9(BB)-2A-RFP		Cloned in our facility	
pcDNA3.1(+)	Mammalian expression vector	V79020	TFS
pJet1.2	Subcloning vector	K1232	TFS
pRRL-MCS90-IRES-RFP	Transfer plasmid	35395	Addgene
pRRL-MCS90-IRES-GFP		Cloned in our facility	

3.7. Buffers

Buffer	Component	Volume
Cell lysis buffer	10X Cell lysis buffer	100 μL
	PIC	60 μL
	PMSF	10 μL
	2mM Na_3VO_4/dH_2O	830 μL
6X DNA loading dye	Glycerol	30 mL
	Bromophenol blue	10 mg
	Set the pH to 8.0	
	dH_2O	to 100 ml
6X Laemmli buffer	20 % SDS	4 mL
	Glycerol	4 mL
	1.0 M Tris HCl pH 6.8	2 mL

	Bromophenol blue	5 mg
LB medium	LB-Medium (Luria/Miller)	25g
	dH$_2$O	to 1L
LB plates	LB-Medium (Luria/Miller)	25g
	Agar-agar Kobe 1	15g
	dH$_2$O	to 1L
Phosphate-buffered saline (PBS)	NaCl	800g
	KCl	20g
	Na$_2$HPO$_4$	142g
	KH$_2$PO$_4$	24.5g
	Set the pH to 7.4	
	dH$_2$O	to 1L
PBS-T	Tween 20	0,05% (v/V)
	PBS	to 1L
Running buffer	Tris base	
	Glycine	
	SDS	
	dH$_2$O	
Transfer buffer	Tris base	
	Glycine	
	dH$_2$O	
Stripping buffer	Glycine	
	SDS	
	Tween 20	
	Set the pH to 2.2	
	dH$_2$O	

TBE	Tris base	216 g
	Boric acid	110 g
	0.5 M EDTA (pH 8.0)	80 mL
	dH$_2$O	to 2L
TE (Tris-EDTA) buffer	Tris base	10 mM
	EDTA	1mM
	Set the pH to 8.0	
	dH$_2$O	to 1L

3.8. Kits

Product	Catalog number	Company
Cloning Kit (CloneJET)	K1231	TFS
cDNA Reverse Transcription Kit	4368813	TFS
Human Stem Cell Nucleofector Kit 2	VPH-5022	Lonza
Maxwell RNA isolation kit	AS1270	Promega
Plasmid Plus Maxi Kit	12965	Qiagen
Zymoclean Gel DNA Recovery Kit	D4002	Zymo
Zyppy Plasmid Miniprep Kit	D4037	Zymo

3.9. Softwares

Name	Company	Version	Usage
FACSDiva	BD Biosciences	8.0.1	Collection of FACS data
FlowJo	FlowJo	10_2	Examination of FACS data
ImageLab	BioRad	6.0.1	Obtaining and analyzing data from agarose gel electrophoresis and Western blot techniques
NanoDrop 2000	TFS	1.6.198	Evaluation of DNA/RNA purity

Prism	GraphPad	8.04.2000	Creation of graphs and statistical analysis

3.10. Primers

Primer name	Sequence (5' > 3')	Usage
LA5_IL1RL2_fw	ATGCTTCCGGAATGTGGTCCTTG	SDM
LA6_IL1RL2_rev	GGCGATATCGATTTATCACTTATCGTCGTC	
LA63_F_IL1RL2_Age I	GGATCCACCGGTTCGAATCGATGGC	
LA64_R_IL1RL2_Spe I	GTCCGGACTAGTTTATCACTTATCGTCGTC ATCCT	
LA39_GAPDH_F	TGCTGGGGAGTCCCTGCCACA	Real-Time PCR
LA40_GAPDH_R	GGTACATGACAAGGTGCGGCTC	
LA45_CXCL10_qF	TGCTTCCAAGGATGGACCACACAGA	
LA46_CXCL10_qR	ACCTTCCTACAGGAGTAGTAGCAGC	
LA49_CCL20_qF	TTTGCTCCTGGCTGCTTTGATGT	
LA50_CCL20_qR	GCAAGTGAAACCTCCAACCCCA	
LA67_IL6_qF	AAGCGCCTTCGGTCCAGT	
LA68_IL6_qR	CATGTCTCCTTTCTCAGGGCT	
LA41_IL8_qF	ACTCCAAACCTTTCCACCCCAAAT	
LA42_IL8_qR	ACAACCCTCTGCACCCAGTTTT	
LA73_IL1RL2_sF	CCCGGGCTGTTTTAATTGTGAGTT	Sanger Sequencing
LA74_IL1RL2_sF	GGATGGCACCATGCTTCTGTTT	
LA149_U6_fw	GAGGGCCTATTTCCCATGATTCC	
pJet_sF	CGACTCACTATAGGGAGAGCGGC	
pJet_sF	AAGAACATCGATTTTCCATGGCAG	
YY147_pRRL_MCS_ Fw	CAATCAGCCTGCTTCTCGCTT	
YY148_pRRL_MCS_ Rev	AGCAGCGTATCCACATAGCGTA	

4.   METHODS

4.1.   Cell Culture

This study utilized colorectal carcinoma cells HCT116 (ATCC® CCL-247™) and human induced pluripotent stem cells (iPSCs; Helmholtz Center Munich) lines. Cell cultures were routinely confirmed to be free of mycoplasma contamination.

4.1.1.   Maintenance of HCT116 colon carcinoma cell line

The HCT116 cells were plated in 24- or 96-well plates and flasks and maintained in a standard humidified incubator at 37°C in a 5% CO_2 atmosphere. Cells were cultured in DMEM containing fetal bovine serum (FBS; 10%), L-glutamine (1%), penicillin (1%), HEPES (10 mM), and sodium pyruvate (1%). Cells were subcultured once a week, and the medium was routinely refreshed during culturing with pre-warmed medium to 37°C before usage.

4.1.2.   Maintenance of iPSC line

iPSCs were generated from male foreskin fibroblasts. iPSCs were cultured on multi-well plates or dishes coated with Matrigel. The Matrigel was suspended in Advanced Dulbecco's Modified Eagle's Medium (DMEM)/F12 in a 1:100 ratio, and the coated plates were kept at 37°C for 1 hour prior to implementation. Once the Matrigel polymerized, plates/dishes were rinsed with PBS, and iPSCs suspended in mTeSRplus medium were plated. The cells were spread evenly by shaking and then plated in a humidified incubator at 37°C and 5% CO2. The medium was removed by aspiration for subculturing, and iPSC colonies were rinsed with PBS once. The cells were incubated with 1 mg/mL Collagenase IV for 60 minutes at 37°C. After incubation, colonies were fragmented by pipetting. mTeSRplus medium was added to block the Collagenase IV reaction. The colonies were spun at 200g for 3 minutes at RT. The supernatant was carefully removed following centrifugation. Subsequently, colonies were resuspended in mTeSRplus medium and divided among prewarmed plates that had been coated beforehand. The medium was refreshed daily or every 2 days, depending on colony density.

Colonies were harvested using Collagenase IV and fragmented via pipetting for the cryopreservation of iPSCs. Subsequently, the colonies were centrifuged at 200g for 3 minutes at RT, mixed with Bambanker solution, and then promptly frozen at –80°C. The next day, they

were transferred to liquid nitrogen for prolonged preservation. To defrost cryopreserved iPSCs, cell culture plates/dishes were prepared following previously established methods above. The frozen cell suspension was thawed in a 37°C water bath and promptly transferred to prewarmed Advanced DMEM/F12. Following centrifugation of the colonies at 200g for 3 minutes at RT, they were mixed in mTeSRplus and seeded on plates. Additionally, a 10 µM Rho kinase inhibitor (Y-27632) was incorporated into medium for one day. Subsequently, the medium was refreshed every 1-2 days contingent on the cell density.

4.2. PBMC Isolation from Human Blood

The blood samples of patients, family members, and healthy donors (HDs) were collected aseptically by venipuncture using EDTA an anticoagulant. Anticoagulated blood was kept at RT until processing. The blood was mixed with PBS and gently added to the surface of the Ficoll reagent. The blood/Ficoll mixture was spun at 2200 rpm for 20 minutes at RT. The centrifuge was set with an acceleration of 9 and a deceleration of 5. After centrifugation, the top layer (serum/PBS fraction) from the Ficoll preparation was aspirated, and peripheral blood mononuclear cells (PBMCs) from the Ficoll phase were collected in a 50 mL Falcon tube. Once all PBMCs were isolated, the tube containing PBMCs was filled with PBS and centrifuged at 1500 rpm for 10 minutes at 4°C. The supernatant was then removed, and the PBMC pellet was mixed in cold PBS and placed on ice. The PBMCs were counted using trypan blue solution in the Neubauer cell counting chamber. The PBMCs were used for macrophage and dendritic cell differentiation.

4.3. Macrophages/dendritic cell differentiation from human blood monocytes

$CD14^+$ monocytes were enriched by magnetic bead isolation from human PBMCs (see PBMC isolation in section 4.2) according to manufacturer descriptions. $CD14^+$ monocytes were further differentiated into macrophages by adding macrophage colony-stimulating factor (M-CSF; 100 ng/ml) or DCs by adding GM-CSF (100 ng/ml) for 7 days. After 7 days of differentiation, the cells were treated with IL-36γ (100 ng/ml) for 2 and 4 hours to assess gene expression by real-time PCR. After stimulation, the cells were resuspended in a homogenization buffer for RNA isolation (see section 4.12).

4.4. Genetic engineering facilitated by CRISPR/Cas9

Guide RNAs (gRNAs) and templates for homologous-directed repair (HDR) were meticulously designed using Benchling (www.benchling.com) and the Synthego Clustered Regularly Interspaced Short Palindromic Repeats (CRISPR) Design Tool (www.synthego.com), following established protocol [154]. Subsequently, the guide RNAs (refer to Table 1) were procured from Integrated DNA Technologies (IDT, USA).

Table 1: Guide RNAs targeting *IL1RL2* for CRISPR-mediated engineering.

Name	Sequence
Guide for KI at intron 10 forward	CACCGTCGATGACATTGGCCACGGC
Guide for KI at intron 10 reverse	AAACGCCGTGGCCAATGTCATCGAC
Guide for KI at exon 11 forward	CACCGAAAACGTTAAGCTGTGCAGG
Guide for KI at exon 11 reverse	AAACCCTGCACAGCTTAACGTTTTC
Guide for KO at exon 2 forward	CACCGCTTCCACTGTCTGTCACAGC
Guide for KO at exon 2 reverse	aaacGCTGTGACAGACAGTGGAAGC
Guide for KO at exon 5 forward	CACCGCTTTTGGTGAGCAATGTCT
Guide for KO at exon 5 reverse	aaacAGACATTGCTCACCAAAAGC

The gRNAs were cloned into linearized plasmids expressing CRISPR-associated protein 9 (Cas9) derived from *Streptococcus pyogenes*, along with either green fluorescent protein (GFP) or red fluorescent protein (RFP). Linearization was performed using the reaction procedure outlined in Table 2.

Table 2: Reaction mixture for linearization of PX458 plasmid

Reagent	Amount
PX458 plasmid	1 μg
10x FastDigest Buffer	5 μL
BpiI	2 μL
Alkaline Phosphatase	2 μL
Nuclease-free water (NFW)	to 50 μL

The linearization was performed at 37 ^{0}C for 1 hour, and the enzymatic reaction was stopped by incubating the reaction at 85 ^{0}C for 15 minutes. The plasmids' backbone was separated using agarose gel electrophoresis and purified using DNA extraction (see section 4.7). The DNA concentration was measured using Nanodrop spectrophotometry. The gRNAs were annealed and phosphorylated before cloning following the reactions and incubations in Table 3. The reaction was incubated at 37 ^{0}C for 30 minutes and at 95 ^{0}C for 50 minutes and then cooled down slowly. After annealing, oligos were diluted 1:250 in NFW.

Table 3: The reaction mixture for annealing and phosphorylation of gRNAs

Reagent	Amount
100 µM gRNA forward	2 µL
100 µM gRNA reverse	2 µL
10x T4 Ligation buffer	2 µL
T4 PNK	1 µL
NFW	To 20 µL

Annealed gRNAs and the linearized PX458 plasmid backbone were ligated using the reaction described in Table 4.

Table 4: Reaction mixture for ligation

Reagent	Amount
Linearized backbone	100 ng
Oligos	2 µL
10x T4 buffer	2 µL
T4 ligase	1 µL
NFW	To 20 µL

The ligation mixture was incubated at 22 ^{0}C for a duration of 1 hour. After ligation, the transformation was performed according to section 4.8.

4.5.   Site-Directed Mutagenesis, PCR and Cloning

The PCR-based site-directed mutagenesis (SDM) technique was utilized to create the index patient's variants. Firstly, the commercially available Human *IL1RL2* (NM_003854.2) ORF clone (standard vector: pcDNA3.1+/C-(K)DYK) from GenScript was employed to generate the patient's mutations. AgeI and SpeI restriction sites were introduced using PCR (Tables 5 and 6).

Table 5: PCR mixture for SDM

Reagent	Volume (µL)
Q5 reaction buffer	2
dNTPs	2
DMSO	1
Forward primer	1
Reverse primer	1
Q5 High Fidelity Polymerase	0,5
PCR product	10 ng
NFW	To 20

Table 6: PCR programme for SDM

Temperature (^{0}C)	Duration	Cycles
Lid to 110	-	
98	5 min	1
98	30 sec	
50	30 sec	10
72	30 sec	
98	2 min	1
98	30 sec	1
66	30 sec	30
72	45 sec	
72	10 min	
4	∞	1

Subsequently, the PCR product underwent agarose gel electrophoresis, and the PCR fragment was isolated, as detailed in section 4.6. The PCR fragment containing the mutation and restriction sites was ligated into the blunt-end pJet1.2 vector using the CloneJET PCR Cloning Kit (Table 7).

Table 7: The ligation mixture aimed for blunt-end cloning into the vector pJet1.2.

Reagent	Volume (µL)
2X reagent buffer	10
pJet1.2/blunt	1 (0,05 pmol
PCR product	0,15 pmol
T4 ligase	1
NFW	to 20

The ligation mixture was left to incubate overnight at 4°C and then directly subjected to transformation into bacteria, which were plated on ampicillin[+] agar plates. The bacteria clones were expanded and then isolated for Sanger analysis to confirm the clones with the patient's mutations and restriction sites. After confirmation, the pRRL-MSC90-IRES-RFP backbone and pJet1.2-IL1RL2 (clones with WT gene and index patient mutation) were digested with AgeI and SpeI (Table 8) to generate stable heterologous cell lines overexpressing *IL1RL2* with index patient variants. The digested backbone and mutant genes were run on agarose gel and isolated (see section 4.6). The mutant or WT *IL1RL2* genes were ligated with linerizaed pRRL-IRES-RFP (Table 9). The transformation was performed (see section 4.8).

Table 8: Digestion mixture for AgeI and SpeI

Reagent	Volume (µL)
Plasmid	0,5-1 µg
FD Age I	0,5
FD SpeI	0,5
10X FastDigest buffer	1
NFW	to 10

Table 9: Ligation process for pRRL-MCS90-IRES-RFP

Reagent	Volume (µL)
Backbone plasmid	1-2 µg
Insert	1
T4 Ligase	1
10X Ligation buffer	2
NFW	to 20

4.6.   DNA Electrophoresis and DNA Recovery

Agarose gel electrophoresis is employed to separate DNA fragments based on their respective sizes. Initially, a 0.5-1% agarose gel is prepared by dissolving it in TRIS-Acetate-EDTA buffer (TAE), followed by boiling and casting into electrophoresis cassettes containing ethidium bromide (5 µg/ml). The DNA samples are then mixed with loading dye and subjected to electrophoresis in TAE buffer, facilitating their migration based on molecular size. To measure the DNA fragment's size, either the peqGOLD 1kb or the 100-3000bp DNA ladder is utilized. When necessitated for subsequent applications, the DNA bands are cut from the agarose gel under UV illumination using a scalpel and subsequently purified utilizing the Zymoclean Gel DNA Recovery Kit. The purified DNA fragment is mixed with buffer and heated to 55°C for 10 minutes to dissolve the agarose gel. The liquefied agarose gel is transferred onto a Zymo-Spin Column, positioned in a collection tube, and spun at 16,000 x g for 1 minute. Following this, the column tube is washed twice with DNA Wash buffer. Subsequently, the DNA elution buffer is added to the spin column, and centrifugation is carried out to elute the DNA into the collection tube. This comprehensive process ensures the isolation and purification of DNA fragments from the agarose gel for downstream applications.

4.7.   DNA preparation and ligation

The target gene was generated using SDM, and pRRL-MCS90-IRES-RFP/GFP was digested with AgeI and SpeI restriction enzymes (1 U/µl). Digestion was conducted for two hours at 37°C in the thermocycler and verified by electrophoresis separation. Following separation, DNA fragments were excised from the agarose gel. A 5:1 ratio of insert to plasmid backbone

was mixed with T4 ligase (1 µl), 2x buffer (5 µl), and NFW (2 µl) to ligate the target insert into the plasmid backbone. The mixture was then left to incubate at 4°C overnight.

4.8. Transformation

To reproduce the vectors containing the cloned DNA fragment, competent Escherichia coli were thawed on ice, and the ligated DNA to the pRRL-MCS90-IRES-RFP/GFP plasmid was added. The mixture underwent an initial incubation period on ice for 30 minutes, followed by a brief exposure to elevated temperature (42°C) for 40 seconds, and then returned to ice for 2 minutes. Following this, 500 µl of plain LB medium was mixed with the reaction mixture, and the bacteria were grown at 37°C for one hour at 400 rpm in a thermocycler to facilitate recovery. Subsequently, bacterial samples were inoculated onto LB agar plates supplemented with ampicillin and incubated overnight at 37°C. Colonies displaying resistance to ampicillin were selected and transferred into 4 ml of LB broth supplemented with ampicillin, followed by overnight incubation in a shaker incubator set at 200 rpm for 12 hours, maintained at 37°C.

4.9. Plasmid DNA purification from bacteria

Plasmids were obtained from transformed bacterial cultures cultured overnight in LB medium supplemented with ampicillin under agitation at 37°C. Plasmid extraction was carried out employing either the Zyppy Plasmid Miniprep Kit or the Qiagen MaxiPrep kit, adhering strictly to the protocols provided by the respective manufacturers. The quantification and quality assessment of the extracted plasmids were performed using NanoDrop spectrophotometry, employing UV light absorbance to determine nucleic acid concentration.

4.10. Lentiviral Transduction of HCT116 Cells

The Polyethylenimine (PEI) transfection technique was utilized for the production of lentivirus in the HEK293T cell line by employing Helper plasmids encoding the Vesicular Stomatitis Virus Glycoprotein, group antigen, reverse transcriptase, and mRNA export helper protein as a packaging mixture. One day before transfection, HEK293T cells were seeded onto 10 cm cell culture dishes. HEK293T cells were used for transfection at approximately 50-60% confluency, and the media were refreshed before transfection. The complete DMEM medium was transferred into a 1.5 ml Eppendorf tube as a solvent to prepare the transfection mixture, followed by the addition of plasmid DNA and PEI. The transfection mixture was incubated for

30 minutes at RT before being added to the cells. One day after transfection, the medium was replaced with a 15 ml DMEM complete medium following 72 hours of culturing.

Next, the medium containing lentiviral particles was collected, and cell debris was removed through centrifugation followed by filtration using a 0.45 µm syringe filter. Ultracentrifugation was performed at 4°C, 24,000 rpm for 2.5 hours using a SW32Ti rotor to concentrate lentiviral particles. The lentiviral particle pellets were resuspended in 500 µl of DMEM medium, and aliquots were stored at -80°C for transduction.

Thirty thousand HCT116 cells were seeded in 24-well plates one day before transduction. The medium was replaced with 250 µl OptiMEM containing 50 µl virus aliquot. The cells were spinoculated at 2000 rpm for 60 minutes at 32°C. After spinoculation, the cells were cultured overnight at 37°C. One day after spinoculation, the medium was changed to a fresh, prewarmed medium. Transduction efficiency was evaluated by measuring RFP expression using Fluorescence-Activated Cell Sorting (FACS). The pRRL-MCS90-IRES-GFP plasmid, lacking *IL1RL2*, served as the control plasmid.

4.11. Western Blot

4.11.1. Preparation of Sodium Dodecyl Sulfate-Polyacrylamide Gel (SDS-PAGE)

The SDS-PAGE was prepared manually, utilizing a Mini-PROTEAN 3 Multi-Casting Chamber. Firstly, the separating gel (Table 10) was mixed and filled into the casting chamber. Isopropanol (1 ml) was added to flatten the gel's surface and prevent bubble formation. The separating gel was then kept at RT for 30 minutes for polymerization. Subsequently, the excess isopropanol was cleaned up, and the stacking gel (Table 10) was cast on top of the polymerized separating gel. The gel was again kept at RT for 30 minutes to complete polymerization.

Table 10: Preparation of SDS-PAGE

Separating Gel (10%)	
H_2O	3,10 μL
0,5 M Tris HCl (pH 8.8)	2,9 mL
Acryl-Bisacrylamid	2,6 mL
10% SDS	77,50 μL
Temed	5,75 μL
20% APS	37,60 μL
Staking Gel (6%)	
H2O	1950 μL
0.5 M Tris HCl (pH 6.8)	360,00 μL
Acryl-Bisacrylamid	487,50 μL
10% SDS	28,75 μL
TEMED	2,87 μL
20% APS	18,80 μL

4.11.2. Protein sample preparation

The supernatant was aspirated from the cells, followed by harvesting the cells via trypsinization. The pellet was then lysed in 1x cell lysis buffer, as detailed in Table 11.

Table 11: 1x Cell lysis buffer

Reagent	Volume (μl)
Na_3Vo_4	830
10x cell lysis buffer	100
PIC	60
PMSF	10

The cell/lysis buffer mix was incubated on ice for 45-60 minutes to allow the lysis reaction to proceed. After lysis, the cell/lysis buffer mixture was spun at 15,000 rpm at 4°C for 15 minutes. The proteins in the supernatant were transferred into Eppendorf tubes. 6x Laemmli buffer containing 3% β-Mercaptoethanol was mixed with the proteins, which were then kept at 95°C for 10 minutes for protein denaturation. After denaturation, the protein solution was kept on ice for 2 minutes before loading onto the gel.

4.11.3. Electrophoresis and Protein Transfer

The gel containing protein samples was first subjected to electrophoresis at 80 V until the samples migrated into the separating gel. Subsequently, the voltage was increased to 120 V in a 1x running buffer, and the electrophoresis was continued for 3 hours. After electrophoresis, the gel, fiber pad, Whatman filters, and PVDF membrane were activated in ethanol for 1 minute, followed by soaking in 1x transfer buffer for 2 minutes. The protein-loaded membrane was subsequently positioned devoid of bubbles within the transfer cassette. The cassette was then introduced into a Mini-PROTEAN Tetra Vertical Electrophoresis Cell, which was pre-filled with 1x transfer buffer and surrounded by ice packs. The transfer process was executed under an applied voltage of 100 V for a duration of 60 minutes.

4.11.4. Blocking and Antibody staining

Following the transfer, the PVDF membrane underwent a 60-minute blocking step at RT in a BSA (5%) solution prepared in PBS. Subsequently, it was incubated with primary antibodies overnight at 4°C. The membrane underwent three rounds of washing with PBS-T for 10 minutes each, succeeded by a 60-minute period of incubation with corresponding HRP-conjugated isotype-specific secondary antibodies at RT (RT). Subsequent to this, three additional washes with PBS-T were conducted for 10 minutes each. Visualization was accomplished via enhanced chemiluminescence utilizing the Super Signal West Dura Extended Duration Substrate and the ChemiDoc XRS+ System. For multiple protein analyses, the membrane was treated to remove previous antibody staining by immersion in homemade Stripping buffer for 15-30 minutes at RT, followed by PBS-T washes. Finally, the membrane was subjected to incubation with primary and secondary antibodies, adhering to the previously delineated procedure.

4.12. RNA extraction, Reverse transcription and Real-time PCR

Total RNA was isolated from stimulated patient cells, the heterologous HCT116 cell line, iPSC-derived macrophages, and organoids using the Maxwell® 16 Tissue LEV Total RNA Purification Kit, following the manufacturer's instructions. Subsequently, the concentration and quality of the RNA were assessed using the NanoDrop 2000. The extracted total RNA underwent reverse transcription using a transcription kit and a conventional PCR method. The

reverse transcription mixture was prepared according to the manufacturer's instructions, as detailed in Tables 12 and 13 below.

Table 12: Mixture of reverse transcription reaction

Reagent	Volume (µl)
10x reverse transcription buffer	1
10x Random primers	1
25x dNTPs	0,2
RiboLock	0,5
Reverse Transcriptase	0,5
Total RNA	Up to 1 µg
NFW	Up to 10

Table 13: The PCR program for reverse transcription reaction

Temperature (^{0}C)	Time [minute]
Lid at 110	indefinite
25	10
37	120
85	5
4	indefinite

After reverse transcription, the gene expression levels of interested genes were evaluated by quantitative real-time PCR using the FAST SYBR Green method, following the reaction mixture and program outlined in Tables 14 and 15. The quantitative real-time PCR was conducted on the StepOnePlus Real-Time PCR system. Subsequently, the StepOnePlus Software was employed to analyze the real-time PCR results using the ΔΔCT method to calculate fold changes.

Table 14: qRT-PCR mixture

Reagent	Volume (µl)
Fast SYBR Green	3,5
Forward primer	0,5
Reverse primer	0,5
cDNA	10,5 ng
NFW	Up to 10

Table 15: qRT-PCR program

Temperature (^{0}C)	Time [min]	Cycles
Lid at 110	-	-
50	120	1
95	120	1
95	3	40
60	30	
95	15	1
60	60	1
Ramping from 0.3 increments to 95°C for the melting curve		
95	15	1

4.13. Flow cytometry-based Apoptosis

An Annexin V apoptosis detection kit and a flow cytometry-based apoptosis assay were utilized to assess cell death. Following TNF-α and cycloheximide stimulation, a medium containing dead cells was collected in a falcon tube, and attached cells were trypsinized for harvesting and added to the tube. Annexin V at a ratio of 5:100 was mixed with cells for staining at RT for 20 minutes after washing with 1x Annexin V binding buffer. Following that, the cells were spun at 300g for 5 minutes at RT, washed again with 1x Annexin V binding buffer, and mixed in 100 µL PBS. Before measurements, 100 µL of DAPI solution (1 µg/ml in PBS) was added to the cells. The measurement was performed using a Fortessa LSR.

4.14. CRISPR/Cas9-mediated genetic engineering of iPSC

The iPSCs were maintained according to section 4.1.2. To reduce cytotoxicity, the iPSCs were treated with Rho kinase inhibitor (10 µM Y-27632) for 24 hours before electroporation. The Matrigel-coated plate was prepared 1 hour before usage and kept at 37°C with mTeSRplus medium. The medium from iPSC cells was removed, and cells were rinsed with PBS once. Accutase was added to the top of the iPSCs and incubated for 10 minutes at 37°C. The mTeSRplus medium was added to stop the Accutase reaction. The cells were collected and spun at 200g for 3 minutes at RT. The supernatant was removed, the iPSC pellet was mixed in mTeSRplus medium, and the cells were counted. For each electroporation reaction, 0.5-1.5 x 10^6 cells were used.

The electroporation mixture was prepared following the manufacturer's instructions: 8 µL supplement, 82 µL nucleofector solution, and 5 µg CRISPR vector. A 5-10 µL HDR template was also added to generate knock-ins. The cells were mixed with a 100 µL prewarmed electroporation mixture. The electroporation was conducted using program B016 and the Nucleofector II device in the electroporation cuvette. After electroporation, iPSCs were transferred into a plate prepared before nucleofection and cultured, as described in section 4.1.2. One day after nucleofection, 10 µM SCR7 was added to knock-in cells to inhibit non-homologous end joining. The iPSCs were harvested with Accutase, centrifuged at 200g for 3 minutes at RT, and resuspended in 200 µL prewarmed mTeSRplus medium prepared by adding 10 µM Y-27632 two days after electroporation. The cells were sorted into Eppendorf tubes containing mTeSRplus and 10 µM Y-27632 and 1% v/v Penicillin-Streptomycin using a FACSAria III machine. The sorted cells were seeded in a 10 cm Matrigel-coated cell culture dish in a medium containing fresh mTeSRplus and conditioned medium. The conditioned medium was prepared by filtering the supernatants of the wild-type iPSC cells and adding 10 µL of Y-27632 and 1% v/v Penicillin-Streptomycin. 3000-5000 single iPSCs were seeded and cultured according to section 4.1.2. The rest of the sorted iPSCs were used to genotype the cells. On days 2 and 3, the medium was refreshed with medium containing fresh mTeSRplus and conditioned medium. Subsequently, the culture medium was refreshed with fresh mTeSRplus every other day until the colonies attained sufficient size. Upon reaching the desired size, half of each colony was carefully aspirated using a pipette and transferred to a pre-coated 24-well plate. The remaining portion of the colony was utilized for genotypic analysis. Clones exhibiting confirmed edits were propagated for subsequent experimentation, including differentiation towards macrophages and colonic organoids.

4.15. Differentiation of iPSC towards macrophages

The iPSCs were maintained according to section 4.1.2. When iPSCs reached sufficient size and density, the cells were rinsed with PBS once, and Collagenase (1 mg/ml) was added. The iPSCs were treated with Collagenase (1 mg/ml) for 30 to 60 minutes at 37°C. The cells were collected by pipetting, transferred into a Falcon tube, and pelleted at 10g for 1 minute at RT. The medium was removed, and the pellet of the colonies was resuspended in mTeSRplus. The colonies were counted, and 10-20 colonies were plated in 6-well plates coated with Matrigel. The colonies were cultured until their size reached a diameter of approximately 1 mm. The medium was changed with fresh prewarmed mTeSRplus after two days of seeding and later every day until the colonies reached sufficient size. When the colonies reached sufficient size and density, hematopoiesis was induced. According to Table 16, the medium was changed with cytokines/inhibitors on days 0, 2, 4, and 6 during hematopoiesis induction. Six colonies were selected based on the size and morphology of the colony on day 6 of the differentiation. The remaining colonies were removed by aspiration. On days 9, 12, and 15, half of the medium was refreshed based on Table 16, and the differentiation was characterized by checking CD45, CD34, CD33, and CD14 by collecting the floating cells while the medium was being refreshed. On days 18, 22, and 26 CD14$^+$ monocytes were enriched from floating cells utilizing the EasySep Human CD14$^+$ Selection Kit II. The CD14$^+$ monocytes were cultured for 6-7 days with M-CSF in RPMI 1640+Glutamax supplement medium containing FBS (10%), Penicillin-Streptomycin (1%), HEPES (10 mM), and Sodium pyruvate (1 mM). After differentiation, the mature macrophages were used for polarization (see section 4.16), for analyzing the inflammasome (see section 4.17), or for the human colony-forming unit assay (see section 4.18).

Table 16: Macrophage differentiation cytokines/inhibitor refreshing routine

Day	Reagent	Concentration	Unit	Medium
0-2	BMP4	80	ng/ml	mTeSRplus
	VEGF	80		
	CHI99021	3	μM	
2-4	VEGF	80	ng/ml	Essential 6
	SCF	50		
	bFGF	25		
	SB431542	2	μM	
4-6	SCF	50	ng/ml	StemPro-34
	IL-3	50		
	TPO	5		
	FLT3L	50		
	VEGF	50		
6-9	M-CSF	50		StemPro-34
	SCF	50		
	TPO	5		
	IL-3	50		
	FLT3L	50		
9-12	M-CSF	50		StemPro-34
	GM-CSF	25		
	FLT3L	50		

4.16. Macrophages polarization

50,000 to 200,000 macrophages differentiated from human blood monocytes or iPSC-derived monocytes were seeded in RPMI 1640+Glutamax supplement medium (see section 4.15) without M-CSF in 24-well plates for 24 hours under the conditions described in Table 17 below.

Table 17: Cytokines cocktails for macrophage subsets

Subset	Cytokines	Concentration(ng/ml)
M0	-	-
M1	LPS	50
	IFN-γ	20
M2	IL-4	20
	IL-10	20
	TGF-β	20

After 24 hours, the supernatant was removed, and the macrophages were rinsed with pre-warmed PBS once and harvested with Versene for 10 minutes at 37°C. The cells were stained with macrophage surface markers at RT for 20 minutes for FACS analysis (refer to Table 18).

Table 18: Antibodies for macrophages polarization

Marker	Dilution
CD206-APC	0,5
CD86-BV421	1
CD163-PE	1
CD14-FITC	0,75
HLA-DR-PE-Cy7	0,75

4.17.   Inflammasome

iPSC-derived macrophages were initially treated with either LPS (200 ng/ml) or IL-36γ (100 ng/ml) for 3 hours. Subsequently, the iPSC-derived macrophages were exposed to 6.5 μM Nigericin for 30 minutes in a complete RPMI medium. Following stimulation, the supernatant was harvested for subsequent analysis, while the cells were lysed using lysis buffer for immunoblotting to examine IL-1β levels in both the cell lysate and supernatant.

4.18.   Human Colony Forming Unit

iPSC-derived HSPCs were differentiated according to Table 17 in Section 4.15. The proliferation and differentiation capacity were analyzed using the colony-forming unit (CFU) assay. Specifically, iPSC-derived HSPCs were harvested on day 9 (see Table 17) and pelleted at 300g for 5 minutes at 4°C. The cells were then mixed in IMDM medium and counted. 10,000

cells were mixed in the methylcellulose semi-solid matrix and seeded in dishes, followed by culture at 37°C and 5% CO2 in a humidified incubator until analysis.

4.19. Colonic Organoid Differentiation from iPSC

The iPSCs were maintained and split according to Section 4.1.2. Briefly, when the iPSCs reached sufficient size and density, they were rinsed once with PBS. Subsequently, the cells were treated with Collagenase (1 mg/ml) for 45-60 minutes at 37°C. Afterward, mTeSRplus medium was added to halt the Collagenase reaction. The colonies were then fragmented by pipetting, and the fragmented iPSCs were transferred into a falcon tube and centrifuged at 200g for 3 minutes at RT. The fragmented iPSCs were seeded in 24-well plates coated with Matrigel. The Matrigel-coated plate was prepared at least 1 hour before seeding. The medium was changed daily until cells reached 60-70% confluency. Subsequently, differentiation was initiated with definitive endoderm (DE) differentiation for 72 hours. For this, the medium was replaced, and the cells were cultured in DE medium 1 for 24 hours, followed by DE2 medium for another 24 hours, and finally, DE3 medium for a further 24 hours. After definitive endoderm differentiation, the cells were differentiated into hindgut endoderm (HE) by changing DE3 medium to HE medium for 4 days, with medium renewal every 24 hours. After 4 days, spheroids formed. These spheroids were scraped off, transferred into tubes, and allowed to settle by gravity. The supernatant was removed, and the pellet was centrifuged at 10g for 60 seconds. The pellet was resuspended in Matrigel and seeded in 24-well plates prewarmed as domes for colonic organoid (CO) differentiation. During CO differentiation, the spheroids were cultured in CO medium for 3 days, with daily medium replacement. After 3 days, the CO medium was replaced with an organoid growth medium (refer to Tables 19 and 20).

Table 19: Mediums for organoid differentiation from iPSC

Medium	Basal medium	Supplements				Stimuli 1	Stimuli 2
		GlutaMax	P/S	FBS	Others		
DE1	RPMI 1640	2 mM	1%	0%	-	25 ng/mL Wnt3a	100ng/mL Activin A
DE2	RPMI 1640	2 mM	1%	0.2 %	-	100 ng/mL Activin A	
DE3	RPMI 1640	2 mM	1%	2%	-	100 ng/mL Activin A	-
HE	Advanced DMEM/F12	2 mM	1%	2%	1X B27	3µM CHIR99021	500 ng/mL FGF4
CO	Advanced DMEM/F12	2 mM	1%	2%	1X B27, 1X N2 HEPES	100 ng/mL EGF	100 ng/mL BMP2

The colonic medium was refreshed every 2-3 days for 7-9 days. Afterwards, the organoids were mechanically passaged weekly and pelleted by centrifugation. Following centrifugation, the supernatant was removed, and the organoid pieces were mixed with Matrigel. The organoids suspended in Matrigel were then added to 24-well plates as domes and incubated for 45 minutes at 37°C for polymerization. Once polymerized, a fresh organoid medium containing Rock inhibitor and EGF was added. After 6 days of colonic organoid seeding, the organoids in the domes were used for monolayer organoid differentiation. For monolayer organoid culture, Matrigel-coated 24-well plates were prepared 2 hours before usage and rinsed once with PBS prior to use. The medium from the organoids embedded in Matrigel domes was aspirated. The organoids were then treated with a gentle cell dissociation reagent after incubation at RT for 1 minute. Subsequently, the organoids were pipetted vigorously several times and pooled into 15 ml Falcon tubes. These tubes were gently agitated at RT for 10 minutes. Afterward, the tubes were centrifuged at 200g for 5 minutes at 4°C. Following the removal of the supernatant, the organoids were mixed with pre-warmed Trypsin-EDTA and incubated in a 37°C water bath for 5 minutes. Post-incubation, the organoids were vigorously vortexed and pipetted multiple times to ensure proper dissociation. Cold Advanced DMEM/F-12 was added to neutralize the Trypsin-EDTA, and the organoids were pelleted by spinning at 200g for 5 minutes at 4°C. The

supernatant was then aspirated, and the organoids were rinsed once with cold Advanced DMEM/F-12 supplemented with 10% FBS before being spun again at 200g for 5 minutes at 4°C. Subsequently, the organoids were resuspended in IntestiCult™ Monolayer Growth Medium containing IntestiCult™ ODM Human Basal Medium, Organoid Supplement, and Y-27632. The organoids were then plated onto a Matrigel-coated 24-well plate and cultured for 2 days. Afterward, the medium was refreshed with IntestiCult™ Monolayer Growth Medium without Y-27632 until the culture reached approximately 80% confluency.

Table 20: Organoid basal medium and growth medium

Basal medium	
Component	**Volume**
Advanced DMEM/F12	500 mL
1x GlutaMax	5 mL
10 mM HEPES	5 mL
1x Penicilin/Streptomycin	5 mL
Growth medium	
Component	**Volume**
Basal Medium	25 mL
Wnt3 A	10 mL
Rspo	10 mL
Noggin	5 mL
B27	1 mL
nAc	125 µL
A83-01	5 µL
SB202190	16,6 µL
hEGF	5 µL
ROCK inhibitor	5 µL

4.20. Wound Healing Assay

HCT116 cells and iPSC-derived colonic monolayer organoids expressing *IL1RL2* variants were seeded in 24-well plates. One day after seeding for HCT116 cells and three days after seeding for monolayer organoids, a wound was created by scratching the cell monolayer using pipette tips. After washing once with medium, the cells with the wound were incubated at 37°C, either

with or without stimulation, with 100 ng/ml IL-36γ. Wound healing was monitored, and images were captured every 24 hours. The wound size was measured manually.

4.21. Sanger Sequencing

The sequence of the DNA of interest from patients or cell samples engineered with the CRISPR/Cas system, or plasmids used in cloning to generate stable heterologous cell lines, was determined by Sanger sequencing. First, DNA was purified from the patient's samples utilizing the Qiamp DNA Blood Mini Kit. Primers were designed for targets to amplify the DNA region of interest, employing the AmplifX software/algorithm. After amplification, excess primers and nucleotides were cleaned by enzymatic cleanup (alkaline phosphatase ExoSAP) of the amplified PCR fragment. The sequencing reaction was executed by Eurofins Genomics (Ebersberg) or GENEWIZ (Leipzig) service providers. Sequencing data analysis was conducted using ApE software (version 2.0.49).

4.22. Statistical Analysis

Statistical analysis of the experimental data was performed employing a two-tailed paired Student's t-test through GraphPad Prism version 6 (GraphPad Software, USA). Randomization and blinding techniques were not implemented, and no predetermined sample size was established for the analyses. The results are visually represented as mean values accompanied by the standard error of the mean (SEM). A significance threshold of $p < 0.05$ was employed, with values falling below this threshold considered statistically significant. Data were regarded as statistically insignificant unless explicitly stated otherwise.

5. RESULT

5.1. Identification of patients with *IL1RL2* deficiency and VEO-IBD

In a genome screening conducted in our laboratory, two unrelated IBD patients were identified with germline biallelic mutations in *IL1RL2*. The index patient (designated as A.II-1 or P1) with VEO-IBD was from Germany and was directed to us for genetic analysis at the age of 6 years. The second patient was from Iran (referred to as B.II-1 or P2).

Patient 1 (P1) presented with gastrointestinal manifestations, notably non-bloody diarrhea and a perianal fissure. Endoscopic examination revealed a spectrum of gastrointestinal involvement characterized by mild, non-specific antrum gastritis in the stomach, chronic moderate florid inflammation accompanied by ulceration and epithelial regeneration in the distal and terminal ileum, and moderate colitis affecting components of the large intestine with notable epithelioid cell aggregates observed in the ascending and transverse colon. Additionally, a solitary granuloma was identified. Hematological analysis indicated a decreased hemoglobin level (11.2 g/dl), while white blood cell count (7.13 cells/µl) and platelet count (2638 cells/µl) fell within normal parameters. Serum immunoglobulin levels remained within reference ranges (2.12 g/l IgA; 15.9 g/l IgG; 1.52 g/l IgM), although anti-Saccharomyces cerevisiae antibodies (ASCA) were positive, with antineutrophil cytoplasmic antibody (ANCA) and antinuclear antibody (ANA) tests yielding negative results. Therapeutically, the patient was managed with a regimen comprising anti-inflammatory and immunosuppressive agents. However, the patient exhibited intolerance to Azathioprine-induced pancreatitis before the age of 13, necessitating subsequent treatment with Methotrexate, which was discontinued due to adverse effects such as vomiting. Infliximab was administered until the age of 17, followed by Adalimumab until the age of 19, and subsequently, Golimumab from ages 19 to 22. Additionally, the patient received Ustekinumab therapy from ages 20 to 21. In pursuit of elucidating the genetic etiology underlying VEO-IBD in patients P1 and P2, we conducted WES analysis. This comprehensive genetic screening revealed a compound heterozygous missense mutation in P1, characterized by alterations at positions c.952A>G (resulting in p.Asn318Asp) and c.965A>C (resulting in p.Glu322Ala), as annotated by the reference sequence NM_001351446.2 and ENST00000264257.2. Concurrently, P2 exhibited a homozygous mutation at position c.12984C>T, located within a splice region.

To affirm the correlation of these sequence variants with the disease phenotype observed in P1 and P2, we conducted a Sanger sequencing analysis (Figure 7). In pedigree A (the index family),

the c.952A>G variant was inherited from A.I-1, while the c.965A>C variant was inherited from A.I-2. Notably, individual A.II-2 harbored the heterozygous c.952A>G variant. In pedigree B, individual B.II-1 (P2) exhibited a homozygous c.12984C>T variant, while parents exhibited a heterozygous variant.
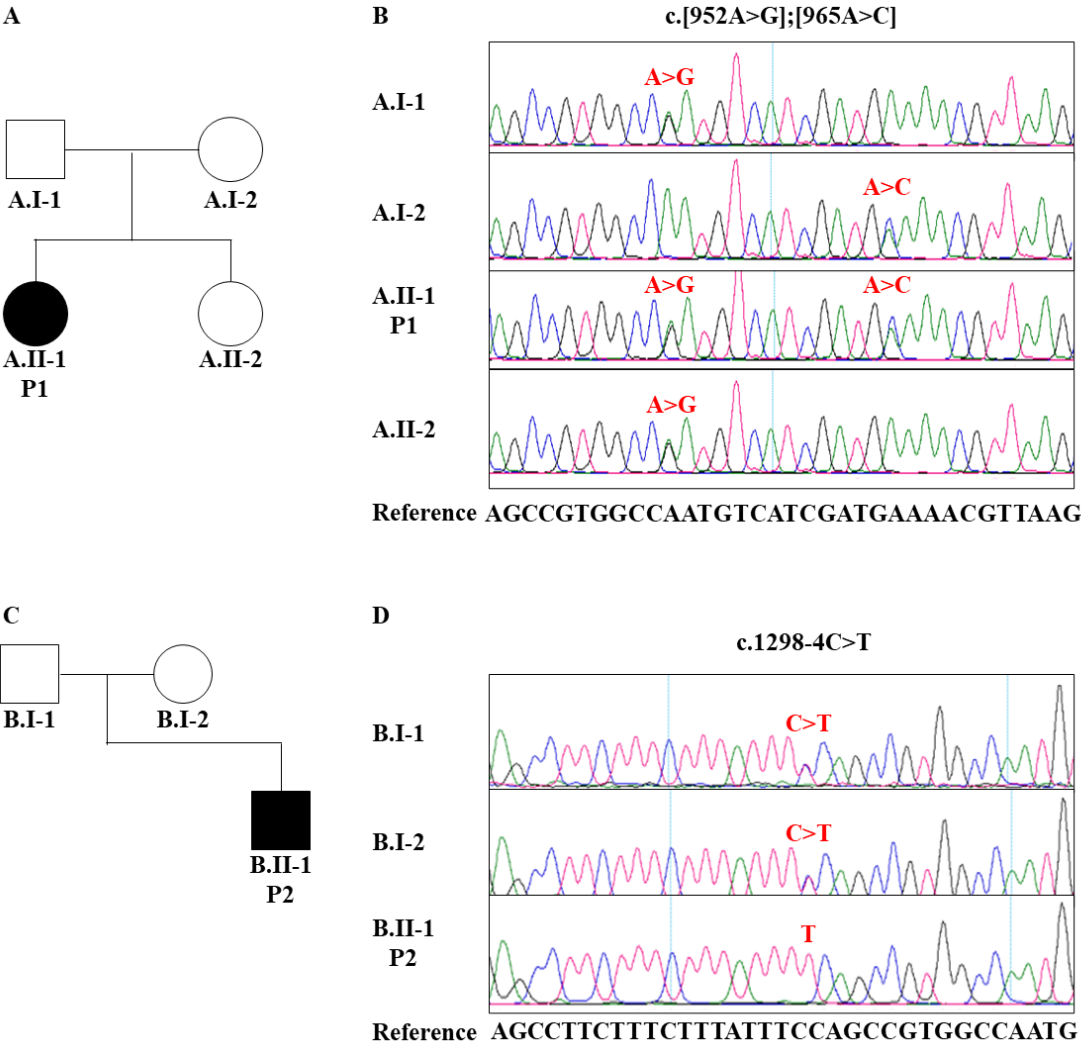

Figure 7: Segregation analysis of the *IL1RL2* mutations in the patients A. II-1 and B.II-1 by Sanger sequencing.
Sanger sequencing analysis confirmed that the compound heterozygous mutation (c.[952A>G];[965A>C]) of P1 in Pedigree A (A and B) and splice region mutation of P2 (c.12984C>T) in Pedigree B (C and D) are segregated from parents. In pedigree A, segregation analysis revealed the presence of the c.952A>G variant in individual A.II-2. Mutations are highlighted in red within the pertinent diagram and corresponding position.

5.2. Structural analysis of the identified IL1RL2 mutations in the index patient

The IL1RL2 receptor is synthesized as a heterodimer and both heterodimers have a toll-like domain [104]. The index patient's mutation affects the amino acids p.Asn318Asp and p. Glu322Ala in the TIR domain of IL1RL2. When iCn3D analysis was performed based on the SWISS model, it was determined that the surface area of the WT protein structure was 606.36 A, but in the presence of the p.Asn318Asp mutation, the surface area of the protein changed to 601.95 A and in the presence of the p. Glu322Ala variant, the protein surface area changed to 994.57A. In addition, while the distance between amino acids is 5 A in WT, it was measured as 5.1 A in the p.Asn318Asp and 6 A in p. Glu322Ala variants (Figure 8).
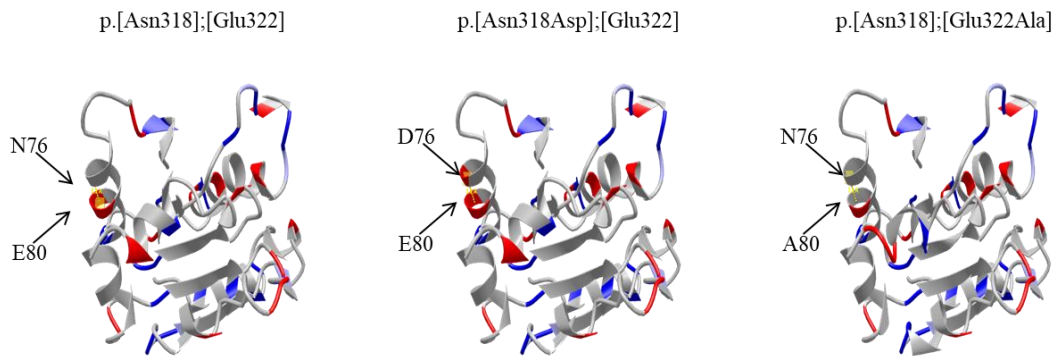

Figure 8: Modelling of the index patient mutation predicts structural variations.
The iCn3D analysis, which relies on the SWISS model is depicted in the picture. The core of the protein is depicted as ribbons, with coiled structures representing alpha-helices and flat structures representing beta-sheets. The gray color represents the backbone of the protein. Red denotes negatively charged amino acids, whereas blue represents positively charged amino acid residues. Arrows indicate the position of the variant in the index patient.

5.3. Analysis of NFκB and MAPK activation in the index patient with a compound heterozygous mutation

To evaluate whether the determined *IL1RL2* mutation of the index patient (P1; c.[952A>G];[965A>C]) has any effects on the phosphorylation of the NFκB and MAPK pathways in patient monocyte-derived macrophages, we conducted a Western blot on macrophages treated with IL-36β (100 ng/ml) for 0, 5, 15, and 30 min after 4 hours starvation. The Western blot analysis showed that the P1 exhibited reduced phospho-NFκB, p44/42 MAPK, and p38 compared to the father (c.[952A>G];[965A]) and HD (c.[952A];[965A]) (Figure 9).
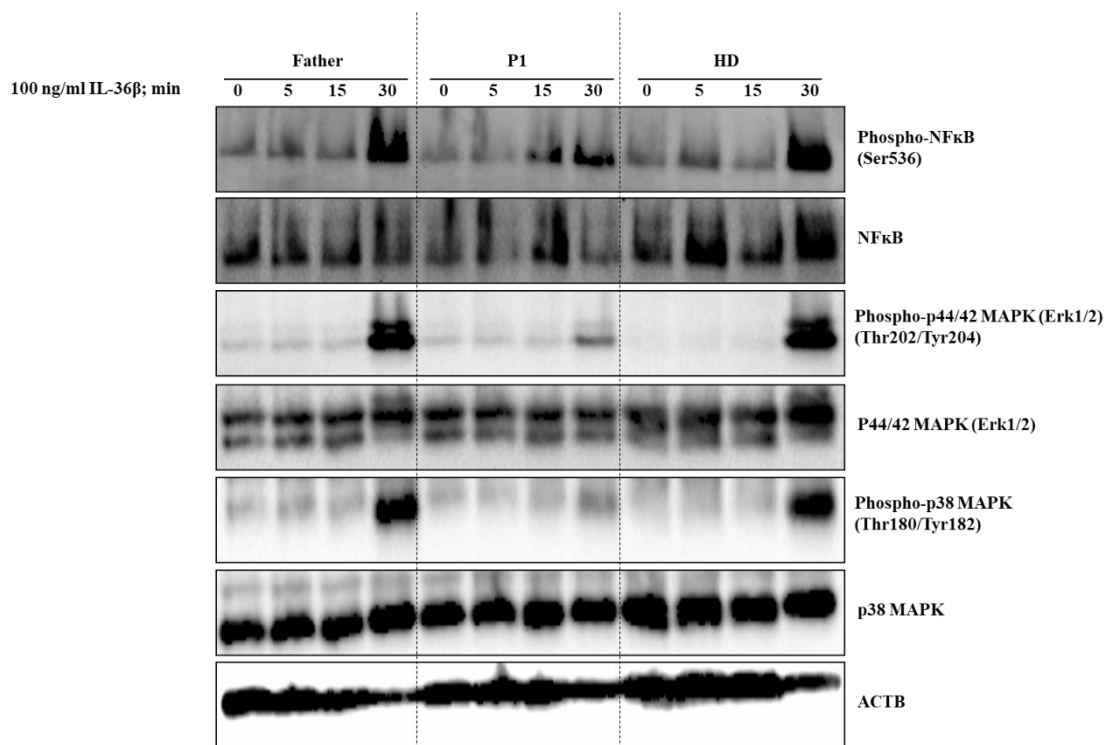

Figure 9: The phosphorylation of NFκB and MAPK was reduced in P1.
Western blot analysis was performed on primary monocyte-derived macrophages following stimulation with IL-36β to evaluate phosphorylation of NFκB, -P44/42 ERK1/2, and -p38 proteins in (n=1). In the patient cells (P1), phosphorylation levels of NFκB, p44/42 ERK1/2, and p38 were found to be lower compared to phosphorylation in the father and the healthy donor (HD).

5.4. Evaluation of inflammatory gene expression in the patients

The IL1RL2 receptor pathway influences the expression of various proinflammatory genes, including *IL6*, *IL8,* and *CXCL10*, through the NFκB and MAPK pathways. To demonstrate whether the index P1's mutation affects the expression of proinflammatory genes, we stimulated DCs derived from the patient's monocytes with IL-36β (100 ng/ml) for 2 or 4 hours.

Our findings revealed higher basal expression levels of *IL6* and *IL8* in the patient compared to the HD and the father. Moreover, upon IL-36β stimulation, *IL6* and *IL8* expression were elevated in the patient (c.[952A>G];[965A>C]) in comparison to the HD (c.[952A];[965A]) (Figure 10).
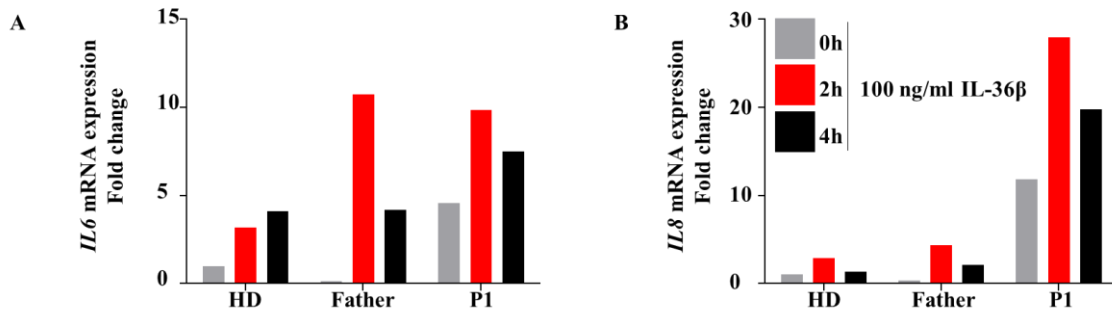

Figure 10: Evaluation of proinflammatory inflammatory gene expression in P1 in monocytes derived dendritic cells by real-time PCR.
The DCs derived from primary monocytes were treated with IL-36β (100 ng/ml) for 2 and 4 hours (n=1). Fold changes in *IL6* expression (A) and *IL8* expression (B) are shown. IL6 and IL8 expression were higher in the P1 in comparison to the healthy donor (HD).

To determine how the mutation affected the *IL6* expression in the P2 patient, we stimulated the DCs derived from monocytes with IL-36β (100 ng/ml) for 4 hours. We found that *IL6* expression in P2 was higher at the basal level and after stimulation than the HD, mother, and father (Figure 11).
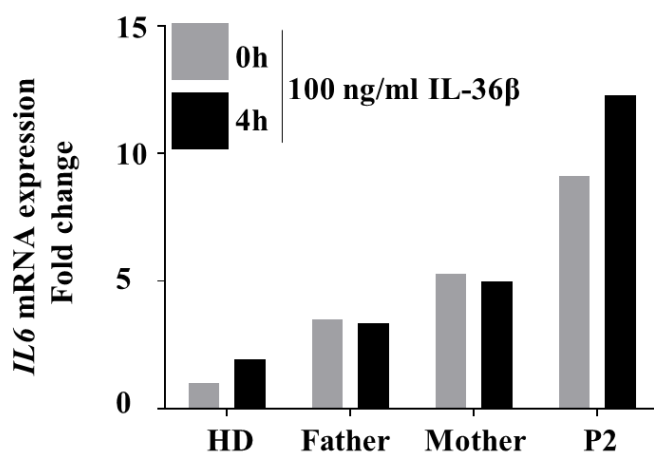

Figure 11: *IL6* expression was increased in P2.
IL6 expression was analyzed in derived DCs derived primary monocytes stimulated with IL-36β (100 ng/ml) for 4 hours. *IL6* expression was higher in P2 compared to healthy donor (HD) (n=1).

To analyze whether *CXCL10* expression was affected by the P1, we stimulated the patient's DCs derived from monocytes with IL-36β (100 ng/ml) for 2 or 4 hours. We found that *CXCL10* expression was lower in the index family than in the HD. In addition, we found that *CXCL10* expression was lower in the patient compared to family members (Figure 12).
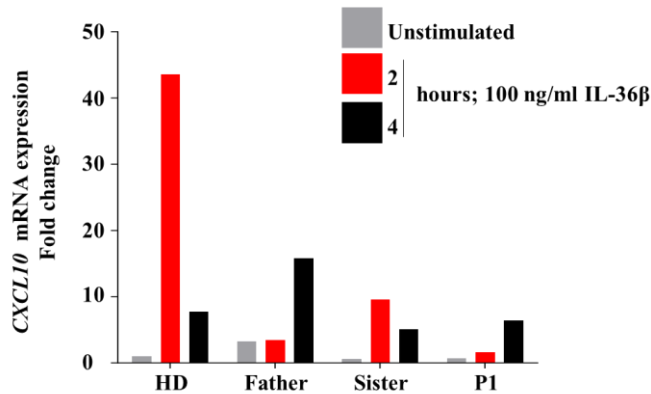

Figure 12: *CXCL10* expression was diminished in the P1.
The analysis of *CXCL10* expression was conducted in DCs derived from primary monocytes after stimulation with IL-36β (100 ng/ml) for durations of 2 and 4 hours (n=1). *CXCL10* expression was less in P1, Sister, and Father compared to healthy donor (HD).

5.5. Analysis of macrophage polarization in the index patient with compound heterozygous mutation

To evaluate the impact of the index patient mutation on macrophage activation, primary monocytes were differentiated into macrophages over 7 days. Subsequently, these macrophages were polarized into M1 pro-inflammatory or M2 anti-inflammatory states for 24 hours. Macrophage activation markers CD14, CD274, CD273, CD163, CD86, and HLA-DR were analyzed using FACS. Our findings indicated that CD14 expression was decreased in both P1 and the sister across M0, M1, and M2 macrophages. The expression of CD274 remained unchanged in activated macrophages of P1. CD273 expression was diminished in both P1, and the sister compared to HD in M0 resting and M2 anti-inflammatory macrophages, although no change was observed in M1 macrophages. CD163 expression was decreased in both P1 and the sister in M0, M1, and M2 macrophages. Additionally, CD163 expression was specifically reduced in M0 resting and M2 anti-inflammatory macrophages of P1 but not in M1 macrophages. CD86 expression was increased in M0 and M2 macrophages only in P1, with no changes observed in M1 macrophages compared to HD. Although HLA-DR expression increased in both the father and the sister, the increase was more pronounced in P1 (Figure 13).
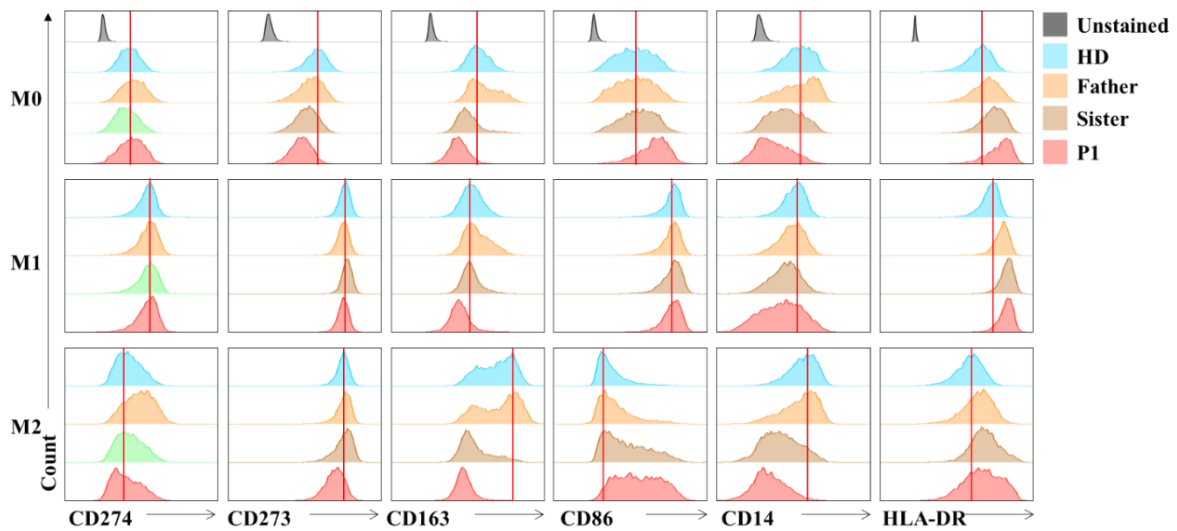
Figure 13: Index patient mutation affected monocyte-derived macrophage activation.
FACS analysis was conducted to assess macrophage subtype-specific markers CD274, CD273, CD163, CD86, CD14, and HLA-DR in patient-derived monocytes (n=1). In M0 resting macrophages, the expression of CD273, CD163, and CD14 was reduced in both Patient 1 (P1) and their sibling. Conversely, CD86 and HLA-DR expression levels were elevated in both P1 and the sibling. In M1 macrophages, CD14 expression was decreased in P1 and slightly in the sibling. However, HLA-DR expression increased in P1, the sibling, and the father. In M2 macrophages, CD163 and CD14 expression decreased in both P1 and the sibling. On the other hand, HLA-DR and CD86 expression levels were increased in P1 and slightly in the sibling compared to healthy donor (HD).

5.6. Investigation of *IL1RL2* mutations on macrophage differentiation from iPSC

Accessing patients' primary cells is challenging due to both the clinical conditions of the patients and the difficulty in transporting the patient material to our facility. Therefore, patient mutations were successfully generated in iPSC by using the CRISPR/Cas9 system. The clones with encoding for the patient mutation (Figure 14A) and with KO clone with delCACAG in exon 5 (Figure 14B) were confirmed by Sanger sequencing.
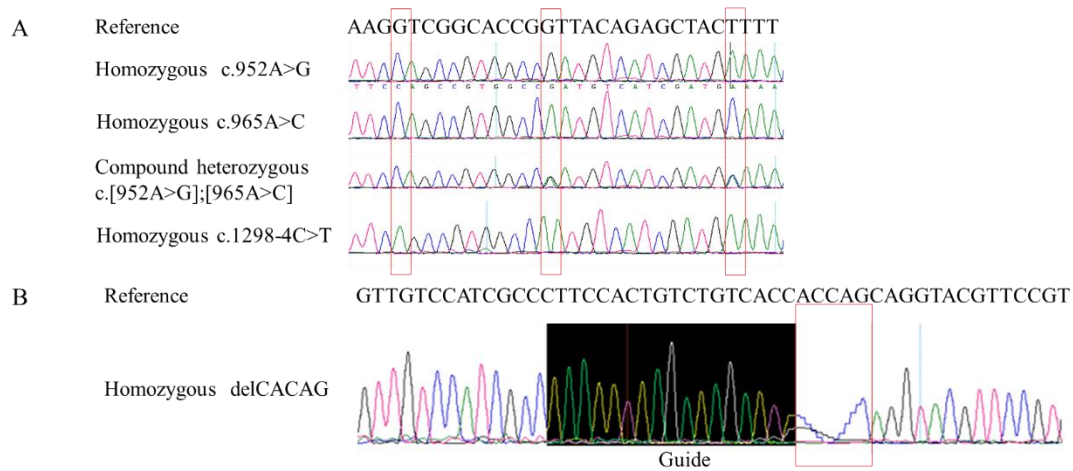
Figure 14: Confirmation of clones with patient mutations generated with CRISPR/Cas system. The Sanger sequencing results of KI clones with the patient's mutation are shown in the A, while the KO clone is in the B. The location of the mutation is indicated by the red rectangle.

The differentiation efficiency of iPSCs into macrophage cells was evaluated using FACS analysis at 12, 15, and 18 days (Figure 15). On day 12, most CD45$^+$ hematopoietic cells derived from iPSCs expressed CD34, a stem cell marker, and CD33, a myeloid lineage marker. At this early stage, CD14 expression was low compared to the late stage of the differentiation on day 15 and 18. By day 15, CD45$^+$ cells also expressed CD33 (99% CD33$^+$). Additionally, CD14 expression increased significantly, with 76-85% of cells expressing CD14. Since the CD33$^+$ population had already reached 100% on day 15, only CD45 and CD14 expressions were analyzed on day 18. At this stage, CD14 expression reached approximately 100%.

Throughout the differentiation process, patient variants did not affect the expression of CD33, CD34, or CD14. The timing and efficiency of differentiation were consistent across all variants. These findings indicate a robust and reproducible protocol for macrophage differentiation from iPSCs. The data suggest that patient-specific variants in *IL1RL2* do not alter the differentiation timeline or marker expression.
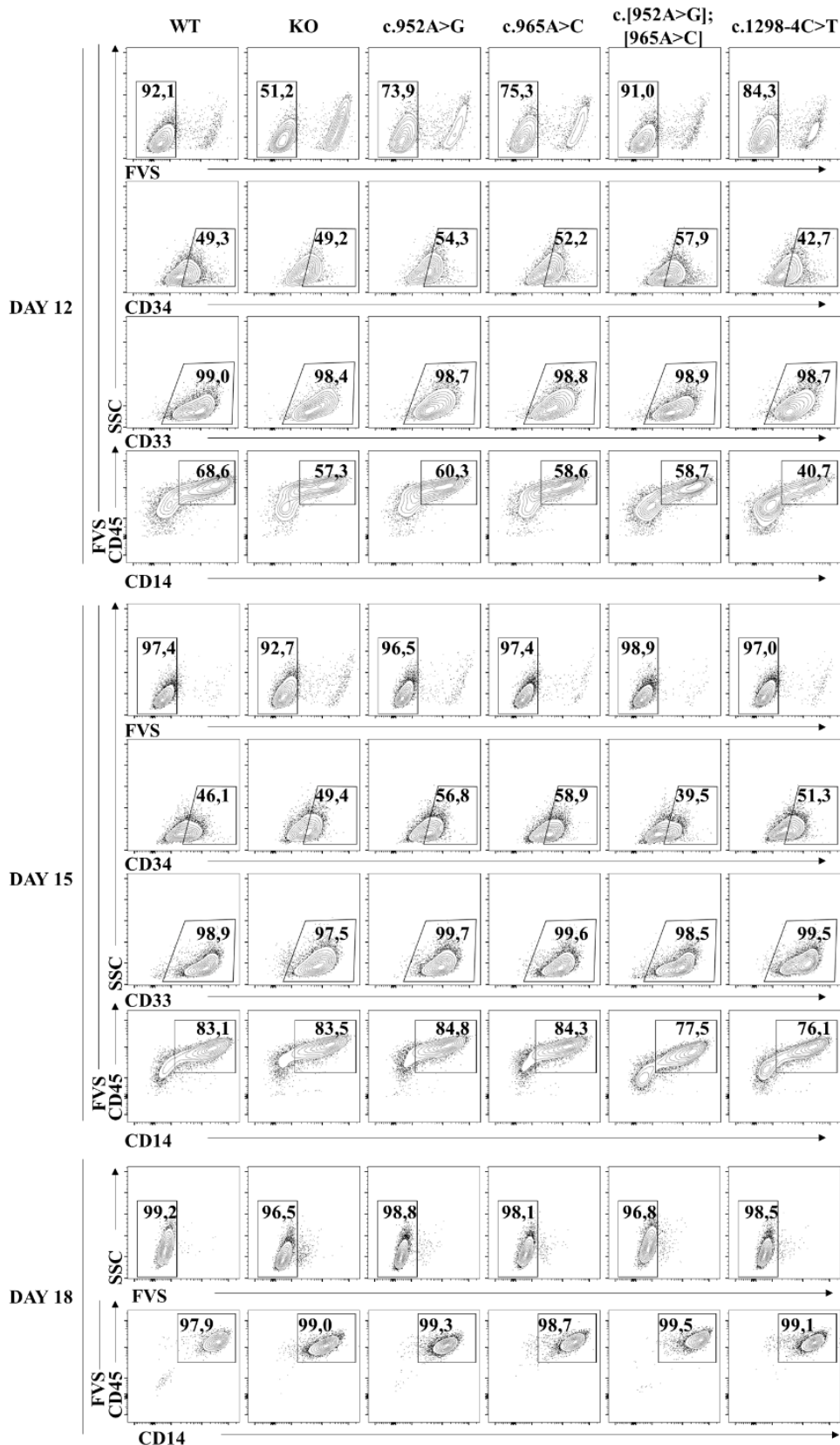
Figure 15: Characterization of the macrophages differentiated from iPSC.
A demonstrative FACS analysis of hematopoietic cell surface markers throughout the maturation process of macrophages from WT, KO, and patient-specific mutation expressing iPSCs, namely P1 and P2, exhibits the effective generation of $CD45^+ CD14^+$ monocytes or macrophages over time (n=3).

To evaluate the impact of the index patient mutation (P1; c.[952A>G];[965A>C]) and the second patient mutation (P2; c.1298-4C>T) on macrophage differentiation, we conducted a CFU assay on day 9 of macrophage differentiation to assess the total number of macrophage colonies. The results indicated that the majority of cells formed were macrophages. Notably, the total number of colonies significantly decreased in KO cells (*p<0.0001) and significantly increased in cells with the second patient mutation (*p=0.0432; c.1298-4C>T) compared to the WT controls. Although a comparable increasing trend in the colony number was observed in cells with the index patient mutation, this difference was not statistically significant (Figure 16).
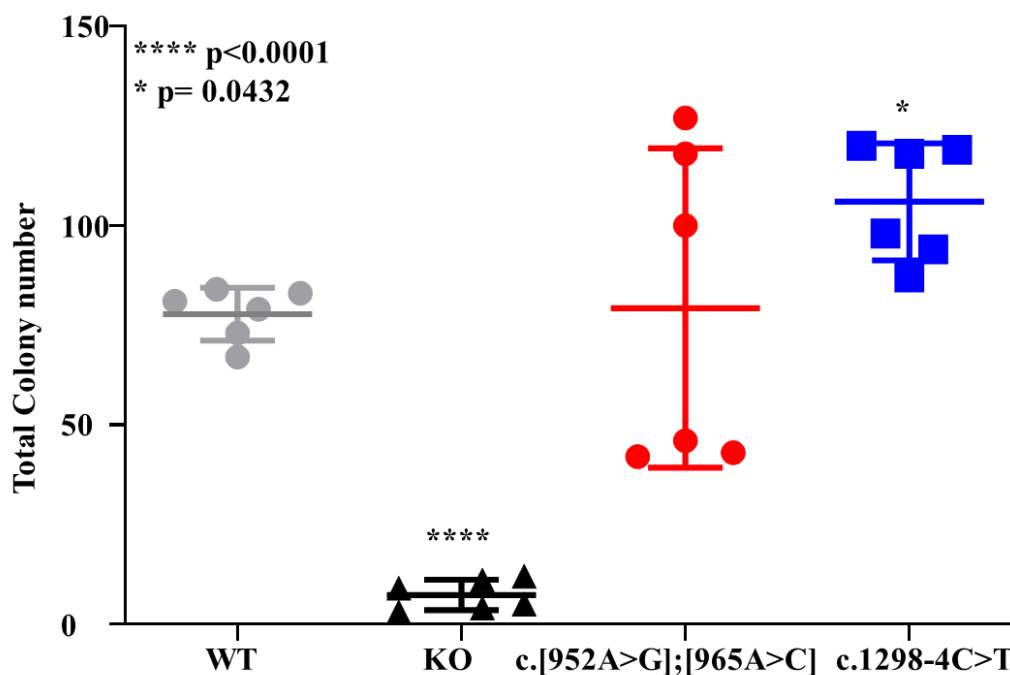

Figure 16: The number of colonies was affected by *IL1RL2* deficiency in iPSC.
The human colony-forming assay in iPSC-derived hematopoietic cells with patient variants is depicted (n=2). The knock-out (KO) cells form colonies with a significant decrease (****p<0.0001), while the increase in colonies for the c.[952A>G];[965A>C] variant is not statistically significant. Cells expressing the c.1298-4C>T variant form significantly increased colonies (p=0.0432).

5.7. Examination of the impact of *IL1RL2* mutations on the polarization of macrophages derived from iPSCs

On day 18 of monocyte differentiation from iPSCs, CD14^{+} monocytes were selectively enriched and subsequently differentiated into macrophages for 7 days. Subsequently, these macrophages were polarized into either M1 proinflammatory or M2 anti-inflammatory

phenotypes for 24 hours. Using FACS, we examined the expression levels of macrophage polarization markers including CD274, CD273, CD86, CD14, and HLA-DR.

Our analysis revealed a reduction in CD274 expression within *IL1RL2* deficient M0 resting macrophages (KO, c.952A>G, c.965A>C, c.[952A>G];[965A>C], and c.1298-4C>T) compared to WT cells. However, this reduction was not observed in either M1 or M2 macrophages.

Similarly, CD273 expression decreased in M1 cells displaying *IL1RL2* deficiency (KO, c.952A>G, c.965A>C, c.[952A>G];[965A>C], and c.1298-4C>T) compared to WT cells. Notably, CD273 expression increased only in M2 anti-inflammatory cells carrying the c.[952A>G];[965A>C] mutation compared to WT cells. No notable variances in CD273 expression were seen in M0 macrophages.

CD86 expression exhibited an increase solely in M1 and M2 macrophages displaying the c.[952A>G];[965A>C] mutation compared to WT cells.

Furthermore, CD14 expression decreased in both M0 resting and M1 proinflammatory macrophages exhibiting *IL1RL2* deficiency (KO, c.952A>G, c.965A>G, c.[952A>G];[965A>C], and c.1298-4C>T), while it remained unchanged in M2 macrophages.

Regarding HLA-DR expression, M0 macrophages displayed an increase in expression levels in both KO and homozygous c.952A>G cells, while expression remained unaltered in homozygous c.965A>C cells and compound heterozygous c.[952A>G];[965A>C] cells. Conversely, a noticeable shift in HLA-DR expression was evident in polarized macrophages harboring the c.1298-4C>T mutation. In M1 cells, HLA-DR expression exhibited a reduction across all variants except for c.[952A>G];[965A>C] compound heterozygous mutations. However, no alterations were observed in M2 cells (Figure 17).
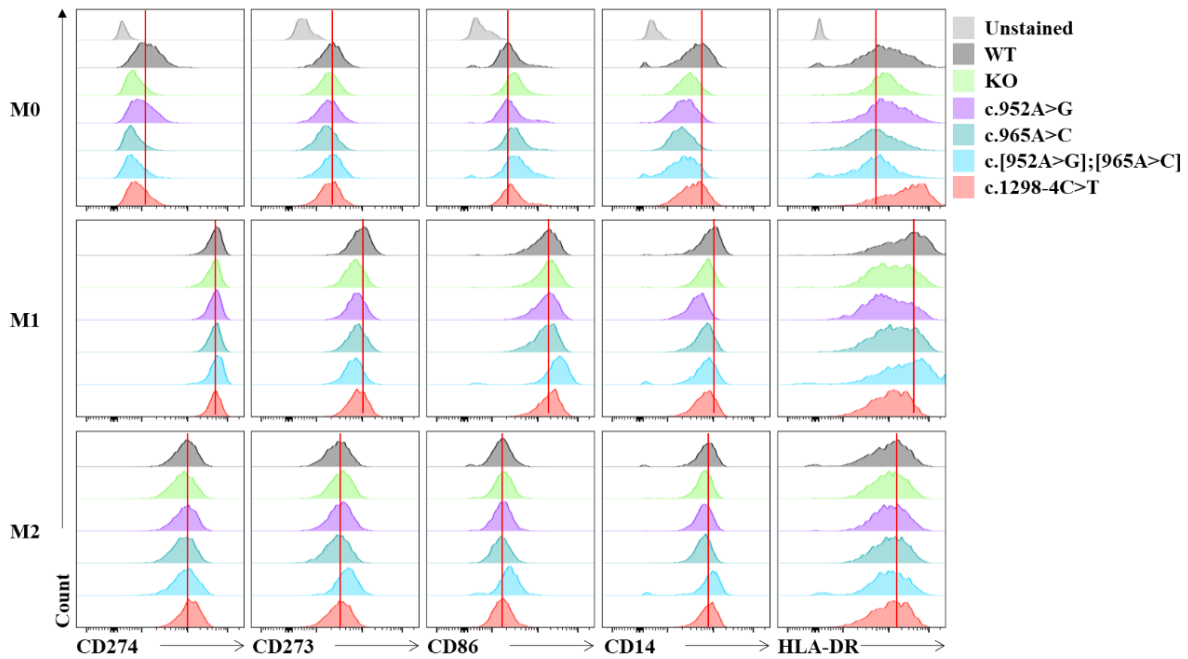
Figure 17: *IL1RL2* variants affected activation of iPSC-derived macrophages.
FACS analysis of macrophage subtype-specific markers CD274, CD273, CD86, CD14, and HLA-DR was performed in knock-out (KO), P1 (c.[952A>G];[965A>C]), and P2 (c.1298-4C>T) variant-expressing iPSC-derived macrophages. In M0 resting macrophages, the expression of CD274 and CD14 was decreased in all cells expressing *IL1RL2* variants compared to wild-type (WT) cells. HLA-DR expression was higher only in M0 cells expressing the c.1298-4C>T variant. In M1 cells, the expression of CD273, CD14, and HLA-DR was decreased in all cells expressing *IL1RL2* variants compared to WT cells. In M2 cells, CD14 expression was slightly decreased in all cells expressing *IL1RL2* variants compared to WT cells (n=3).

5.8. Investigation of inflammasome activation in iPSC-derived macrophages expressing index patient variants

IL-36 cytokines, including IL-36α, IL-36β, and IL-36γ, are known for their ability to induce the activation of the NLRP3 inflammasome, which represents a pivotal step in the production of inflammatory cytokines such as IL-1β and IL-18. Notably, research has demonstrated that IL-36γ can initiate NLRP3 inflammasome activation in macrophages via a TLR4/MyD88-dependent pathway, resulting in the generation of mature IL-1β, thus amplifying the inflammatory cascade [137]. In order to investigate how the mutations c.952A>G and c.965A>C impact inflammasome activation, we primed iPSC-derived macrophages with either IL-36γ or LPS. Following this priming step, the cells were subjected to a 3-hour treatment with Nigericin. Our analysis revealed a similar upregulation in both IL-1β production and its cleavage following stimulation with IL-36γ or LPS, irrespective of whether the cells were WT

or mutated. These findings suggest that, under these experimental conditions, the studied mutations did not significantly alter the inflammasome activation pathway (Figure 18).
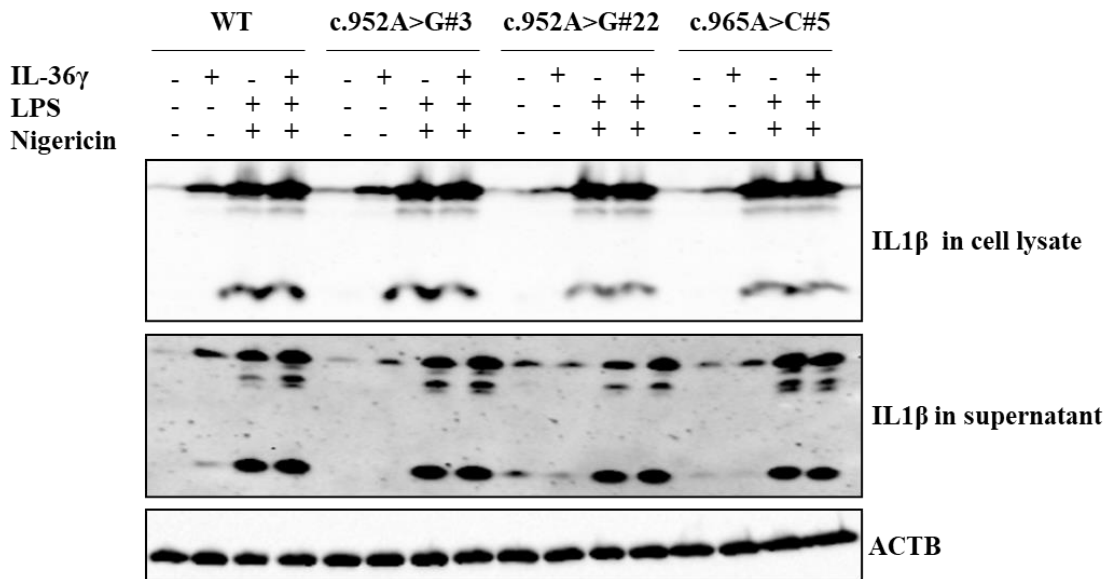

Figure 18: Inflammasome activation upon IL-36γ or LPS stimulation was not affected by index patient variants in iPSC-derived macrophages.
Western blot analysis of inflammasome activation (n=2). The iPSC-derived macrophages were primed with LPS or IL-36γ for 3 hours, followed by treatment with 6.5 μM Nigericin for 30 minutes. Semiquantitative immunoblots were reacted with anti-IL-1β and anti-ACTB antibodies. No difference was observed in inflammasome activation between wild-type (WT) cells and cells expressing the c.952A>G or c.965A>C variants.

5.9. Analysis of NFκB and MAPK activation in HCT116 cells overexpressing index patient variants

IL1RL2 is expressed in epithelial cells and is known to activate pathways such as NFκB and p38 [85, 89]. To investigate the impact of the index patient's mutations on the NFκB and p38 pathways, the patient's mutation was generated in *IL1RL2* cDNA by SDM and transduced into HCT116 colon carcinoma cells by the lentiviral transduction method. The transduction efficiency was confirmed both by measuring the expression of RFP by FACS and by analyzing *IL1RL2* expression by the qPCR method. The transduced cells were RFP[+] compared to plain cells. In addition, *IL1RL2* expression in WT and homozygous mutant cells reached 2500-4000-

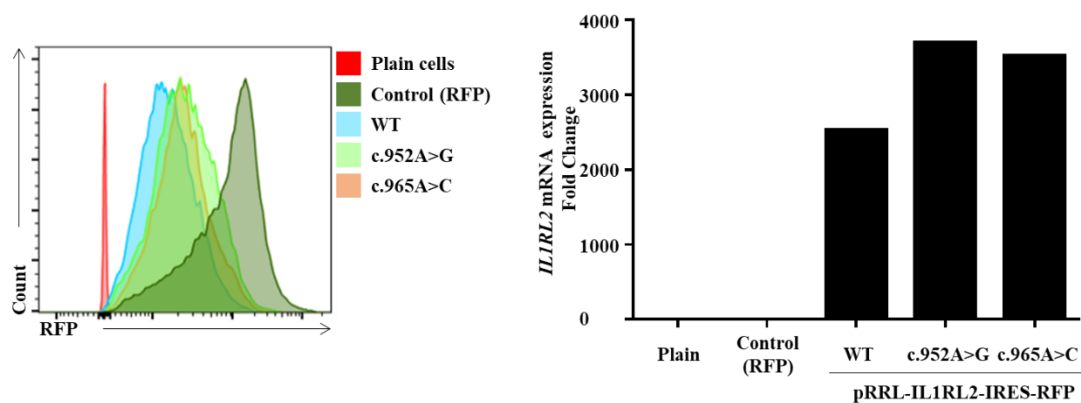fold   change   compared   to   plain   cells   (Figure   19).

Figure 19: Confirmation of transduction efficiency by FACS and qPCR.
FACS analysis of transduction efficiency by measuring RFP (A). qPCR analysis of *IL1RL2* showing the transduction efficiency (B). Plain cells were not transduced. Control cells were transduced only with empty pRRL-IRES-RFP plasmid. c.952A>G and c.965A>C showing transduction of index patient variants (n=2).

HCT116 cells overexpressing the variants of the index patient (P1) were starved for 20 hours and then induced with IL-36γ (100 ng/ml) for 0, 5, and 15 minutes. NFκB and p38 activation were analyzed using the Western Blot. We found that NFκB and p38 pathways were not activated upon IL36γ stimulation in control cells transduced with RFP alone. Although NFκB and p38 phosphorylation increased in WT and c.952A>G variant-expressing cells after 5 minutes, we did not observe an activation in c.965A>C variant-expressing cells. We found that there was no difference between WT and c.952A>G variant-expressing cells after 5 minutes of stimulation. Although phosphorylation increased in both WT and c.952A>G variant-expressing cells after 15 minutes of stimulation, both NFκB and p38 phosphorylation increased more in c.952A>G cells than in WT. However, NFκB and p38 activation are lower in c.965A>C variant-expressing cells than in WT and c.952A>G cells after 5 and 15 minutes of activation (Figure 20).
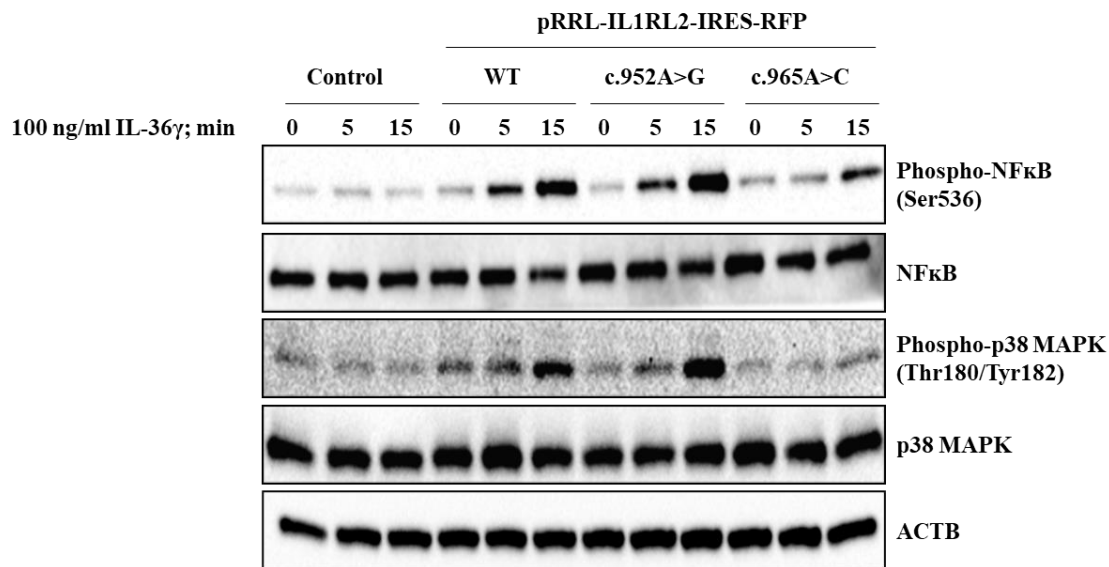
Figure 20: NFκB and p38 activation changed in HCT116 cells overexpressing index patient (P1) variant.
Western blot analysis of NFκB and p38 MAPK in HCT116 cells induced with IL-36γ (100 ng/ml) for 5- and 15 minutes following 20 hours of serum starvation (n=4). The Semiquantitative immunoblots reacted with anti-phospho- NFκB, - total NFκB, phospho-p38, -total p38, and -ACTB antibodies.

5.10. Analysis of cell death in HCT116 cells overexpressing index patient variants

Numerous investigations have indicated that disrupted epithelial cell death plays a pivotal role as a pathogenic element in intestinal inflammation. [138]. To evaluate epithelial cell death response, we analyzed the apoptosis in HCT116 colon carcinoma cells overexpressing *IL1RL2* index patient variants. The cell death was induced with TNF-α and cycloheximide for 0, 2, and 6 hours under both wounded and unwounded conditions. Apoptosis was assessed by the Annexin V/DAPI method.

Under unwound conditions, we did not observe differences after 2 hours but early apoptotic cells (Annexin V$^+$/DAPI$^-$ cells) were increased after 6 hours. The early apoptotic cell number was higher in the cells expressing c.965A>C variant (70.1%) compared to WT cells (55.9%) after 6 hours. Although the percentage of early apoptotic cells increased in cells expressing the c.952A>G variant, it remained lower than that in the WT cells.

On the contrary, under wound conditions, we observed an increased apoptotic cell numbers (Annexin V$^+$/DAPI$^+$) in the c.952A>G variant expressing cells (13.6%) and c.965A>C variant-expressing cells (30.3%) compared to WT (0.33%) and control cells (0.84%). We found more early apoptotic cells in the c.965A>C variant-expressing cells (41.3%) compared to WT (15.3%) or c.952A>G variant-expressing cells (23.7%) (Figure 21).
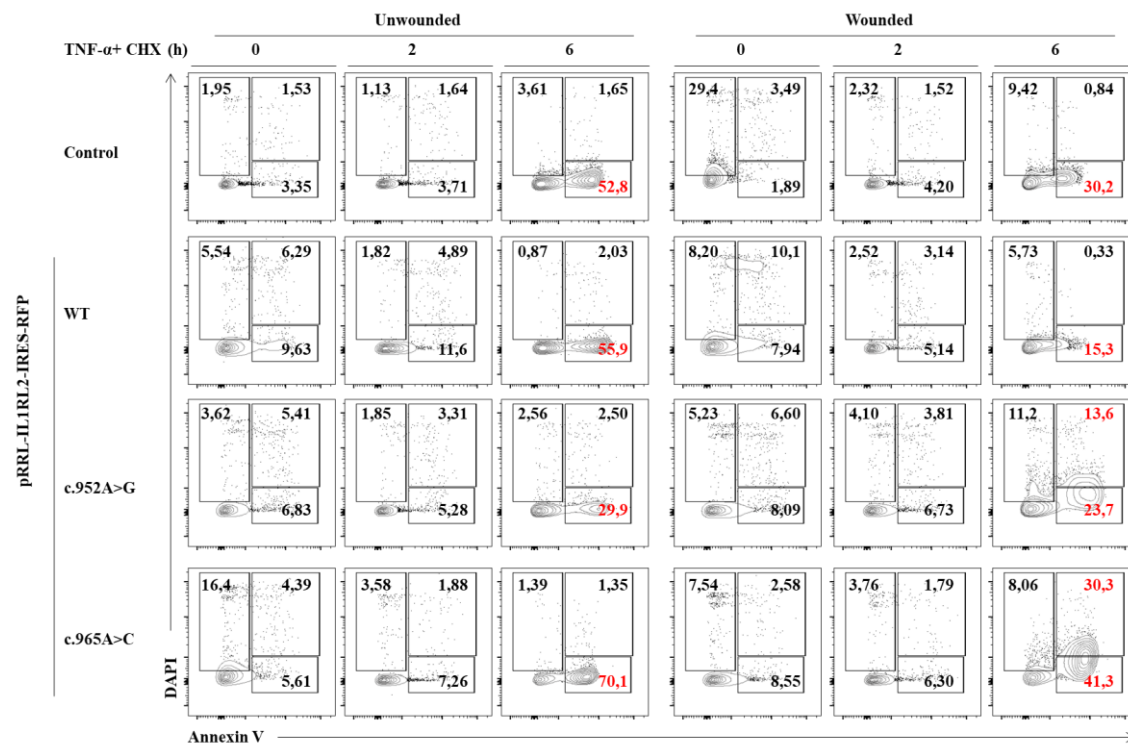
Figure 21: c.952A>G and c.965A>C variants affected cell death in HCT116 cells.
FACS analysis of cell death by using Annexin V/DAPI staining in HCT116 cells expressing index patient variants (c.952A>G and c.965A>C treated with TNF-α and CHX for 2 and 6 hours (n=1). Annexin V^+/DAPI$^-$ signifies early apoptotic cells, while Annexin V^+/DAPI$^+$ indicates late apoptotic cells. Annexin V^-/DAPI$^+$ indicates dead cells, whereas Annexin V^-/DAP^{I-} signifies viable cells.

5.11. Investigation of wound healing and *CCL20* expression in HCT116 cells overexpressing index patient variants

Several studies have shown that the IL1RL2 pathway contributes to the healing of colon wounds by activating the NFκB and MAPK pathways [85, 91, 139]. To investigate the effect of mutations of the index patient on wound healing, we transduced the HCT116 colon carcinoma epithelial cell line with index patient variants by lentiviral transduction methods. The wounds were created on the cells using the scratch assay method. The cells with wounds were stimulated with IL-36γ. Phase contrast images were captured at 24-hour intervals to observe the progression of wound healing. The control cells are transduced with an empty plasmid, expressing only the RFP fluorescent gene as control of the transduction. We observed that the wound closure occurred in WT cells at 24 hours (p=0.028) and was nearly complete at 48 hours (p=0.0009) in comparison to control cells. While wound healing was observed in cells expressing the c.952A>C and c.965A>G variants, it was not completed. Upon stimulation with IL-36γ, the wounded cells showed closure of the wound after 48 hours in WT cells (p=0.0227).

Conversely, the process of wound healing was delayed in cells expressing the c.952A>C or c.965A>G variants, as well as in control cells, in comparison to WT cells (Figure 22).
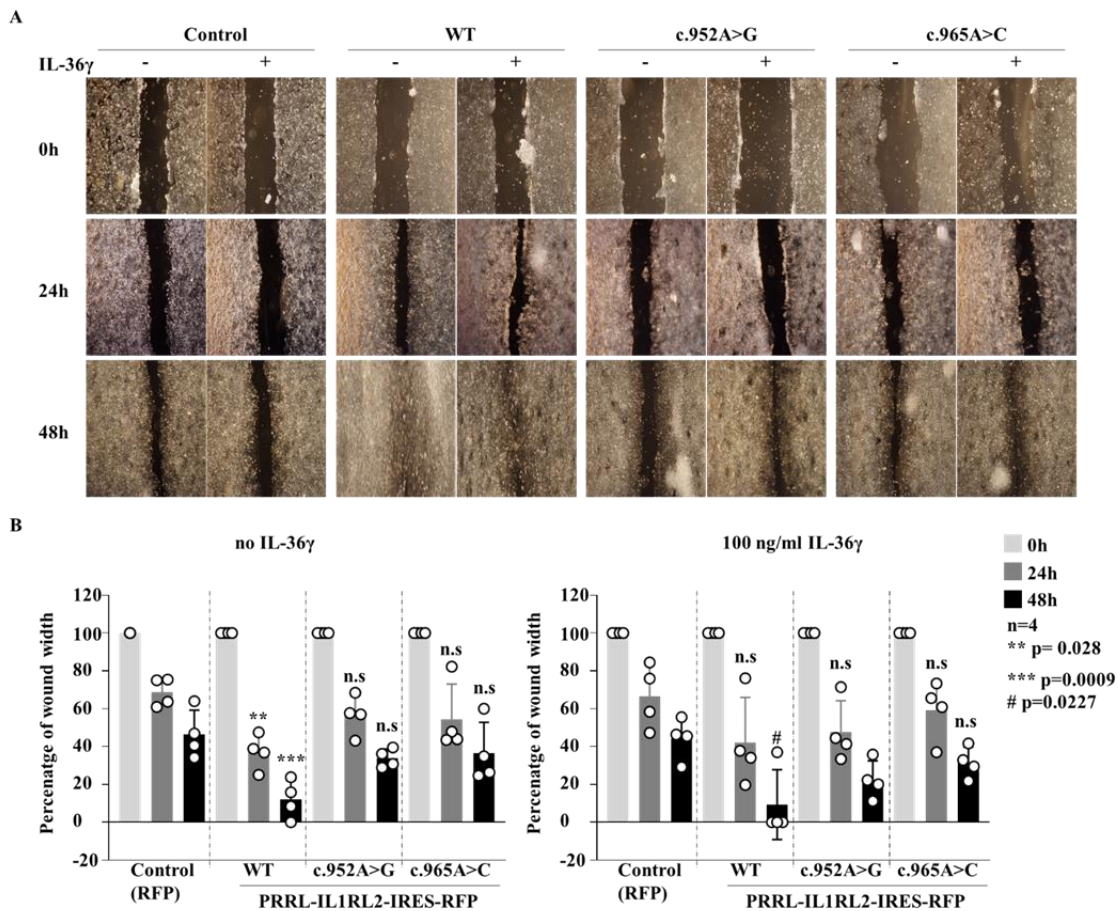

Figure 22: Index patient variants affected wound healing in the HCT116 colon carcinoma cells.
Phase contrast images of the scratch assay were used to monitor wound healing in HCT116 cells expressing index patient variants over time (n=4) (A). Quantitative analysis of wound width showed that the wound closed in wild-type (WT) cells under both conditions: without IL-36γ (**p=0.028 for 24 hours; *p=0.0009 for 48 hours) and with 100 ng/ml IL-36γ (#p=0.0227 for 48 hours). However, wound healing was delayed in cells expressing the c.952A>G or c.965A>C variants compared to WT cells (B).

It has been shown in various studies that CCL20 contributes to wound healing in epithelial cells [140]. We found that *CCL20* expression was increased in both WT and mutant cells after IL-36γ stimulation, and the increase was higher in cells expressing the c.952A>G variant than in WT (p<0.0001 for unwounded conditions and p=0.0052 for wounded conditions). Although the expression in unwounded and wounded cells was less in c.965A>G variant expressing cells than in the c.952A>G variant expressing cells, we did not observe any significant difference in comparison to WT cells (Figure 23).
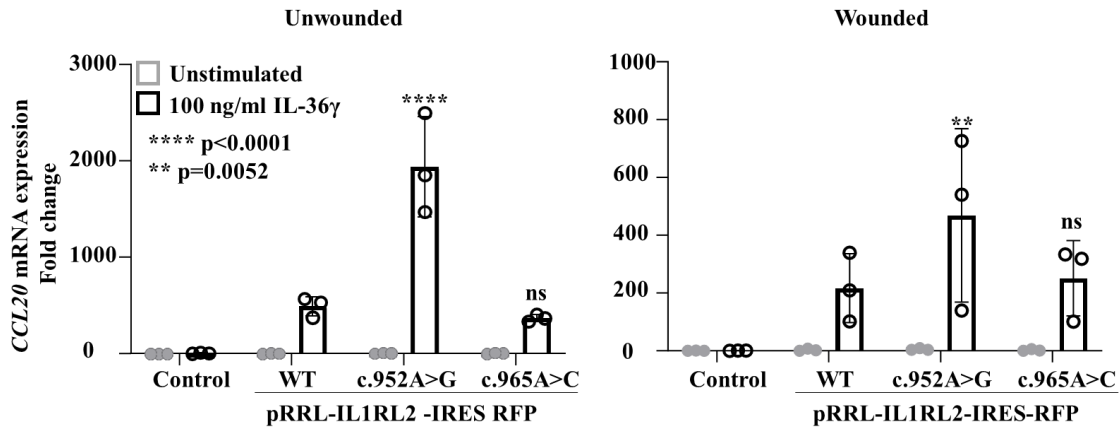
Figure 23: c.952A>G mutation affected *CCL20* expression in HCT116 colon carcinoma cells.
qPCR analysis was conducted to assess CCL20 expression in HCT116 cells expressing index patient variants (n=3). The cells were induced with IL-36γ (100 ng/ml) for 24 hours. A significant increase in CCL20 expression was observed in cells expressing the c.952A>G variants under both unwounded (****p>0.0001) and wounded (**p=0.0052) conditions compared to wild-type (WT) cells. However, the increase in cells expressing the c.965A>C variant was insignificant compared to WT cells.

5.12. Investigation of wound healing and *CCL20* expression in iPSC-derived colonic organoids expressing *IL1RL2* variants

To examine the effects of the index (P1) and second patient (P2) mutations on intestinal epithelial cells, we generated a 3D and monolayer colonic organoid model differentiated from iPSC genetically engineered with patient mutations (c.[952A>G];[965A>C] or c.1298-4C>T) by using the CRISPR/Cas9 engineering system.

First of all, we analyzed the effect of c.[952A>G];[965A>C] index patient mutation (P1) and c.1298-4C>T mutation (P2) on the *IL1RL2* and *CCL20* expression. We found that *IL1RL2* expression increased in both c.[952A>G];[965A>C] (***p=0.0004) and c.1298-4C>T (**p=0.029) mutated colonic organoids compared to WT organoids. However, *CCL20* expression increased in just c.1298-4C>T mutant organoids compared to WT cells (p<0.0001) (Figure 24).
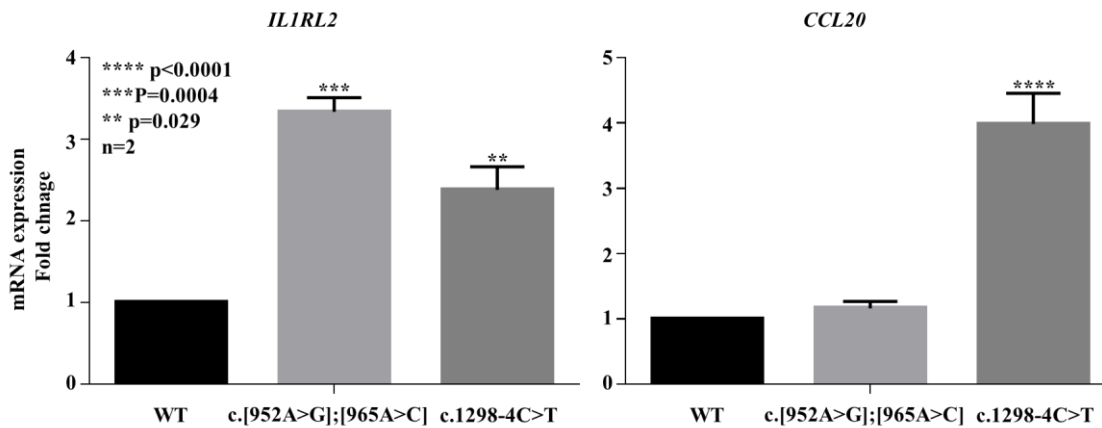
Figure 24: Basal level of *IL1RL2* and *CCL20* expression is higher in iPSC-derived colonic organoids.

qPCR analysis of *IL1RL2* and *CCL20* in iPSC-derived 3D colonic organoids (n=2). *IL1RL2* expression was higher in c.[952A>G];[965A>C] (***p=0.0004) and c.1298-4C>T (**p=0.029) compared to wild-type (WT) cells. *CCL20* expression was higher in c.1298-4C>T variants expressing cells (****P>0.0001) compared to WT cells but there was no difference between c.[952A>G];[965A>C] variant expressing cells and WT.

The 3D organoid was treated with IL-36γ (100 ng/ml) for 4, 8, and 24 hours, and *CCL20* expression was analyzed by qPCR. As shown in Figure 25, we found that *CCL20* expression was significantly increased in cells with c.1298-4C>T (P2) mutation compared to WT cells after IL-36γ stimulation (** p=0.0021 for 4 hours; ## p=0.0013 for 8 hours; ++ p=0.0058 for 24 hours). Although cells expressing the c.[952A>G];[965A>C] compound heterozygous mutation (P1) showed increased *CCL20* expression; the observed discrepancy did not reach statistical significance.
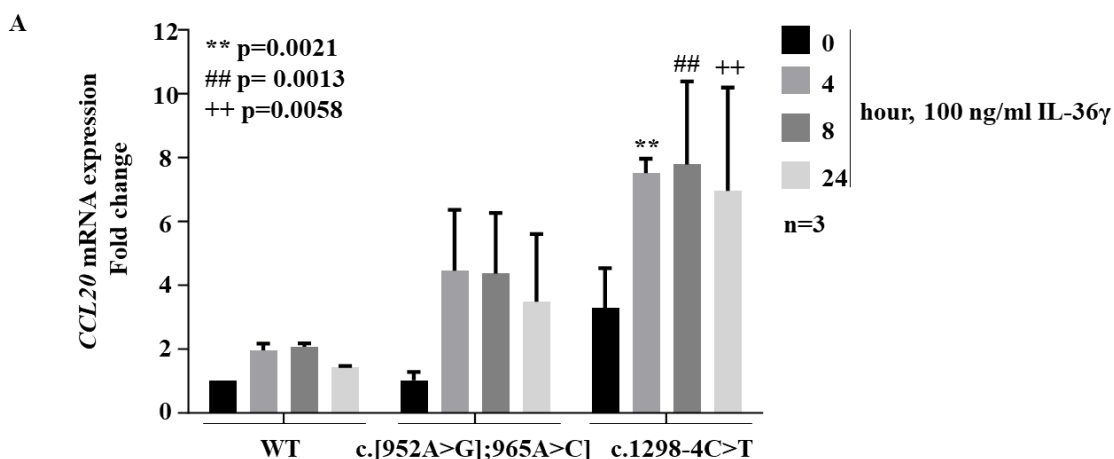

Figure 25: *CCL20* expression altered in iPSC-derived 3D colonic organoids.

qPCR analysis of *CCL20* in iPSC-derived 3D colonic organoids stimulated with IL-36γ for 4, 8, and 24 hours. *CCL20* expression increased in organoids expressing the c.1298-4C>T variant (**p=0.0021 for 4 hours; ##p=0.0012 for 8 hours; ++p=0.0058 for 24 hours) (n=3).

We examined the impact of P1 and P2 mutations on wound healing in iPSC-derived monolayer colon organoids. After creating scratches in the monolayer organoids, we monitored the wound over 4 days, capturing phase contrast images every 24 hours. In WT cells, wounds typically healed within 24 to 72 hours. However, in cells with the c.[952A>G];[965A>C] variant, wound healing was delayed, with closure occurring between 48 and 72 hours. Notably, wounds in cells with the P2 mutation remained unhealed even after 96 hours (p = 0.0266) (Figure 26).
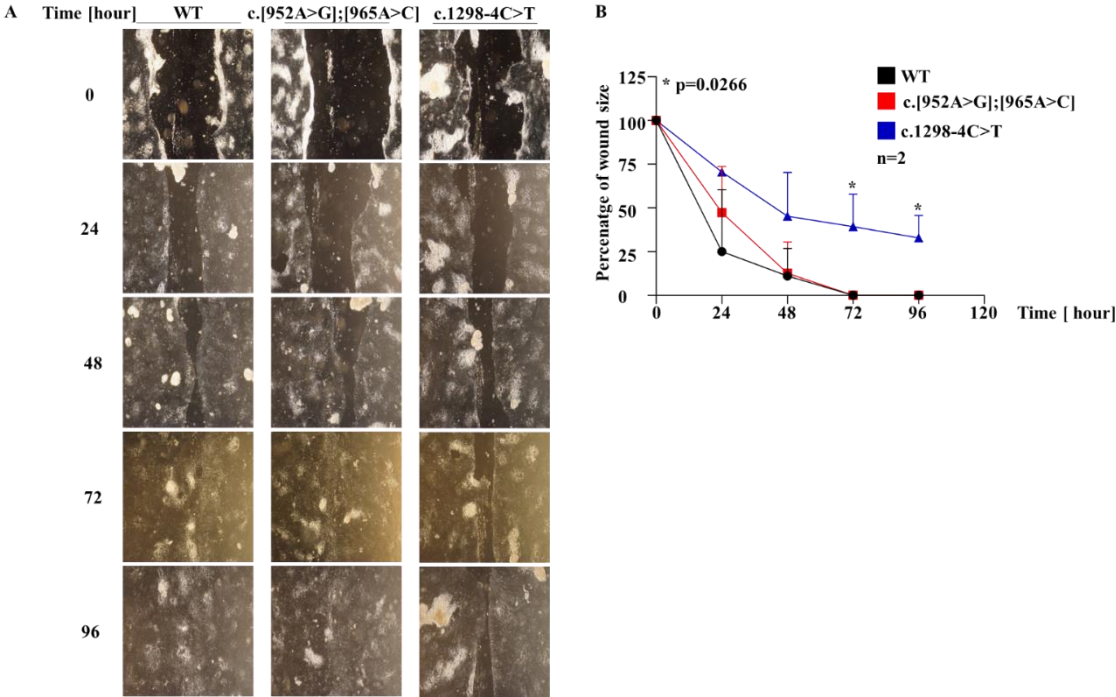
Figure 26: *IL1RL2* variants caused impaired wound healing in iPSC-derived monolayer colonic organoids.
Phase contrast images of the scratch assay were used to monitor wound healing in iPSC-derived monolayer colonic organoids (A). Quantitative analysis of wound width showed that the wound closed in wild-type (WT) organoids after 72 hours. The wound in organoids expressing the c.[952A>G];[965A>C] variant also closed after 72 hours, even though healing was delayed until that time. The wound did not close in organoids expressing the c.1298-4C<T variant (*p=0.0266) (B).

6. DISCUSSION

6.1. IL1RL2 deficiency - A newly identified monogenic risk factor for VEO-IBD

Pediatric patients diagnosed with VEO-IBD, distinguished by onset before the age of 6, manifest unique inflammatory profiles distinct from those observed in adult presentations. These include a higher incidence of colonic inflammation, a tendency for perianal diseases such as fistulas and abscesses, and a more severe course of the condition [141]. Although VEO-IBD is rare, its global incidence has increased significantly in recent decades, and it currently accounts for approximately 15% of pediatric IBD cases [142]. Identifying monogenic diseases has illuminated the crucial roles of immune dysfunctions and genetic factors in VEO-IBD among children. The advent of next-generation sequencing has uncovered over 100 monogenic loci associated with IBD-like symptoms, offering valuable insights into the genetic foundations of VEO-IBD. To further investigate these genetic complexities, our laboratory has conducted a comprehensive WES analysis involving one of the largest international cohorts, comprising over 1000 VEO-IBD patients. This endeavor aims to uncover new genetic contributors to the pathomechanism of VEO-IBD, potentially paving the way for personalized therapeutic interventions and improved patient care. Our extensive genome-wide analysis identified two unrelated VEO-IBD patients with either a compound heterozygous missense mutation or a splice region mutation in *IL1RL2*, indicating a novel monogenic risk factor for IBD. The patient designated P1 in Pedigree A (Figure 7) exhibited a severe and treatment-resistant disease course, characterized by symptoms such as non-bloody diarrhea and perianal fissures, along with early onset of perianal complications, including inflammation/ileitis with ulceration. The second patient, referred to as P2 in Pedigree B (Figure 7), is identified as a VEO-IBD patient from Iran. However, additional information regarding P2, including clinical symptoms, age, treatment, and other details, is missing.

IL1RL2 has emerged as a significant regulator of intestinal homeostasis [85, 91, 103, 126, 128, 143]. IL1RL2 is activated by IL-36 cytokines, which triggers the activation of immune cells and leads to inflammation. [127]. Additionally, IL1RL2-mediated signaling influences tissue repair mechanisms and wound healing in the intestine [92, 124, 128]. Our studies suggest that in VEO-IBD patients with mutations in *IL1RL2*, the dysregulation of IL-36 signaling may lead to exaggerated inflammatory responses and impaired wound repair, contributing to the severe and refractory disease course observed in these individuals. Our studies underscore the significance of IL1RL2-mediated signaling in regulating intestinal inflammation and

maintaining homeostasis. Elucidating the role of IL1RL2 in VEO-IBD can enhance our understanding of disease mechanisms and guide the development of targeted therapies for affected patients.

6.2.   The *IL1RL2* variants altered the structural conformation of the TIR domain

The IL1RL2 receptor is essential for immune responses and regulation of inflammation [110, 117, 128, 131]. Guanghui et al. showed that N-linked glycosylation and disulfide bonds influence IL1RL2-mediated signaling by controlling receptor formation and trafficking to the cell membrane [87]. It has been shown that SNPs in the TIR domain affect the activation of NFκB. For example, the single nucleotide polymorphisms V352I and L550P exhibited only minimal effects on signaling in the presence of all three IL-36 cytokines. Conversely, A471T diminished NFκB promoter activation in response to IL-36 cytokines compared to WT, and the reduction is identical for all cytokine responses [87]. Correspondingly, our findings determined that the index patient's specific mutations at amino acids p.Asn318Asp and p.Glu322Ala within the TIR domain of IL1RL2 underscore the functional importance of these residues. iCn3D analysis, employing the SWISS model, has enlightened changes in the protein's surface area and interatomic distances due to these mutations (Figure 8). The reduction in surface area associated with the c.952A>G mutation suggests a structural rearrangement that could influence ligand binding or receptor dimerization. Similarly, the notable increase in surface area with the c.965A>C variant indicates significant conformational changes, potentially impacting protein-protein interactions or signaling cascades.

Moreover, alterations in interatomic distances and hydrogen bond numbers provide insights into the structural ramifications of these mutations, potentially affecting the receptor's essential stability and conformational dynamics. These observations highlight the intricate relationship between protein structure and function, emphasizing the significance of structural investigations in elucidating the molecular basis of genetic disorders and informing potential therapeutic approaches. However, more sophisticated structural analysis is still required.

6.3.   *IL1RL2* variants reduced the phosphorylation of NFκB and MAPK and altered gene expression in the index patient

IL1RL2 receptor activation has a major role in regulating inflammatory responses, mediated via activating key signaling pathways, including NFκB and MAPKs [97, 126, 144, 145]. Upon ligand binding, IL1RL2 triggers a cascade of events that activates the NFκB and MAPK

pathways. Several gene expressions in inflammation, immunity, and cell survival are regulated by NFκB as a transcription factor. IL1RL2 activation induces the engagement of adaptor protein MyD88 to its intracellular domain. MyD88 further recruits IRAKs, leading to the activation of the IKK complex, which phosphorylates the IκB (inhibitor of NFκB), directing to its degradation and subsequent release of NFκB. The NFκB subsequently moves to the nucleus, where it affects the transcription of pro-inflammatory genes. Additionally, IL1RL2 can activate MAPK pathways, including ERK, JNK, and p38 MAPK, which transduce signals to the nucleus and mediate gene expressions associated with inflammation and immune responses [146]. Following activation, NFκB or MAPKs move to the nucleus, binding to specific DNA parts within the promoters of target genes and initiating transcription [85]. The NFκB and MAPK pathways orchestrate robust inflammatory responses, essential for immune defense, by enhancing cytokines like IL-6, IL-8, and chemokines, including CXCL10 and CCL20, crucially involved in inflammatory disease [147]. IL-6, produced by various cell types, contributes to inflammation, tissue damage, and immune dysregulation [148]. IL-6 plays a complex role in IBD. While it has pro-inflammatory effects, complete IL-6 blockade can exacerbate gut inflammation in IBD patients, particularly by suppressing Tregs while promoting the IL-1β/Th2 pathway [149, 150]. Conversely, the deletion of IL-6 in IL-10 deficient mice, a model of VEO-IBD, exacerbates colitis and induces systemic inflammation, suggesting a protective role for IL-6 [149]. IL-8 is a potent chemotactic factor recruiting neutrophils to sites of inflammation, exacerbating tissue damage [151]. CXCL10 assumes a critical function in the inflammatory process of the intestines by attracting immune cells to localize at the inflamed site within the intestinal tract [152-154].

The *IL1RL2* mutation (c.[952A>G];[965A>C]) found in the index patient (P1, A.II-1) was thoroughly examined to delineate its impact on NFκB and MAPK pathway phosphorylation. Monocyte-derived macrophages obtained from A.II-1, alongside cells from A.I-1 and a HD, were subjected to IL-36β stimulation. Western blot analysis revealed diminished phosphorylation levels of NFκB, p44/42 MAPK, and p38 in P1 (c.[952A>G];[965A>C]) compared to both the father (c.[952A>G];[965A]) and the HD (c.[952A];[965A]). These findings intimate a significant functional alteration attributed to the mutation (Figure 9), potentially elucidating aspects of the patient's phenotype. In parallel, similar investigations were achieved utilizing a heterologous HCT116 colon carcinoma cell line engineered via lentiviral transduction to express the *IL1RL2* mutation (c.952A>G or c.965A>C). We found that in cells expressing WT *IL1RL2* or the c.952A>G variant, phosphorylation of NFκB and p38 increased after 5 minutes, contrasting with the less NFκB and p38 activation in response to IL-36γ

stimulation in c.965A>C expressing cells. While control cells only transduced with RFP exhibited no activation of NFκB and p38 pathways upon IL-36γ stimulation, which indicates the contribution of the IL1RL2 on the activity of NFκB and MAPK pathways. Notably, after 15 minutes, the c.952A>G mutation demonstrated heightened phosphorylation compared to WT, while the c.965A>C mutation showed less activation relative to both WT and c.952A>G cells. Our findings imply the impact of *IL1RL2* mutations on NFκB and p38 pathway activation, potentially providing insights into the mechanisms driving the patient's phenotype (Figure 20). To evaluate the effect of the index patient mutation on *CXCL10* expression, we stimulated macrophages derived from the patient's monocytes with IL-36β and analyzed the mRNA expression by qPCR. Significantly, our study unveiled a notable decrease in *CXCL10* expression levels within the index family when contrasted with those of a HD, with the patient exhibiting considerably lower expression levels than other family members (Figure 12). This finding aligns with our previous observations correlating reduced NFκB and MAPK phosphorylation, as depicted in Figure 9, with the downregulation of *CXCL10*. Overall, the results from our assay underscore the potential involvement of the index patient mutation in modulating *CXCL10* expression dynamics via NFκB and MAPK pathways. It has been demonstrated that inhibitors targeting the NFκB and MAPK pathways can decrease inflammatory cytokines and chemokines levels, such as CXCL10 [156]. Reduced expression of *CXCL10* may indicate an impaired capacity to recruit immune cells to locations of inflammation, thus weakening the body's capacity to mount a robust immune defense against pathogens or gut tissue damage [157, 158].

We observed that the P1 mutation (c.[952A>G]; [965A>C]) led to increased expression of both *IL6* and *IL8* in monocyte-derived DCs upon IL-36β stimulation. Similarly, the P2 mutation (c.1298-4C>T) resulted in elevated *IL6* expression under the same conditions. However, basal gene expression levels were higher in both patients compared to HDs (Figure 10 and Figure 11). The elevated baseline expression of *IL6* symbolizes a continuous state of inflammation within these individuals, as this proinflammatory cytokine recreates a key role in modulating various immune reactions, particularly in regulating inflammation [159-161]. The elevated baseline levels of *IL6* suggest ongoing immune activation. The rise in basal *IL6* levels could indicate how severe VEO-IBD is, as *IL6* is closely tied to the disease's development and activity, suggesting more severe symptoms and highlighting the immune system's imbalance seen in IBD.

Given the elevation in basal levels of IL6 and IL8 expression, the observed increase in expression following IL-36beta stimulation remains negligible. It suggests that IL-36beta

stimulation does not significantly alter expression levels in the patient's monocytes-derived DCs. However, obtaining patient material limited our ability to conduct further studies with patient cells. Therefore, additional replication studies on mRNA expression are necessary to elucidate the impact of *IL1RL2* variants on pro-inflammatory genes.

In the context of IBD, reduced CXCL10 levels in DCs suggest an alteration in the immune response. CXCL10, a chemokine crucial for recruiting and activating T cells at sites of inflammation, plays a significant role in the inflammatory processes characteristic of IBD. Lower levels of CXCL10 may indicate impaired T-cell recruitment to the intestinal mucosa, potentially affecting the disease's inflammatory response. This reduction might reflect a protective mechanism against excessive inflammation, as indicated by more basal levels of IL6 and IL8 expression in the P1 and P2, or it might signify compromised immune activation. Additionally, changes in CXCL10 levels might correlate with disease severity and activity, serving as a potential marker for disease monitoring.

In IBD, the balance and regulation of cytokines and chemokines are critical. Elevated IL-6 and IL-8 levels are typically associated with active disease and severe inflammation. Reduced CXCL10 expression in this context might reflect a regulatory attempt to mitigate excessive immune cell recruitment and inflammation or indicate a shift in the type of immune response predominant in the affected tissues.

6.4. Deficiency in *IL1RL2* altered macrophage activation in patient monocyte-derived and iPSC-derived macrophages

Activated macrophages play a central role in IBD pathogenesis. In IBD, the inflamed intestinal mucosa recruits many macrophages, which cause metabolic alterations and excessive activation. Macrophages in IBD are predominantly of the pro-inflammatory M1 phenotype, which produces increased levels of TNF-α. These M1 macrophages contribute significantly to intestinal damage and the development of IBD. In contrast, the anti-inflammatory M2 macrophages are lowered in IBD. Modulating macrophage polarization is considered a promising therapeutic strategy in IBD. Inhibiting the M1 subset or inducing the M2 phenotype can effectively ameliorate IBD. Under homeostasis, macrophages maintain intestinal barrier integrity. However, in IBD, dysbiosis leads to excessive activation of macrophages, which disrupt the epithelial barrier and cause inflammation. The dysregulation of intestinal macrophage homeostasis, with excessive M1 activation and reduced M2 polarization, is an important factor in the progression of IBD.

In view of the fact that we investigated macrophage activation in both P1 monocyte-derived macrophages and iPSC-derived macrophages expressing P1 or P2 specific mutation by utilizing the CRISPR/Cas9 system. The differentiation of primary monocytes into macrophages, followed by their polarization into M1 proinflammatory or M2 anti-inflammatory phenotypes, allowed for a comprehensive evaluation of macrophage activation markers. Using FACS analysis, we examined CD274, CD273, CD163, CD86, CD14, and HLA-DR expression levels, revealing distinct patterns associated with the P1 mutation, c.[952A>G]; [965A>C] (Figure 13). While CD274 expression remained unchanged in P1, CD273 expression decreased in both M0 resting and M2 anti-inflammatory macrophages, which might indicate impairment in acquiring the full M2 phenotype. It has been shown that a reduction in CD273 expression on M0 and M2 macrophages is likely to weaken their ability to suppress immune responses and exert anti-inflammatory effects, both of which are fundamental characteristics of the alternatively activated M2 phenotype [162].

CD163 expression significantly decreased across all activation states in P1. In the context of intestinal inflammation, diminished CD163 expression has several implications [163]. For instance, reduced CD163 in M0 macrophages may impair their homeostatic functions, such as the clearance of apoptotic cells and the maintenance of gut homeostasis [163]. In M1 macrophages, decreased CD163 expression could exacerbate their inflammatory phenotype by dysregulating anti-inflammatory pathways typically regulated by CD163 [163] Similarly, in M2 macrophages, reduced CD163 may hinder their capacity to resolve inflammation and promote tissue repair in IBD [163, 164].

Furthermore, CD86 expression increased in M0 and M2 macrophages. Increased CD86 on M0 macrophages indicates a shift towards a more activated, pro-inflammatory phenotype in the context of IBD, potentially impairing their homeostatic functions and contributing to the loss of tolerance to commensal bacteria and self-antigens in the gut [165, 166]. The further increase in CD86 expression on M1 macrophages would enhance their capacity to activate pathogenic T cells, thereby exacerbating the excessive T-cell responses and chronic intestinal inflammation characteristic of IBD [164]. This dysregulation of macrophage phenotypes and functions due to elevated CD86 levels could contribute to the breakdown of tolerance, the perpetuation of chronic inflammation, and the tissue damage observed in the pathology of IBD [164].

Additionally, CD14 expression decreased in all macrophage states in the P1. The reduced expression of CD14 on M0, M1, and M2 macrophages has significant implications. M0 macrophages, which normally maintain gut homeostasis through CD14 expression, exhibit an altered phenotype in IBD due to reduced CD14 levels, potentially compromising their ability

to clear apoptotic cells and handle microorganism's antigens [164, 167]. Similarly, decreased CD14 expression on M1 macrophages, which are heightened in number and pro-inflammatory activity in IBD lesions, may disrupt their responsiveness to bacterial products and their production of inflammatory molecules [164, 167]. Despite this reduction, the pro-inflammatory impact of M1 macrophages may persist. Furthermore, reduced CD14 on M2 macrophages, which play a regulatory and anti-inflammatory role in IBD, could further impair their ability to resolve inflammation and promote tissue repair [164, 167]. This dysregulation of macrophage phenotypes and functions due to decreased CD14 levels likely contributes to the breakdown of gut homeostasis, the perpetuation of chronic inflammation, and the impaired resolution of inflammation observed in IBD pathology [164, 167].

Notably, HLA-DR expression showed a heightened shift in P1 across all activation conditions. The increased expression of HLA-DR on M0, M1, and M2 macrophages in IBD is indicative of important immune activation and has several implications [164, 167]. Typically, M0 macrophages exhibit low HLA-DR expression, but in the IBD setting, elevated levels suggest their activation and acquisition of a more pro-inflammatory phenotype, potentially disrupting their homeostatic functions in maintaining gut immune tolerance and bacterial clearance [164, 167]. Meanwhile, M1 macrophages, already pro-inflammatory and increased in numbers in IBD lesions, display further heightened HLA-DR expression, indicating an enhanced activated state and amplifying their ability to present antigens and drive pathogenic T cell responses, thus exacerbating chronic inflammation. Conversely, M2 macrophages, which are generally decreased in IBD but have a regulatory, anti-inflammatory role, show increased HLA-DR expression, signifying an altered activation state that may impair their normal functions in resolving inflammation, promoting tissue repair and maintaining gut homeostasis [164, 167].

The assessment of macrophage activation markers in iPSC-derived macrophages revealed distinct patterns across different mutations and KO cells compared to WT cells. In resting M0 cells, CD274 expression was consistently reduced across all mutations and KO cells compared to WT cells. However, this reduction was not observed in M1 pro-inflammatory cells and M2 anti-inflammatory cells, indicating a mutation-specific effect in the resting state. Contrary to the lack of change in CD273 expression in M0 cells, an increase was observed in M1 cells. Notably, this increase was only significant in M2 cells expressing P1 compound heterozygous mutation (c.[952A>G]; [965A>C]) and P2 a splice region mutation (1298-4C>T), suggesting modulation of CD273 expression in the inflammatory and anti-inflammatory states. It has been studied that reduced CD273 expression in resting macrophages impairs interaction with Tregs,

crucial for Treg homeostasis. CD273, a ligand for PD-1 on T cells, facilitates this interaction. Blocking CD273 reduces Treg-macrophage contact, compromising Treg survival. Thus, CD273 plays a vital role in macrophage-mediated Treg regulation [168]. Regarding CD86 expression, no significant alterations were noted across all macrophage activation states. However, CD14 expression displayed a consistent decrease in M0 and M1 cells compared to WT cells across all deficient cells, similar to findings in the index patient monocytes-derived macrophages, while no change was observed in M2 macrophages. Decreased CD14 expression in these macrophage populations would likely result in impaired inflammatory profile, which could have implications for their functional roles in P1 and P2 patient phenotypes. There is evidence from several studies that reduced CD14 levels are associated with increased inflammation [171-173]. For example, in the experimental IBD model utilizing mice, the absence of CD14 resulted in increased disruption of the intestinal barrier, greater inflammation based on histological scores, and higher levels of pro-inflammatory cytokines such as IL-1β, IL-6 and, TNF-α in contrast to mice with normal CD14 levels. Administering external CD14 improved the function of the intestinal barrier and decreased inflammation [172].

HLA-DR expression exhibited distinct changes among different sets of macrophages. In M0 cells, HLA-DR expression increased in deficient cells compared to WT cells, suggesting enhanced antigen presentation capabilities. Conversely, in M1 cells, HLA-DR expression decreased across all mutations, implying a modulation of antigen presentation in the pro-inflammatory state. However, no significant change in HLA-DR expression in M2 cells indicated differential regulation across activation states (Figure 17). The decreased HLA-DR expression on these cells is believed to have significant functional consequences, compromising their antigen-presenting capacity and overall immune response, which may increase susceptibility to infections in sepsis patients [174]. Overall, the evaluation of macrophage activation markers in iPSC-derived macrophages highlights mutation-specific and activation state-dependent alterations, providing an understanding of the complicated regulation of macrophage function in *IL1RL2* mutations of our P1 and P2 patients. Further investigation is warranted to elucidate the underlying mechanisms and potential therapeutic targets associated with these findings.

Furthermore, the investigation of macrophage activation in both P1 monocyte-derived and iPSC-derived macrophages with specific mutations utilizing the CRISPR/Cas9 system reveals mutation-specific effects on macrophage activation markers. While alterations in CD273, CD86, and HLA-DR expression suggest impaired immune regulation and antigen presentation capabilities, reduced CD14 expression across all macrophage states implies compromised

homeostatic functions and inflammatory response dampening, potentially affecting disease pathogenesis in IBD. The distinct changes observed underscore the complexity of macrophage regulation in IBD and highlight the need for further research to elucidate underlying mechanisms and identify potential therapeutic targets.

6.5. The *IL1RL2* deficiency altered the number of macrophage colonies

Accessing primary cells directly from patients can be logistically and clinically challenging, necessitating alternative approaches. In our study, we addressed this issue by using iPSCs and the CRISPR/Cas system to introduce patient-specific mutations. We then differentiated the genetically engineered iPSCs with *IL1RL2* variants into macrophages. To confirm macrophage differentiation, we monitored the expression of CD14, CD45, CD34, and CD33 during differentiation using FACS analysis. Initially, on day 12, we observed CD34 and CD33 expression with low CD14. By day 15, CD14 expression increased, and CD33 expression became nearly total. By day 18, CD14 expression reached nearly 100%, indicating advanced differentiation (Figure 15). The progression in marker expression over time suggests successful differentiation of iPSCs into macrophages, with the marker CD14 showing significant increases, which are indicative of macrophages.

To assess the impact of the P1 (c.[952A>G];[965A>C]) and P2 (c.1298-4C>T) mutations on macrophage differentiation, we conducted a colony-forming unit assay on Hematopoietic progenitor cells on day 9 of differentiation stage. Results revealed a notable reduction in total colony numbers in KO cells ($p > 0.0001$), indicating a significant impairment in differentiation efficiency related to *IL1RL2* deficiency. While the c.[952A>G];[965A>C] mutation (P1) showed similar colony numbers to WT cells, c.1298-4C>T (P2) was associated with increased colony numbers ($p = 0.0432$). These findings suggest differential effects of the mutations on macrophage differentiation (Figure 16). The CFU data suggests a lack of *IL1RL2* significantly reduced the total number of colonies. Surprisingly, the P2 mutation enhances colony formation and differentiation potential compared to the WT, whereas the P1 mutation has no significant impact on this process. These different effects of the mutations indicate distinct influences on IL1RL2 function and the differentiation of macrophages from hematopoietic progenitors.

6.6. *IL1RL2* variants caused impaired wound healing in intestinal epithelial cells

IL1RL2 pathway has revealed its pivotal role in orchestrating wound healing processes, primarily by activating key signaling pathways like NFκB and MAPK [85, 143]. Several studies

demonstrate that IL1RL2 signaling is vital in promoting intestinal wound healing [91, 128]. Following mucosal damage, releasing IL1RL2 ligands triggers the activation of IL1RL2[+] colonic fibroblasts. This activation prompts the expression of GM-CSF and IL-6, promoting intestinal epithelial cell and antimicrobial protein production [143, 175]. Administering IL1RL2 ligands to experimental intestinal wounds notably quickened mucosal healing in vivo. [175]. Impaired IL1RL2 signaling confers heightened susceptibility to acute dextran sodium sulfate colitis [175]. IL1RL2 has the capability to trigger IL-22 production, which in turn promotes epithelial proliferation and restitution, fostering the secretion of antimicrobial peptides, and exhibits protective effects against intestinal inflammation. These findings underscore the beneficial role of IL1RL2 signaling in acute intestinal wound healing [91, 128]. Overall, IL1RL2 signaling in intestinal epithelial cells and fibroblasts facilitates mucosal healing by stimulating epithelial cell proliferation, promoting antimicrobial protein production, and facilitating IL-22-mediated epithelial restitution. The modulation of the IL1RL2 pathway presents itself as a promising therapeutic approach for eliciting mucosal healing IBD [91, 128, 143, 175].

We investigated the effect of mutations on wound healing using the HCT116 colon carcinoma cell line engineered with lentiviral transduction and iPSC-derived colonic organoids expressing c.[952A>G];[965A>C] (P1) or c.1298-4C>T (P2) variants. We analyzed the expression of *IL1RL2* and *CCL20* levels by qPCR. Our findings revealed a significant change in *IL1RL2* expression in iPSC-derived colonic organoids carrying c.[952A>G];[965A>C] or c.1298-4C>T variants compared to WT organoids. However, the elevation in *CCL20* expression was observed in organoids with the c.1298-4C>T mutation compared to WT cells (Figure 24). Our finding suggested that the c.[952A>G];[965A>C] and c.1298-4C>T variants have subtle effect on the *IL1RL2* and *CCL20* expression.

To investigate wound healing, we stimulate cells with IL-36γ under wounded conditions. We found that WT cells exhibited significant wound closure within 24 hours compared to control cells, suggesting the involvement of the IL1RL2 pathway in facilitating wound closure. However, control cells expressing only RFP and mutant cells showed delayed wound closure rates, particularly those expressing the c.952A>G and c.965A>C variants compared to WT cells (Figure 22). Upon IL-36γ stimulation, WT cells demonstrated accelerated wound closure, underscoring the pathway's importance in healing. In contrast, mutant and control cells exhibited delayed wound closure, suggesting an impaired response to IL-36γ stimulation due to P1 variants. We investigate *CCL20* expression in unwounded and wounded conditions. Results indicated increased *CCL20* expression in both WT and mutant cells following IL-36γ

stimulation, with higher expression observed in cells harboring specific mutations. Notably, the c.952A>G variant showed a pronounced increase in *CCL20* expression compared to WT cells, highlighting potential genotype-dependent effects on wound healing pathways (Figure 23).

To complement cellular studies, 3D and monolayer colonic organoid models differentiated from iPSCs engineered with patient mutations were utilized. The impact of c.[952A>G];[965A>C] or c.1298-4C>T mutations on iPSC-derived monolayer colon organoids were evaluated over a 4-day wound healing observation period. We found that wound healing was delayed in cells expressing the c.[952A>G];[965A>C] variant expressing cells, while it did not complete in cells with the c.1298-4C>T variant expressing cells, compared to WT cells (Figure 26). These models provided valuable insights into the effects of mutations on wound healing dynamics in a more physiologically relevant context.

Overall, impaired wound healing coupled with *CCL20* levels in HCT116 cells expressing variants from the index patient suggests a compromised inflammatory and immune response at the wound site, potentially leading to slower healing in epithelial cells. Additional functional assays, such as proliferation, migration, and co-culture systems with macrophages, need to be conducted to fully understand the mechanism behind this observed phenotype.

6.7. *IL1RL2* variants showed decreased resistance to apoptosis

Previous studies have elucidated the significant role of the IL-36 signaling pathway in governing apoptosis in epithelial cells [176-178]. Activation of the IL1RL2 can promote programmed cell death, particularly under inflammatory conditions [176, 179]. Specifically, the double-stranded RNA analog poly (I: C) was observed to trigger pyroptosis in human keratinocytes, therefore promoting the extracellular secretion of IL-36γ [178]. However, inhibition of caspase-3/7 and caspase-1 blocked the secretion of IL-36γ [178]. This suggests that the IL-36 pathway is activated by and can promote apoptosis in epithelial cells. It is established that cellular proliferation, differentiation, and apoptosis are regulated by MAPKs. In the context of TNFα/CHX-induced apoptosis, oxidative stress, mitochondrial dysfunction, and activation of caspase-3/7 in intestinal epithelial cells are increased [176, 179]. The available evidence suggests that the IL-36 mediated signaling regulates apoptosis in epithelial cells, and its activation can potentiate programmed cell death induced by inflammatory stimuli like TNFα/CHX [176-179].

To assess epithelial cell death response, we scrutinized apoptosis in HCT116 colon carcinoma cells overexpressing *IL1RL2* with P1 variants, treated with TNF-α and CHX for 0, 2, and 6 hours, under wounded and non-wounded conditions using Annexin V/DAPI method. Under unwound conditions, no differences were observed after 2 hours, but early apoptotic cells increased after 6 hours, with the c.965A>C variant showing a higher percentage (70.1%) compared to WT cells (55.9%), while the c.952A>G variant had fewer early apoptotic cells than WT. Under wound conditions, apoptotic cell numbers increased significantly in both c.952A>G (13.6%) and c.965A>C (30.3%) variants compared to WT (0.33%) and control cells (0.84%). Additionally, early apoptotic cells were more prevalent in the c.965A>C variant (41.3%) than in WT (15.3%) or c.952A>G (23.7%) cells (Figure 21).

These findings show that the c.965A>C variant may enhance apoptosis, especially under wounded conditions, while the c.952A>G variant may have a different effect on apoptosis.

6.8.   Looking Forward: Opportunities and Limitations

The discovery of new mutations in *IL1RL2* using whole exome sequencing sparked an exploration into their molecular workings as part of this thesis work. By employing advanced techniques like CRISPR/Cas9 and iPSC differentiation, this research revealed altered immune responses linked with *IL1RL2* mutations in patients, uncovering deficiencies in macrophage polarization and decreases in NFκB and MAPK activation. Additionally, functional tests on HCT116 cells and organoids expressing *IL1RL2* patient-specific variants shed light on the effect of wound healing and cytokine expression, emphasizing *IL1RL2's* critical role in gut immunity.

While our study sheds light on the role of *IL1RL2* mutations in VEO-IBD and associated molecular mechanisms, several limitations exist.

Firstly, the sample size remains relatively small, particularly regarding patients with *IL1RL2* mutations. A larger cohort would provide more robust insights into these mutations' prevalence and clinical manifestations in VEO-IBD.

Additionally, the lack of comprehensive clinical data, particularly for P2, limits our ability to characterize the phenotype associated with *IL1RL2* mutations entirely. Furthermore, our study primarily focuses on the molecular and cellular aspects of *IL1RL2* variants, warranting further investigation into the clinical implications and therapeutic strategies for patients with these mutations. Integrating multi-omics approaches, functional tests, and in vivo models will be

pivotal in outlining the molecular pathways involved and identifying potential therapeutic of *IL1RL2* for VEO-IBD.

Despite these limitations, our study opens avenues for future research in VEO-IBD and IL1RL2-associated pathogenesis. Further analyses, including different in vitro co-culture systems, like iPSC-derived organoids or macrophages challenged with bacteria, or in vivo models, like mice with P1 or P2 mutations, might expand our knowledge about the interaction between *IL1RL2* mutations and VEO-IBD.

In this study, we used HCT116 cells overexpressing the homozygous single mutation identified within the compound heterozygous mutation in the index patient. The c.952A>G homozygous single mutation typically has modest effects compared to the c.965A>C homozygous single mutation in HCT116 cells on the activation of NFκB/MAPK, wound healing, cell death, and CCL20 expression. However, the compound heterozygous mutation in the index patient, c.[952A>G];[965A>C] shows modest effects on wound healing compared to the c.1298-4C>T mutation in iPSC-derived organoids. To better understand the impact of the index patient's mutation, conducting cell death, proliferation, and migration studies in iPSC-derived organoid models that express the patient's compound heterozygous mutation is necessary. This approach might clarify how these variants affect wound healing and cell death and whether the compound heterozygous mutation and single variant impact differently. By examining these genotype-phenotype correlations, we can gain insight into the role of the IL1RL2 variant in the context of IBD.

Lastly, while our findings suggest potential therapeutic targets, further studies are necessary to validate the efficacy and safety of targeted interventions in VEO-IBD patients with *IL1RL2* mutations.

7. REFERENCES

1. Kaser, A., S. Zeissig, and R.S. Blumberg, *Inflammatory bowel disease.* Annu Rev Immunol, 2010. **28**: p. 573-621.

2. Adolph, T.E., et al., *The metabolic nature of inflammatory bowel diseases.* Nat Rev Gastroenterol Hepatol, 2022. **19**(12): p. 753-767.

3. Sykora, J., et al., *Current global trends in the incidence of pediatric-onset inflammatory bowel disease.* World J Gastroenterol, 2018. **24**(25): p. 2741-2763.

4. Ye, Y., et al., *Prevalence of Inflammatory Bowel Disease in Pediatric and Adult Populations: Recent Estimates From Large National Databases in the United States, 2007-2016.* Inflamm Bowel Dis, 2020. **26**(4): p. 619-625.

5. Seyedian, S.S., F. Nokhostin, and M.D. Malamir, *A review of the diagnosis, prevention, and treatment methods of inflammatory bowel disease.* J Med Life, 2019. **12**(2): p. 113-122.

6. Mendoza, J.L., et al., *[Extraintestinal manifestations in inflammatory bowel disease: differences between Crohn's disease and ulcerative colitis].* Med Clin (Barc), 2005. **125**(8): p. 297-300.

7. Marshall, J.K., *Are there epidemiological differences between Crohn's disease and ulcerative colitis?* Inflamm Bowel Dis, 2008. **14 Suppl 2**: p. S1.

8. Ayada, I., et al., *[Extra-intestinal manifestations associated with Crohn's disease].* Ned Tijdschr Geneeskd, 2024. **168**.

9. Kilic, Y., et al., *Prevalence of Extraintestinal Manifestations in Inflammatory Bowel Disease: A Systematic Review and Meta-analysis.* Inflamm Bowel Dis, 2024. **30**(2): p. 230-239.

10. Odze, R.D., *A contemporary and critical appraisal of 'indeterminate colitis'.* Mod Pathol, 2015. **28 Suppl 1**: p. S30-46.

11. Mulder, D.J., et al., *A tale of two diseases: the history of inflammatory bowel disease.* J Crohns Colitis, 2014. **8**(5): p. 341-8.

12. Xu, F., et al., *Prevalence of Inflammatory Bowel Disease Among Medicare Fee-For-Service Beneficiaries - United States, 2001-2018.* MMWR Morb Mortal Wkly Rep, 2021. **70**(19): p. 698-701.

13. Borowitz, S.M., *The epidemiology of inflammatory bowel disease: Clues to pathogenesis?* Front Pediatr, 2022. **10**: p. 1103713.

14. Danpanichkul, P., et al., *Global Epidemiology and Burden of Elderly-Onset Inflammatory Bowel Disease: A Decade in Review.* J Clin Med, 2023. **12**(15).

15. Rosen, M.J., A. Dhawan, and S.A. Saeed, *Inflammatory Bowel Disease in Children and Adolescents.* JAMA Pediatr, 2015. **169**(11): p. 1053-60.

16.   Murthy, S.K., et al., *High end of life health care costs and hospitalization burden in inflammatory bowel disease patients: A population-based study.* PLoS One, 2017. **12**(5): p. e0177211.

17.   Magro, F., et al., *Burden of Disease and Cost of Illness of Inflammatory Bowel Diseases in Portugal.* GE Port J Gastroenterol, 2023. **30**(4): p. 283-292.

18.   Wang, R., et al., *Global, regional and national burden of inflammatory bowel disease in 204 countries and territories from 1990 to 2019: a systematic analysis based on the Global Burden of Disease Study 2019.* BMJ Open, 2023. **13**(3): p. e065186.

19.   Kaplan, G.G., *The global burden of IBD: from 2015 to 2025.* Nat Rev Gastroenterol Hepatol, 2015. **12**(12): p. 720-7.

20.   Jarmakiewicz-Czaja, S., et al., *Genetic and Epigenetic Etiology of Inflammatory Bowel Disease: An Update.* Genes (Basel), 2022. **13**(12).

21.   Park, S.C. and Y.T. Jeen, *Genetic Studies of Inflammatory Bowel Disease-Focusing on Asian Patients.* Cells, 2019. **8**(5).

22.   Wu, N., et al., *Inflammatory bowel disease and the gut microbiota.* Proc Nutr Soc, 2021: p. 1-11.

23.   Uhlig, H.H., et al., *Clinical Genomics for the Diagnosis of Monogenic Forms of Inflammatory Bowel Disease: A Position Paper From the Paediatric IBD Porto Group of European Society of Paediatric Gastroenterology, Hepatology and Nutrition.* J Pediatr Gastroenterol Nutr, 2021. **72**(3): p. 456-473.

24.   Nameirakpam, J., et al., *Genetics on early onset inflammatory bowel disease: An update.* Genes Dis, 2020. **7**(1): p. 93-106.

25.   Serra, E.G., et al., *Somatic mosaicism and common genetic variation contribute to the risk of very-early-onset inflammatory bowel disease.* Nat Commun, 2020. **11**(1): p. 995.

26.   Ek, W.E., M. D'Amato, and J. Halfvarson, *The history of genetics in inflammatory bowel disease.* Ann Gastroenterol, 2014. **27**(4): p. 294-303.

27.   Ogura, Y., et al., *A frameshift mutation in NOD2 associated with susceptibility to Crohn's disease.* Nature, 2001. **411**(6837): p. 603-6.

28.   Cooney, R., et al., *NOD2 stimulation induces autophagy in dendritic cells influencing bacterial handling and antigen presentation.* Nat Med, 2010. **16**(1): p. 90-7.

29.   Parackova, Z., et al., *Novel XIAP mutation causing enhanced spontaneous apoptosis and disturbed NOD2 signalling in a patient with atypical adult-onset Crohn's disease.* Cell Death Dis, 2020. **11**(6): p. 430.

30.   Nambu, R. and A.M. Muise, *Advanced Understanding of Monogenic Inflammatory Bowel Disease.* Front Pediatr, 2020. **8**: p. 618918.

31.   Loddo, I. and C. Romano, *Inflammatory Bowel Disease: Genetics, Epigenetics, and Pathogenesis.* Front Immunol, 2015. **6**: p. 551.

32.   Jans, D. and I. Cleynen, *The genetics of non-monogenic IBD*. Hum Genet, 2023. **142**(5): p. 669-682.

33.   Szilagyi, A. and X. Xue, *Comparison of geographic distributions of Irritable Bowel Syndrome with Inflammatory Bowel Disease fail to support common evolutionary roots: Irritable Bowel Syndrome and Inflammatory Bowel Diseases are not related by evolution.* Med Hypotheses, 2018. **110**: p. 31-37.

34.   Collaborators, G.B.D.I.B.D., *The global, regional, and national burden of inflammatory bowel disease in 195 countries and territories, 1990-2017: a systematic analysis for the Global Burden of Disease Study 2017.* Lancet Gastroenterol Hepatol, 2020. **5**(1): p. 17-30.

35.   Khalili, H., et al., *Geographical variation and incidence of inflammatory bowel disease among US women.* Gut, 2012. **61**(12): p. 1686-92.

36.   Mak, W.Y., et al., *The epidemiology of inflammatory bowel disease: East meets west.* J Gastroenterol Hepatol, 2020. **35**(3): p. 380-389.

37.   Ng, S.C., et al., *Geographical variability and environmental risk factors in inflammatory bowel disease.* Gut, 2013. **62**(4): p. 630-49.

38.   Chong, C., et al., *Current smoking habits in British IBD patients in the age of e-cigarettes.* BMJ Open Gastroenterol, 2019. **6**(1): p. e000309.

39.   Battistini, C., et al., *Vitamin D Modulates Intestinal Microbiota in Inflammatory Bowel Diseases.* Int J Mol Sci, 2020. **22**(1).

40.   Cosnes, J., *Tobacco and IBD: relevance in the understanding of disease mechanisms and clinical practice.* Best Pract Res Clin Gastroenterol, 2004. **18**(3): p. 481-96.

41.   Turner, D., et al., *Antibiotic Cocktail for Pediatric Acute Severe Colitis and the Microbiome: The PRASCO Randomized Controlled Trial.* Inflamm Bowel Dis, 2020. **26**(11): p. 1733-1742.

42.   Glassner, K.L., B.P. Abraham, and E.M.M. Quigley, *The microbiome and inflammatory bowel disease.* J Allergy Clin Immunol, 2020. **145**(1): p. 16-27.

43.   Bhamre, R., et al., *Psychiatric comorbidities in patients with inflammatory bowel disease.* Indian J Gastroenterol, 2018. **37**(4): p. 307-312.

44.   Ananthakrishnan, A.N., et al., *Ambient air pollution correlates with hospitalizations for inflammatory bowel disease: an ecologic analysis.* Inflamm Bowel Dis, 2011. **17**(5): p. 1138-45.

45.   Belizario, J.E. and M. Napolitano, *Human microbiomes and their roles in dysbiosis, common diseases, and novel therapeutic approaches.* Front Microbiol, 2015. **6**: p. 1050.

46.   Andoh, A., et al., *Terminal restriction fragment length polymorphism analysis of the diversity of fecal microbiota in patients with ulcerative colitis.* Inflamm Bowel Dis, 2007. **13**(8): p. 955-62.

47.   Nishino, K., et al., *Analysis of endoscopic brush samples identified mucosa-associated dysbiosis in inflammatory bowel disease.* J Gastroenterol, 2018. **53**(1): p. 95-106.

48.	Ohkusa, T., et al., *Induction of experimental ulcerative colitis by Fusobacterium varium isolated from colonic mucosa of patients with ulcerative colitis.* Gut, 2003. **52**(1): p. 79-83.

49.	Schaubeck, M., et al., *Dysbiotic gut microbiota causes transmissible Crohn's disease-like ileitis independent of failure in antimicrobial defence.* Gut, 2016. **65**(2): p. 225-37.

50.	Nishida, A., et al., *Gut microbiota in the pathogenesis of inflammatory bowel disease.* Clin J Gastroenterol, 2018. **11**(1): p. 1-10.

51.	Hapfelmeier, S., et al., *Reversible microbial colonization of germ-free mice reveals the dynamics of IgA immune responses.* Science, 2010. **328**(5986): p. 1705-9.

52.	Macpherson, A.J. and N.L. Harris, *Interactions between commensal intestinal bacteria and the immune system.* Nat Rev Immunol, 2004. **4**(6): p. 478-85.

53.	Al Nabhani, Z., et al., *Nod2 Deficiency Leads to a Specific and Transmissible Mucosa-associated Microbial Dysbiosis Which Is Independent of the Mucosal Barrier Defect.* J Crohns Colitis, 2016. **10**(12): p. 1428-1436.

54.	Couturier-Maillard, A., et al., *NOD2-mediated dysbiosis predisposes mice to transmissible colitis and colorectal cancer.* J Clin Invest, 2013. **123**(2): p. 700-11.

55.	Li, E., et al., *Inflammatory bowel diseases phenotype, C. difficile and NOD2 genotype are associated with shifts in human ileum associated microbial composition.* PLoS One, 2012. **7**(6): p. e26284.

56.	Frank, D.N., et al., *Disease phenotype and genotype are associated with shifts in intestinal-associated microbiota in inflammatory bowel diseases.* Inflamm Bowel Dis, 2011. **17**(1): p. 179-84.

57.	Ince, M.N. and D.E. Elliott, *Immunologic and molecular mechanisms in inflammatory bowel disease.* Surg Clin North Am, 2007. **87**(3): p. 681-96.

58.	Guan, Q., *A Comprehensive Review and Update on the Pathogenesis of Inflammatory Bowel Disease.* J Immunol Res, 2019. **2019**: p. 7247238.

59.	Abraham, C. and J.H. Cho, *Inflammatory bowel disease.* N Engl J Med, 2009. **361**(21): p. 2066-78.

60.	Mehandru, S. and J.F. Colombel, *The intestinal barrier, an arbitrator turned provocateur in IBD.* Nat Rev Gastroenterol Hepatol, 2021. **18**(2): p. 83-84.

61.	Wallace, K.L., et al., *Immunopathology of inflammatory bowel disease.* World J Gastroenterol, 2014. **20**(1): p. 6-21.

62.	Kosoy, R., et al., *Deep Analysis of the Peripheral Immune System in IBD Reveals New Insight in Disease Subtyping and Response to Monotherapy or Combination Therapy.* Cell Mol Gastroenterol Hepatol, 2021. **12**(2): p. 599-632.

63.	Lu, Q., et al., *Immunology of Inflammatory Bowel Disease: Molecular Mechanisms and Therapeutics.* J Inflamm Res, 2022. **15**: p. 1825-1844.

64.   Elemam, N.M., S. Hannawi, and A.A. Maghazachi, *Innate Lymphoid Cells (ILCs) as Mediators of Inflammation, Release of Cytokines and Lytic Molecules.* Toxins (Basel), 2017. **9**(12).

65.   Ahluwalia, B., et al., *Immunopathogenesis of inflammatory bowel disease and mechanisms of biological therapies.* Scand J Gastroenterol, 2018. **53**(4): p. 379-389.

66.   Kumric, M., et al., *Role of B-Cell Activating Factor (BAFF) in Inflammatory Bowel Disease.* Diagnostics (Basel), 2021. **12**(1).

67.   Zogorean, R. and S. Wirtz, *The yin and yang of B cells in a constant state of battle: intestinal inflammation and inflammatory bowel disease.* Front Immunol, 2023. **14**: p. 1260266.

68.   Magnusson, M.K., et al., *Macrophage and dendritic cell subsets in IBD: ALDH+ cells are reduced in colon tissue of patients with ulcerative colitis regardless of inflammation.* Mucosal Immunol, 2016. **9**(1): p. 171-82.

69.   Han, X., et al., *Roles of Macrophages in the Development and Treatment of Gut Inflammation.* Front Cell Dev Biol, 2021. **9**: p. 625423.

70.   Hegarty, L.M., G.R. Jones, and C.C. Bain, *Macrophages in intestinal homeostasis and inflammatory bowel disease.* Nat Rev Gastroenterol Hepatol, 2023. **20**(8): p. 538-553.

71.   Dharmasiri, S., et al., *Human Intestinal Macrophages Are Involved in the Pathology of Both Ulcerative Colitis and Crohn Disease.* Inflamm Bowel Dis, 2021. **27**(10): p. 1641-1652.

72.   Rutella, S. and F. Locatelli, *Intestinal dendritic cells in the pathogenesis of inflammatory bowel disease.* World J Gastroenterol, 2011. **17**(33): p. 3761-75.

73.   Hart, A.L., et al., *Characteristics of intestinal dendritic cells in inflammatory bowel diseases.* Gastroenterology, 2005. **129**(1): p. 50-65.

74.   Crosnier, C., D. Stamataki, and J. Lewis, *Organizing cell renewal in the intestine: stem cells, signals and combinatorial control.* Nat Rev Genet, 2006. **7**(5): p. 349-59.

75.   Johansson, M.E., et al., *The inner of the two Muc2 mucin-dependent mucus layers in colon is devoid of bacteria.* Proc Natl Acad Sci U S A, 2008. **105**(39): p. 15064-9.

76.   Dignass, A., et al., *Trefoil peptides promote epithelial migration through a transforming growth factor beta-independent pathway.* J Clin Invest, 1994. **94**(1): p. 376-83.

77.   Taupin, D.R., K. Kinoshita, and D.K. Podolsky, *Intestinal trefoil factor confers colonic epithelial resistance to apoptosis.* Proc Natl Acad Sci U S A, 2000. **97**(2): p. 799-804.

78.   Artis, D., et al., *RELMbeta/FIZZ2 is a goblet cell-specific immune-effector molecule in the gastrointestinal tract.* Proc Natl Acad Sci U S A, 2004. **101**(37): p. 13596-600.

79.   Nair, M.G., et al., *Goblet cell-derived resistin-like molecule beta augments CD4+ T cell production of IFN-gamma and infection-induced intestinal inflammation.* J Immunol, 2008. **181**(7): p. 4709-15.

80.   Eriguchi, Y., et al., *Reciprocal expression of enteric antimicrobial proteins in intestinal graft-versus-host disease.* Biol Blood Marrow Transplant, 2013. **19**(10): p. 1525-9.

81.   Salzman, N.H., *Paneth cell defensins and the regulation of the microbiome: detente at mucosal surfaces.* Gut Microbes, 2010. **1**(6): p. 401-6.

82.   Meyer-Hoffert, U., et al., *Secreted enteric antimicrobial activity localises to the mucus surface layer.* Gut, 2008. **57**(6): p. 764-71.

83.   Greenfeder, S.A., et al., *Molecular cloning and characterization of a second subunit of the interleukin 1 receptor complex.* J Biol Chem, 1995. **270**(23): p. 13757-65.

84.   Debets, R., et al., *Two novel IL-1 family members, IL-1 delta and IL-1 epsilon, function as an antagonist and agonist of NF-kappa B activation through the orphan IL-1 receptor-related protein 2.* J Immunol, 2001. **167**(3): p. 1440-6.

85.   Queen, D., C. Ediriweera, and L. Liu, *Function and Regulation of IL-36 Signaling in Inflammatory Diseases and Cancer Development.* Front Cell Dev Biol, 2019. **7**: p. 317.

86.   Lovenberg, T.W., et al., *Cloning of a cDNA encoding a novel interleukin-1 receptor related protein (IL 1R-rp2).* J Neuroimmunol, 1996. **70**(2): p. 113-22.

87.   Yi, G., et al., *Structural and Functional Attributes of the Interleukin-36 Receptor.* J Biol Chem, 2016. **291**(32): p. 16597-609.

88.   Towne, J.E., et al., *Interleukin-36 (IL-36) ligands require processing for full agonist (IL-36alpha, IL-36beta, and IL-36gamma) or antagonist (IL-36Ra) activity.* J Biol Chem, 2011. **286**(49): p. 42594-42602.

89.   Carrier, Y., et al., *Inter-regulation of Th17 cytokines and the IL-36 cytokines in vitro and in vivo: implications in psoriasis pathogenesis.* J Invest Dermatol, 2011. **131**(12): p. 2428-37.

90.   Gunther, S. and E.J. Sundberg, *Molecular determinants of agonist and antagonist signaling through the IL-36 receptor.* J Immunol, 2014. **193**(2): p. 921-30.

91.   Scheibe, K., et al., *Inhibiting Interleukin 36 Receptor Signaling Reduces Fibrosis in Mice With Chronic Intestinal Inflammation.* Gastroenterology, 2019. **156**(4): p. 1082-1097 e11.

92.   Ngo, V.L., et al., *A cytokine network involving IL-36gamma, IL-23, and IL-22 promotes antimicrobial defense and recovery from intestinal barrier damage.* Proc Natl Acad Sci U S A, 2018. **115**(22): p. E5076-E5085.

93.   Gabay, C. and J.E. Towne, *Regulation and function of interleukin-36 cytokines in homeostasis and pathological conditions.* J Leukoc Biol, 2015. **97**(4): p. 645-52.

94.   Taylor, S.L., et al., *Genomic organization of the interleukin-1 locus.* Genomics, 2002. **79**(5): p. 726-33.

95.   Clancy, D.M., et al., *Extracellular Neutrophil Proteases Are Efficient Regulators of IL-1, IL-33, and IL-36 Cytokine Activity but Poor Effectors of Microbial Killing.* Cell Rep, 2018. **22**(11): p. 2937-2950.

96.   Johnston, A., et al., *IL-1 and IL-36 are dominant cytokines in generalized pustular psoriasis.* J Allergy Clin Immunol, 2017. **140**(1): p. 109-120.

97.   Murrieta-Coxca, J.M., et al., *IL-36 Cytokines: Regulators of Inflammatory Responses and Their Emerging Role in Immunology of Reproduction.* Int J Mol Sci, 2019. **20**(7).

98.   Towne, J.E., et al., *Interleukin (IL)-1F6, IL-1F8, and IL-1F9 signal through IL-1Rrp2 and IL-1RAcP to activate the pathway leading to NF-kappaB and MAPKs.* J Biol Chem, 2004. **279**(14): p. 13677-88.

99.   Penaloza, H.F., et al., *Interleukin-36 Cytokines in Infectious and Non-Infectious Lung Diseases.* Front Immunol, 2021. **12**: p. 754702.

100.   Ainscough, J.S., et al., *Cathepsin S is the major activator of the psoriasis-associated proinflammatory cytokine IL-36gamma.* Proc Natl Acad Sci U S A, 2017. **114**(13): p. E2748-E2757.

101.   Elias, M., et al., *IL-36 in chronic inflammation and fibrosis - bridging the gap?* J Clin Invest, 2021. **131**(2).

102.   Sachen, K.L., C.N. Arnold Greving, and J.E. Towne, *Role of IL-36 cytokines in psoriasis and other inflammatory skin conditions.* Cytokine, 2022. **156**: p. 155897.

103.   Higashiyama, M. and R. Hokaria, *New and Emerging Treatments for Inflammatory Bowel Disease.* Digestion, 2023. **104**(1): p. 74-81.

104.   Zhou, L. and V. Todorovic, *Interleukin-36: Structure, Signaling and Function.* Adv Exp Med Biol, 2021. **21**: p. 191-210.

105.   Boutet, M.A., et al., *Distinct expression of interleukin (IL)-36alpha, beta and gamma, their antagonist IL-36Ra and IL-38 in psoriasis, rheumatoid arthritis and Crohn's disease.* Clin Exp Immunol, 2016. **184**(2): p. 159-73.

106.   Frey, S., et al., *The novel cytokine interleukin-36alpha is expressed in psoriatic and rheumatoid arthritis synovium.* Ann Rheum Dis, 2013. **72**(9): p. 1569-74.

107.   Franzke, C.W., et al., *Epidermal ADAM17 maintains the skin barrier by regulating EGFR ligand-dependent terminal keratinocyte differentiation.* J Exp Med, 2012. **209**(6): p. 1105-19.

108.   Berglof, E., et al., *IL-1Rrp2 expression and IL-1F9 (IL-1H1) actions in brain cells.* J Neuroimmunol, 2003. **139**(1-2): p. 36-43.

109.   Zhu, J., et al., *Interleukin-36beta exacerbates DSS-induce acute colitis via inhibiting Foxp3(+) regulatory T cell response and increasing Th2 cell response.* Int Immunopharmacol, 2022. **108**: p. 108762.

110.   Tu, J., et al., *Acitretin inhibits IL-17A-induced IL-36 expression in keratinocytes by down-regulating IkappaBzeta.* Int Immunopharmacol, 2020. **79**: p. 106045.

111.   Kobayashi, K., et al., *Cigarette Smoke Underlies the Pathogenesis of Palmoplantar Pustulosis via an IL-17A-Induced Production of IL-36gamma in Tonsillar Epithelial Cells.* J Invest Dermatol, 2021. **141**(6): p. 1533-1541 e4.

112.   Gu, J., et al., *Correlations between IL-36 family cytokines in peripheral blood and subjective and objective assessment results in patients with allergic rhinitis.* Allergy Asthma Clin Immunol, 2023. **19**(1): p. 79.

113.   Takahashi, K., et al., *Interleukin (IL)-1beta Is a Strong Inducer of IL-36gamma Expression in Human Colonic Myofibroblasts.* PLoS One, 2015. **10**(11): p. e0138423.

114.   Liu, H., et al., *Staphylococcus aureus Epicutaneous Exposure Drives Skin Inflammation via IL-36-Mediated T Cell Responses.* Cell Host Microbe, 2017. **22**(5): p. 653-666 e5.

115.   Milora, K.A., et al., *Interleukin-36beta provides protection against HSV-1 infection, but does not modulate initiation of adaptive immune responses.* Sci Rep, 2017. **7**(1): p. 5799.

116.   Braegelmann, J., et al., *Candida induces the expression of IL-36gamma in human keratinocytes: implications for a pathogen-driven exacerbation of psoriasis?* J Eur Acad Dermatol Venereol, 2018. **32**(11): p. e403-e406.

117.   Vigne, S., et al., *IL-36R ligands are potent regulators of dendritic and T cells.* Blood, 2011. **118**(22): p. 5813-23.

118.   Mutamba, S., et al., *Expression of IL-1Rrp2 by human myelomonocytic cells is unique to DCs and facilitates DC maturation by IL-1F8 and IL-1F9.* Eur J Immunol, 2012. **42**(3): p. 607-17.

119.   Tao, X., et al., *Interleukin 36alpha Attenuates Sepsis by Enhancing Antibacterial Functions of Macrophages.* J Infect Dis, 2017. **215**(2): p. 321-332.

120.   Nguyen, T.T., et al., *Interleukin-36 cytokines enhance the production of host defense peptides psoriasin and LL-37 by human keratinocytes through activation of MAPKs and NF-kappaB.* J Dermatol Sci, 2012. **68**(1): p. 63-6.

121.   Dietrich, D., et al., *Interleukin-36 potently stimulates human M2 macrophages, Langerhans cells and keratinocytes to produce pro-inflammatory cytokines.* Cytokine, 2016. **84**: p. 88-98.

122.   Ramadas, R.A., et al., *IL-36alpha exerts pro-inflammatory effects in the lungs of mice.* PLoS One, 2012. **7**(9): p. e45784.

123.   Harusato, A., et al., *IL-36gamma signaling controls the induced regulatory T cell-Th9 cell balance via NFkappaB activation and STAT transcription factors.* Mucosal Immunol, 2017. **10**(6): p. 1455-1467.

124.   Medina-Contreras, O., et al., *Cutting Edge: IL-36 Receptor Promotes Resolution of Intestinal Damage.* J Immunol, 2016. **196**(1): p. 34-8.

125.   Foster, A.M., et al., *IL-36 promotes myeloid cell infiltration, activation, and inflammatory activity in skin.* J Immunol, 2014. **192**(12): p. 6053-61.

126.   Ngo, V.L., et al., *IL-36R signaling integrates innate and adaptive immune-mediated protection against enteropathogenic bacteria.* Proc Natl Acad Sci U S A, 2020. **117**(44): p. 27540-27548.

127.   Russell, S.E., et al., *IL-36alpha expression is elevated in ulcerative colitis and promotes colonic inflammation.* Mucosal Immunol, 2016. **9**(5): p. 1193-204.

128.   Scheibe, K., et al., *IL-36R signalling activates intestinal epithelial cells and fibroblasts and promotes mucosal healing in vivo.* Gut, 2017. **66**(5): p. 823-838.

129.   Perse, M. and A. Cerar, *Dextran sodium sulphate colitis mouse model: traps and tricks.* J Biomed Biotechnol, 2012. **2012**: p. 718617.

130.   Eichele, D.D. and K.K. Kharbanda, *Dextran sodium sulfate colitis murine model: An indispensable tool for advancing our understanding of inflammatory bowel diseases pathogenesis.* World J Gastroenterol, 2017. **23**(33): p. 6016-6029.

131.   Ngo, V.L., et al., *IL-36 cytokines and gut immunity.* Immunology, 2021. **163**(2): p. 145-154.

132.   Maarouf, M., M. Kuczma, and T.L. Denning, *IL-36/IL-36R Signaling Promotes CD4+ T Cell-Dependent Colitis via Pro-Inflammatory Cytokine Production.* bioRxiv, 2023.

133.   Mao, R. and F. Rieder, *Cooling Down the Hot Potato: Anti-Interleukin 36 Therapy Prevents and Treats Experimental Intestinal Fibrosis.* Gastroenterology, 2019. **156**(4): p. 871-873.

134.   Leon, G., et al., *IL-36 cytokines imprint a colitogenic phenotype on CD4(+) T helper cells.* Mucosal Immunol, 2022. **15**(3): p. 491-503.

135.   Solitano, V., et al., *TL1A inhibition for inflammatory bowel disease treatment: From inflammation to fibrosis.* Med, 2024. **5**(5): p. 386-400.

136.   Hernandez Santana, Y.E., N. Irwin, and P.T. Walsh, *IL-36: a therapeutic target for ulcerative colitis?* Expert Opin Ther Targets, 2022. **26**(6): p. 507-512.

137.   Chi, H.H., et al., *IL-36 Signaling Facilitates Activation of the NLRP3 Inflammasome and IL-23/IL-17 Axis in Renal Inflammation and Fibrosis.* J Am Soc Nephrol, 2017. **28**(7): p. 2022-2037.

138.   Subramanian, S., H. Geng, and X.D. Tan, *Cell death of intestinal epithelial cells in intestinal diseases.* Sheng Li Xue Bao, 2020. **72**(3): p. 308-324.

139.   Baker, K., et al., *IL-36 signalling enhances a pro-tumorigenic phenotype in colon cancer cells with cancer cell growth restricted by administration of the IL-36R antagonist.* Oncogene, 2022. **41**(19): p. 2672-2684.

140.   Li, Z., et al., *CCL20, gammadelta T cells, and IL-22 in corneal epithelial healing.* FASEB J, 2011. **25**(8): p. 2659-68.

141.   Fonseca, A., J. Sunny, and L.M. Felipez, *Very Early-Onset Inflammatory Bowel Disease (VEO-IBD) Presenting with Recurrent Leukocytoclastic Vasculitis Preceded by Streptococcal Pharyngitis.* Case Rep Pediatr, 2021. **2021**: p. 1996430.

142.   Usami, M., et al., *Clinical features of very early-onset inflammatory bowel disease in Japan: a retrospective single-center study.* Intest Res, 2022. **20**(4): p. 475-481.

143.   Chen, Q., N. Gao, and F.S. Yu, *Interleukin-36 Receptor Signaling Attenuates Epithelial Wound Healing in C57BL/6 Mouse Corneas.* Cells, 2023. **12**(12).

144.   Neurath, M.F., *Targeting cytokines in inflammatory bowel disease.* Sci Transl Med, 2022. **14**(675): p. eabq4473.

145.   Neurath, M., *Current and emerging therapeutic targets for IBD.* Nat Rev Gastroenterol Hepatol, 2017. **14**(11): p. 688.

146.   Neurath, M.F., *IL-36 in chronic inflammation and cancer.* Cytokine Growth Factor Rev, 2020. **55**: p. 70-79.

147.   Iznardo, H. and L. Puig, *Exploring the Role of IL-36 Cytokines as a New Target in Psoriatic Disease.* Int J Mol Sci, 2021. **22**(9).

148.   Yao, X., et al., *Targeting interleukin-6 in inflammatory autoimmune diseases and cancers.* Pharmacol Ther, 2014. **141**(2): p. 125-39.

149.   Ye, M., et al., *Deletion of IL-6 Exacerbates Colitis and Induces Systemic Inflammation in IL-10-Deficient Mice.* J Crohns Colitis, 2020. **14**(6): p. 831-840.

150.   Li, Q.Q., H.H. Zhang, and S.X. Dai, *New Insights and Advances in Pathogenesis and Treatment of Very Early Onset Inflammatory Bowel Disease.* Front Pediatr, 2022. **10**: p. 714054.

151.   Daig, R., et al., *Increased interleukin 8 expression in the colon mucosa of patients with inflammatory bowel disease.* Gut, 1996. **38**(2): p. 216-22.

152.   Vasilyeva, E., et al., *Serum Cytokine Profiles in Children with Crohn's Disease.* Mediators Inflamm, 2016. **2016**: p. 7420127.

153.   Singh, U.P., et al., *Chemokine and cytokine levels in inflammatory bowel disease patients.* Cytokine, 2016. **77**: p. 44-9.

154.   Meitei, H.T., N. Jadhav, and G. Lal, *CCR6-CCL20 axis as a therapeutic target for autoimmune diseases.* Autoimmun Rev, 2021. **20**(7): p. 102846.

155.   Osuala, K.O. and B.F. Sloane, *Many Roles of CCL20: Emphasis on Breast Cancer.* Postdoc J, 2014. **2**(3): p. 7-16.

156.   Zhang, T., et al., *NF-kappaB signaling in inflammation and cancer.* MedComm (2020), 2021. **2**(4): p. 618-653.

157.   Li, X., et al., *CXCL10-armed oncolytic adenovirus promotes tumor-infiltrating T-cell chemotaxis to enhance anti-PD-1 therapy.* Oncoimmunology, 2022. **11**(1): p. 2118210.

158.   Cremonesi, E., et al., *Gut microbiota modulate T cell trafficking into human colorectal cancer.* Gut, 2018. **67**(11): p. 1984-1994.

159.   Shahini, A. and A. Shahini, *Role of interleukin-6-mediated inflammation in the pathogenesis of inflammatory bowel disease: focus on the available therapeutic approaches and gut microbiome.* J Cell Commun Signal, 2023. **17**(1): p. 55-74.

160. Tanaka, T., M. Narazaki, and T. Kishimoto, *IL-6 in inflammation, immunity, and disease.* Cold Spring Harb Perspect Biol, 2014. **6**(10): p. a016295.

161. Atreya, R. and M.F. Neurath, *Involvement of IL-6 in the pathogenesis of inflammatory bowel disease and colon cancer.* Clin Rev Allergy Immunol, 2005. **28**(3): p. 187-96.

162. Mia, S., et al., *An optimized protocol for human M2 macrophages using M-CSF and IL-4/IL-10/TGF-beta yields a dominant immunosuppressive phenotype.* Scand J Immunol, 2014. **79**(5): p. 305-14.

163. Skytthe, M.K., J.H. Graversen, and S.K. Moestrup, *Targeting of CD163(+) Macrophages in Inflammatory and Malignant Diseases.* Int J Mol Sci, 2020. **21**(15).

164. Zhang, K., et al., *Macrophage polarization in inflammatory bowel disease.* Cell Commun Signal, 2023. **21**(1): p. 367.

165. Garrido-Trigo, A., et al., *Macrophage and neutrophil heterogeneity at single-cell spatial resolution in human inflammatory bowel disease.* Nat Commun, 2023. **14**(1): p. 4506.

166. Baumgart, D.C., et al., *Exaggerated inflammatory response of primary human myeloid dendritic cells to lipopolysaccharide in patients with inflammatory bowel disease.* Clin Exp Immunol, 2009. **157**(3): p. 423-36.

167. Isidro, R.A. and C.B. Appleyard, *Colonic macrophage polarization in homeostasis, inflammation, and cancer.* Am J Physiol Gastrointest Liver Physiol, 2016. **311**(1): p. G59-73.

168. Liu, Y., et al., *CD279 mediates the homeostasis and survival of regulatory T cells by enhancing T cell and macrophage interactions.* FEBS Open Bio, 2020. **10**(6): p. 1162-1170.

169. da Silva, T.A., et al., *CD14 is critical for TLR2-mediated M1 macrophage activation triggered by N-glycan recognition.* Sci Rep, 2017. **7**(1): p. 7083.

170. Bain, C.C. and A. Schridde, *Origin, Differentiation, and Function of Intestinal Macrophages.* Front Immunol, 2018. **9**: p. 2733.

171. Barbour, J.D., et al., *Reduced CD14 expression on classical monocytes and vascular endothelial adhesion markers independently associate with carotid artery intima media thickness in chronically HIV-1 infected adults on virologically suppressive anti-retroviral therapy.* Atherosclerosis, 2014. **232**(1): p. 52-8.

172. Buchheister, S., et al., *CD14 Plays a Protective Role in Experimental Inflammatory Bowel Disease by Enhancing Intestinal Barrier Function.* Am J Pathol, 2017. **187**(5): p. 1106-1120.

173. Reed-Geaghan, E.G., et al., *Deletion of CD14 attenuates Alzheimer's disease pathology by influencing the brain's inflammatory milieu.* J Neurosci, 2010. **30**(46): p. 15369-73.

174. Lekkou, A., et al., *Cytokine production and monocyte HLA-DR expression as predictors of outcome for patients with community-acquired severe infections.* Clin Diagn Lab Immunol, 2004. **11**(1): p. 161-7.

175. Grapp, H., et al., *IL36R signaling in intestinal epithelial cells and neutrophils enhances intestinal wound healing.* Zeitschrift fur Gastroenterologie, 2023. **61(03): e63-e64**.

176.   Jin, S., R.M. Ray, and L.R. Johnson, *TNF-alpha/cycloheximide-induced apoptosis in intestinal epithelial cells requires Rac1-regulated reactive oxygen species.* Am J Physiol Gastrointest Liver Physiol, 2008. **294**(4): p. G928-37.

177.   Poudel, M., et al., *Regulation of Interleukin-36gamma/IL-36R Signaling Axis by PIN1 in Epithelial Cell Transformation and Breast Tumorigenesis.* Cancers (Basel), 2022. **14**(15).

178.   Yuan, Z.C., et al., *Biology of IL-36 Signaling and Its Role in Systemic Inflammatory Diseases.* Front Immunol, 2019. **10**: p. 2532.

179.   Babu, D., et al., *TNF-alpha/cycloheximide-induced oxidative stress and apoptosis in murine intestinal epithelial MODE-K cells.* Curr Pharm Des, 2012. **18**(28): p. 4414-25.

ACKNOWLEDGEMENTS

AFFIDAVIT

LMU LUDWIG-MAXIMILIANS-UNIVERSITÄT MÜNCHEN	Promotionsbüro Medizinische Fakultät	MMRS	

Affidavit

ATAC, LEYLA

_____
Surname, first name

Lindwurmstrasse 2A

_____
Street

80337, München, Germany

_____
Zip code, town, country

I hereby declare, that the submitted thesis entitled:

IL1RL2 in immunity and intestinal homeostasis -Insights from patients with VEO-IBD

……………………………………………………………………………………………….

is my own work. I have only used the sources indicated and have not made unauthorised use of services of a third party. Where the work of others has been quoted or reproduced, the source is always given.

I further declare that the dissertation presented here has not been submitted in the same or similar form to any other institution for the purpose of obtaining an academic degree.

Münich, 09.12.2024   Leyla Atac

_____   _____

place, date   Signature doctoral candidate

CONFIRMATION OF CONGRUENCY

Confirmation of congruency between printed and electronic version of the doctoral thesis

ATAC, LEYLA

_____
Surname, first name

Lindwurmstrasse 2A

_____
Street

80337, München, Germany

_____
Zip code, town, country

I hereby declare, that the submitted thesis entitled:

IL1RL2 in immunity and intestinal homeostasis -Insights from patients with VEO-IBD

………………………………………………………………………………………………

is congruent with the printed version both in content and format.

Münich, 09.12.2024   Leyla Atac

_____   _____

place, date   Signature doctoral candidate